Chemical engineering of the electronic properties of ITO-organics interface in Phthalocyanine/C$_{60}$-Fullerene organic solar cells

Inaugural-Dissertation
to obtain the academic degree
Doctor rerum naturalium (Dr. rer. nat.)
submitted to the Department of Biology, Chemistry and Pharmacy
of Freie Universität Berlin

by

Boyan Johnev

from Sofia, Bulgaria

Berlin, November 2005

Prepared at Hahn-Meitner Institut, Berlin, department SE2,

in the group "Organic Solar Cells" of Dr. Konstantinos Fostiropoulos

1st reviewer: Prof. Dr. Helmut Tributsch

2nd reviewer: Dr. Christian-Herbert Fischer

Date of defense:10.02.2006

List of Abbreviations

BCP   Bathocuproine; 2,9-Dimethyl-4,7-diphenyl-1,10-phenanthroline

DBU79   1,8-Diazabicyclo[5.4.0]undec-7-ene

DMF   Dimethylformamide

FTIR   Fourier Transform Infra-Red spectroscopy

I_{sc} Short circuit current of a solar cell [A]

ITO   Indium-Tin Oxide

J_{sc} Short circuit current of a solar cell [A/cm^2]

KPFM   Kelvin Probe Force Microscopy

PEDOT:PSS   Poly-Ethylene DioxyThiophene : Poly-Styrene Sulphonate

P_{light} Power of light reaching a solar cell

P_{max} Maximal electrical power of a solar cell

QCDC   Quartz Crystal Deposition Controllers

R_p Parallel resistance in a solar cell

R_s Serial resistance in a solar cell

SEM   Scanning Electron Microscopy

TCO   Transparent Conducting Oxide

UHV   Ultra-High Vacuum

V_{oc} Open circuit voltage of a solar cell

XPS   X-ray Photoelectron Spectroscopy

ZnPc, Phthalo   Zinc Phthalocyanine

Table of contents

1 Introduction and theoretical part

Energy demands in expanding modern society are constantly growing. Parallel with the industry's permanent search for lower cost energy resources, mankind is also looking for renewable energy, whose exploitation would not affect the fragile nature balance. Earth heat, wind and tide energy are some examples of the potential of renewable sources for the production of energy [1].

With a constantly growing share in renewable energy use is the utilization of Sunlight. So called "solar cells" transform it to electricity with commercial energy conversion efficiencies of 10-15% [1]. The record of solar cell efficiency in present time is being held by single crystalline silicon solar cells, whose highly structured surface, together with some extremely complex light trapping techniques transforms incident light with about 25% efficiency in electricity [2]. These solar high-tech devices are of course very expensive and have, therefore limited use, for example, in space technologies, where very compact and efficient devices are required. On Earth, where space is not a problem, bigger and cheaper devices can be installed. The end cost of silicon panels, even if polycrystalline is quite high, firstly because of material purity requirements and secondly because of the amounts of material used.

1.1 Organic photovoltaic devices

In the last two decades a new branch in photovoltaic research was formed. Scientists all over the world have found a new playground in the face of organic ultra-thin film solar cells. Produced from environment-friendly organic materials, on cheap and flexible plastic substrates, semitransparent, cut in various shapes and sizes – those are the dream properties of the organic photodiodes. Some of these are already achieved, but there's still a long path to walk if one wants to combine all these properties in a single device.

The photovoltaic effect in organic materials is known since the mid 70s [3]. Though as the beginning of organic solar cell research scientists tend to point 1986 from the publishing of the well known C. W. Tang article on a "Two-layer organic

photovoltaic cell" [**4**]. At present time many different organic solar cell device architectures exist. From just an organic substance between two electrodes scientists have expanded the complicated interpenetrating organic mixtures or tandem cells [**5**]. All these concepts have been developing very intensively in the last years and sooner or later it is expected that organic photovoltaic devices reach compatible efficiencies to eventually compete with their expensive silicon or poisonous inorganic relatives. Also the price of an organic device is many times lower than that of inorganic ones mainly because of the quantities of material used. Even at prices of about 200-300$ per gram active layer material, a square centimeter of an organic solar cell is much cheaper than one of a silicon single crystal, because in a couple of nanometers thick layer one uses almost invisible quantities of material. Our estimations show that out of 1 kg organic absorber material at 3% organic solar cell efficiency 1 MW electrical power could be yielded.

1.2 Zn-Phthalocyanine - C$_{60}$ heterojunction cell architecture

In the present work we are dealing with a bi-layer bulk heterojunction, donor acceptor solar cell concept having as an absorber/donor the substance zinc-phthalocyanine (**ZnPc**) and as an acceptor fullerene C$_{60}$ (Figure 1). Beside the active layers there are also two buffer layers – Bathocuproine (**BCP**) (2,9-Dimethyl-4,7-diphenyl-1,10-phenanthroline) and a block copolymer – Poly-Ethylene DioxyThiophene : Poly-Styrene Sulphonate (**PEDOT:PSS**) who's role is to admit only electrons or only holes to the corresponding electrode, respectively. This architecture is sandwiched between two electrodes: Indium-Tin Oxide (**ITO**) - at present the mostly used transparent conducting oxide (**TCO**) and Aluminum (Al).

Layer order scheme	Layer function:
Al	Back electrode
Bathocuproine	Buffer
C$_{60}$	Acceptor=n-type
ZnPc	Absorber=donor=p-type
PEDOT:PSS	Buffer
ITO	Front contact
Glass	Substrate
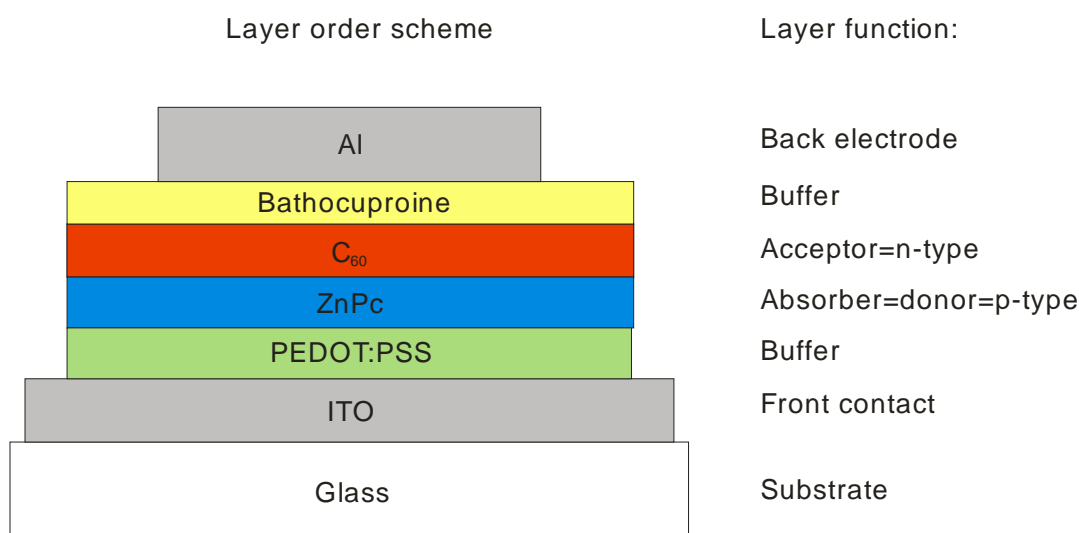
Figure 1. ZnPc/C$_{60}$ solar cell architecture. The two active layers ZnPc and C$_{60}$ are sandwiched between the two buffers, which lay next to the electrodes

After a layer thickness optimization procedure, hereby not conducted by the author, but in the same scientific group, the optimum thickness for each layer of this cell was found. Highest cell efficiency (electrical cell parameters described further in 2.8) was produced by a cell with the following configuration: ZnPc – 30 nm, C$_{60}$ – 30 nm,

BCP – 17 nm and Al – about 150 nm. As concerning PEDOT:PSS thickness, it will be explained later in the experimental section of this work under PEDOT:PSS spin-coating (2.5). Further referenced as a standard cell, this solar cell architecture will be used without the spin-coated PEDOT:PSS buffer, in order to study different chemical ways to manipulate the ITO-organics interface and align the energy band structure for optimum charge carrier transport.

1.3 Theoretical model and energy diagram

After a careful check and comparison of different literature sources, the following energy level diagram for our solar cell could be sketched [6,7,8,9,10,11].
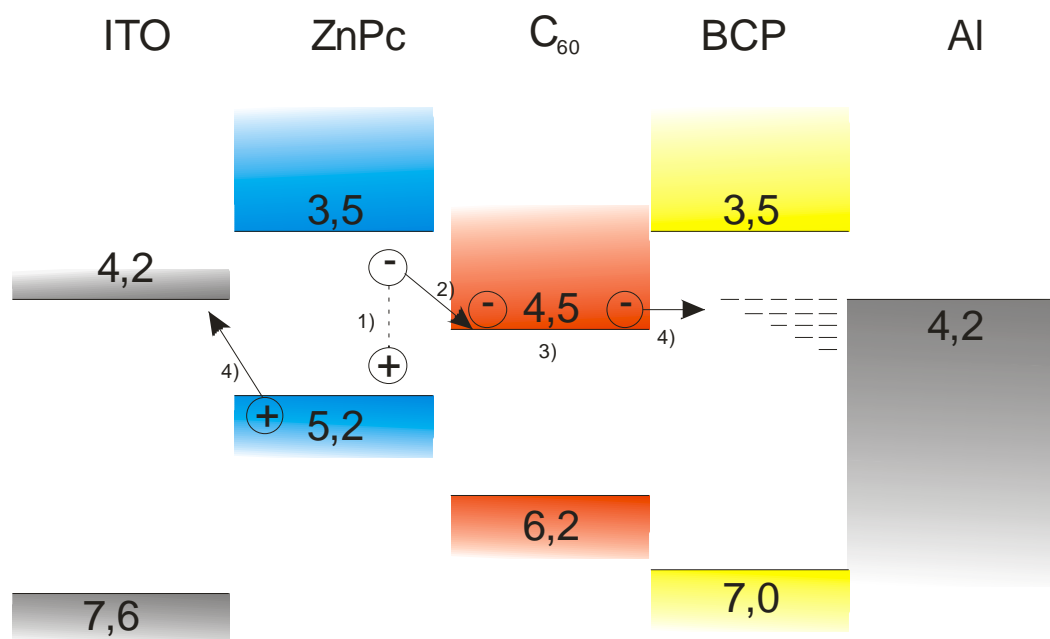
Figure 2. Energy level diagram of the ITO/ZnPc/C$_{60}$/BCP/Al cell; Values in eV. Process 1) stands for exciton creation in absorber layer; process 2) is charge separation on ZnPc-C$_{60}$ interface; process 3) is the diffusion of charges; process 4) is charge transfer to contacts through the buffer layers. Work function of ITO can vary up to 4,7 eV, but 4,2 eV is the value, measured on a clean-sputtered ITO surface

Of course the values for each substance in this diagram vary from publication to publication. Particularly for ITO, a work function value from 4,1 up to 4,7 eV can be found. That's why for this band diagram either mean reference values (ZnPc, C60,

BCP), or values measured by us (ITO) were used. Aluminum, as an element has one, precise value in all sources, namely 4,2 eV.

Sunlight, after being absorbed in organic molecular crystal semiconductors, does not "immediately" create a free electron, but an exciton [12]. This exciton, being a pair of an electron and a hole, held together by Coulomb forces, has some binding energy of ~1 eV in organic materials [13]. It also can diffuse in the ZnPc bulk not more than 30±10 nm [14]. This is the main reason why this material in our cell has an optimum thickness of 30 nm. If it is thinner less light is absorbed leading to lower currents. If it is thicker, less excitons reach the $ZnPc/C_{60}$ interface where charge separation occurs [15]. To be separated, excitons need either more energy, or a favorable arrangement of the surrounding molecular orbitals, where the surrounding field forces them to separate. The electron is transferred to the LUMO of C_{60} and the hole is being transported to ITO. In general, in the transport of charge carriers in organic semiconductors, dominates the so called, hopping mechanism, rather than band-like transport [16].

Further transfer of the electron to the aluminum contact is believed to happen through acquired energetic levels of bathocuproine, which is practically an insulator substance. Its valence band is very low (7,0 eV), thus excluding the possibility of charge transport through its conduction band. The acquired energetic levels in BCP appear after the physical diffusion of the incoming hot aluminum vapor (about 1200°C), during aluminum electrode evaporation. Having a glass point of about 80°C BCP is a "soft" material which allows aluminum to interpenetrate. During this process partially a chemical reaction occurs, which results in an aluminum complex with BCP [17]:

$$Al \underset{+3e^-}{\overset{-3e^-}{\rightleftharpoons}} Al^{3+} \xrightarrow{\text{BCP}} [(Al)_x(BCP)_y]^{3x+}$$
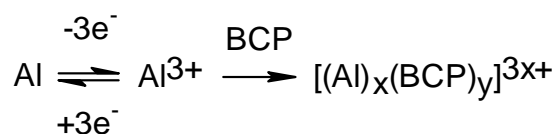
Dispersed in the BCP matrix, this complex creates the additional interpenetrating energy levels which make the transport of electrons to the Al electrode possible. Also the charge of this complex, gathered on the interface C_{60}/BCP blocks holes from proceeding to the aluminum electrode. This way BCP serves as a hole filtering buffer allowing mainly electrons to reach the Al back contact.

1.4 Stability and reproducibility problems

It is a well known fact that organic photovoltaic devices have a much shorter life in comparison with their inorganic or silicon analogues [**18**,**19**,**20**]. It is proven that this is due to the combined effect of light and oxygen traces diffusing in the sample – the so called photo-degradation [**21**]. One hypothetical explanation of degradation are the aggressive oxygen radicals, generated by UV in ITO, which attack the organics and by chemically modifying the organics, create exciton traps, or lower the electro-conductivity of the materials [**22**]. In the literature the degradation is reported in different time scale periods: from hours to days and even months, all depending on different production and encapsulation techniques to keep the aggressive oxygen and humidity out of the device.

The standard cell in the present work (see 1.2) had a half-life of roughly 5 hours, under encapsulation in a Plexiglas container, isolated from atmosphere with pressed rubber O-rings. Unprotected the device degraded in much less time.

Reproducibility of the efficiency results of organic solar cells is also a step stone for scientists. Along with different batches of ITO glass, having different properties, also by the evaporation of the active organic layers there are many parameters which can differ from one to another batch. Vacuum quality, thickness measurement accuracy, evaporation rate, substrate temperature – these are some of the parameters that need to be kept constant in order to achieve reproducible results. Of course this is difficult and that is why statistical quantity of experiments has to be conducted in order to say: "This cell now has that defined efficiency".

Knowing all these difficulties and problems of the organic photovoltaic device that we are dealing with, we can define the topics of the present work.

1.5 Topics and goals of the present work

Analytical studies:

- Study of the ITO substrate and extraction of data about its surface (appearance, roughness, work function), its thickness, temperature behavior (resistance), different substrate types (ITO thickness, resistance);
- Test of the chemical stability of organic cell materials under O_2 and UV irradiance;
- Study of the cell by means of optical simulation;
- Comparison of different methods for layer thickness determination;

Preparative studies:

- Testing different means of ITO passivation in order to avoid the PEDOT:PSS buffer layer, but attaining cell efficiency;
- With all gained experience, engineering and testing of a new chemical passivation on ITO;
- Up-scaling our current standard cell ($0,032 \text{ cm}^2$) to 1 cm^2, to be able to conduce space resolved I/V measurements;
- Experimentation with different (from Aluminum) metal counter-electrodes, to observe cell behavior through counter-electrode work function change

2 Experimental part: Methods, Reagents, Syntheses

The experiments done in behalf of this thesis, due to the high cleanliness demands of the application, were undertaken with a serious consideration of chemical purity and clean environment.

2.1 Environments

All substrate washing, spin-coating and ITO passivation dipping procedures were performed in a Laminar-flow Box from Micro CleanRoom Technology GmbH with an "Astrocell II$^{®}$" air cleaning facility.

Applications which needed protection from humidity or air oxygen have been performed in an InterTec GmbH Glove Box, under nitrogen gas with impurities less than 1 ppm.

Evaporation of organic substances for the production of solar cells has been done in a Balzers ultra-high-vacuum (UHV) evaporation chamber under pressure of about 10^{-7} mbar.

Chemical synthetic preparations, sensitive to humidity have been performed in a fume hood, with glassware under nitrogen gas flow.

2.2 Chemicals, reagents and materials

Chemicals used for cell preparation through UHV evaporation: ZnPc, C60 and BCP, were delivered from the company Covion. They had highest purity grade: 99%.

Other chemicals, used for ITO passivations were delivered from Sigma-Aldrich with a grade "Pure for analysis".

Chemicals from the sources mentioned above were used without further purification.

Chemicals synthesized by us were cleaned as described in synthesis (2.6.2).

Indium-Tin Oxide glass substrates were delivered by Präzisions Glas & Optic GmbH, readily cut in the desired size. The conducting oxide has been sputtered on polished float glass. Substrates used in the present work had a square resistance of 5, 10, 20, 50 and 100 Ω. For a standard solar cell, only 5 Ω/ glass was used for reproducibility.

PEDOT:PSS for spincoating on ITO was obtained from A. C. Starck (BAYER) with no further notice about purity, ingredients, composition.

2.3 Cleaning procedure for ITO

ITO, as received, is of course too contaminated for the purposes of solar cell production. That is why it needs to pass a thorough cleaning procedure to ensure that its surface is clean and more important - dust free. This cleaning procedure was applied as follows:

1. The ITO substrates after being wiped with absolute ethanol are placed in a beaker and ultrasonically cleaned for 20 minutes with acetone.
2. After that the solvent is being changed to 2-propanole and again 20 minutes in the ultrasonic bin are applied.
3. Then, after rinsing each piece of ITO glass with deionized water (MILLIPORE®), 2 different soap solutions from N. Bucher AG are being applied for further 20 minutes each in the ultrasonic bin.
4. Subsequently substrates were rinsed with plenty of deionized water and then dried, using ionized nitrogen gas gun.

Further no plasma or any other surface treatments were applied due to the fact that these change the surface work function of ITO [23,24]. For reproducibility all ITO substrates used in the current work were cleaned using the same cleaning procedure, described above. After the cleaning procedure the ITO substrates were used immediately, to avoid recontamination by storage.

2.4 ITO Passivations

ITO passivations applied in the current work are mostly wet dippings with exception of 8-Hydroxyquinoline which is a gas phase deposition and ZnO/Soluble Phthalocyanine which is an electrodeposition product.

The dipping solutions had the following concentrations:

- HCl 1M
- H_3PO_4 1M,
- HIO_4 1M,
- NH_3 1M,
- Zinc Phthalocyaninetetraphosphonic acid ($ZnPc(PO_3H)_4$) 10^{-4}M.

Deposition of 8-Hydroxyquinoline will be described in 2.6.1.

Co-electrodeposition of ZnO and $CuPc(SO_3H)_4$ was carried out of a mixed solution with concentrations: $0,1M$ $Zn(NO_3)_2$ and $5.10^{-4}M$ $CuPc(SO_3H)_4$ at a voltage of $-1,1V$ at 70ºC for different time durations, depending on the desired thickness [**25**].

2.5 Conventional treatment – PEDOT:PSS Spin-coating

Coating ITO substrates with PEDOT:PSS was performed on a Delta 6RC spin-coater. The PEDOT:PSS solution, as received was too concentrated, that is why it was additionally diluted with deionized water to 60%, 70%, 80% and 90%. Different concentrations of this material yield also different thicknesses, which is anyway irrelevant to the current work. The highest cell efficiency was yielded with 70% concentration, so any reference to a cell with PEDOT:PSS will be done for this concentration. After applying the PEDOT:PSS solution on the ITO glass substrate it was pre-spinned at 200 rpm for 10 seconds, so that the complete surface gets covered with the solution. Then the spinning is continued at 2000 rpm to let the substrate dry. After this the substrate is heated 15 minutes at 100ºC to let the PEDOT:PSS dry and bind to the surface.

2.6 Syntheses

2.6.1 8-Hydroxyquinoline deposition

For the deposition of 8-Hydroxyquinoline on the surface of ITO a two stage process was used [**26,27**] (see reaction scheme – Figure 4), where in each reaction only the first monolayer reacts with the substrate. The first reaction was the deposition of a bridging molecule, followed by the 8-hydroxyquinoline after that. The natural OH-passivation of ITO [**28**] was used for the first step.
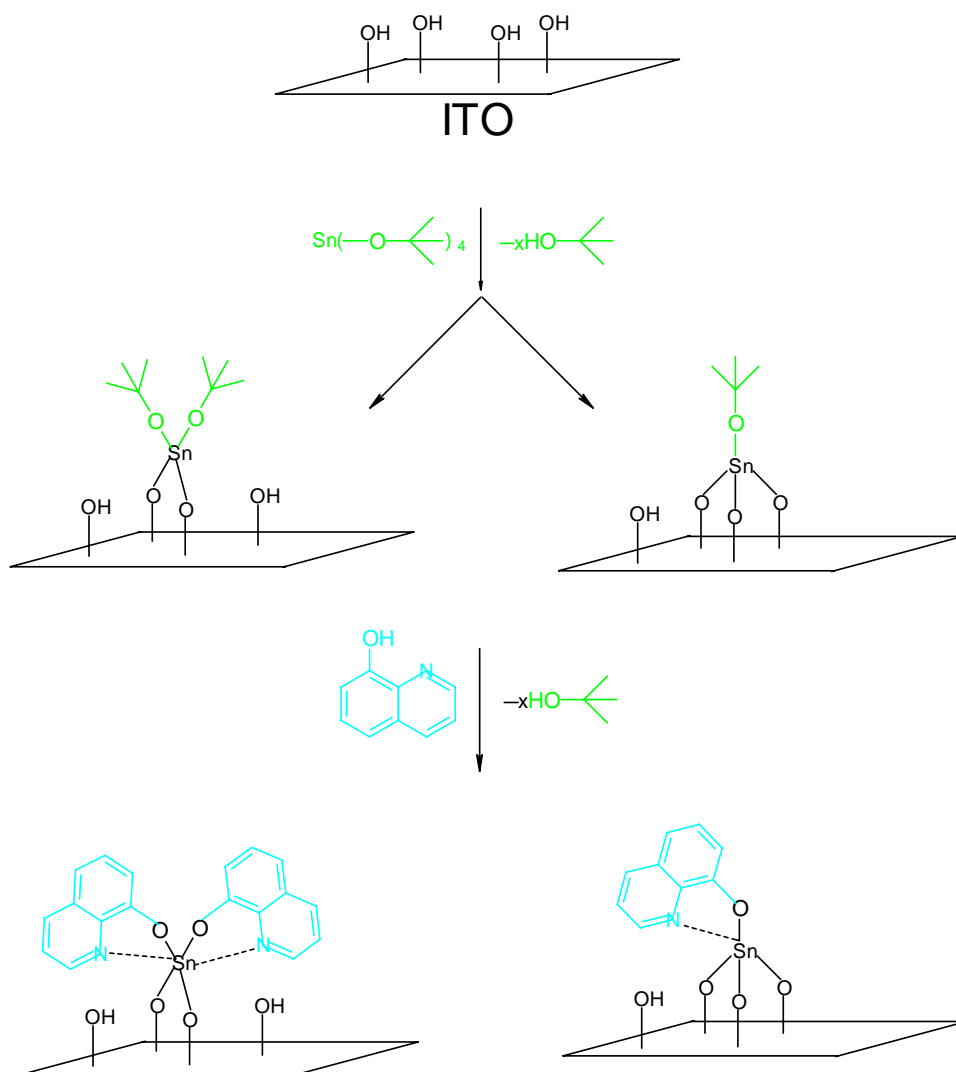

Figure 3. Two stage reaction of passivating ITO with 8-Hydroxyquinoline. At the first stage, a monolayer of tetra(tert-butoxy)tin is deposited on the surface, which is then used for the second reaction, for depositing a monolayer of 8-hydroxyquinoline
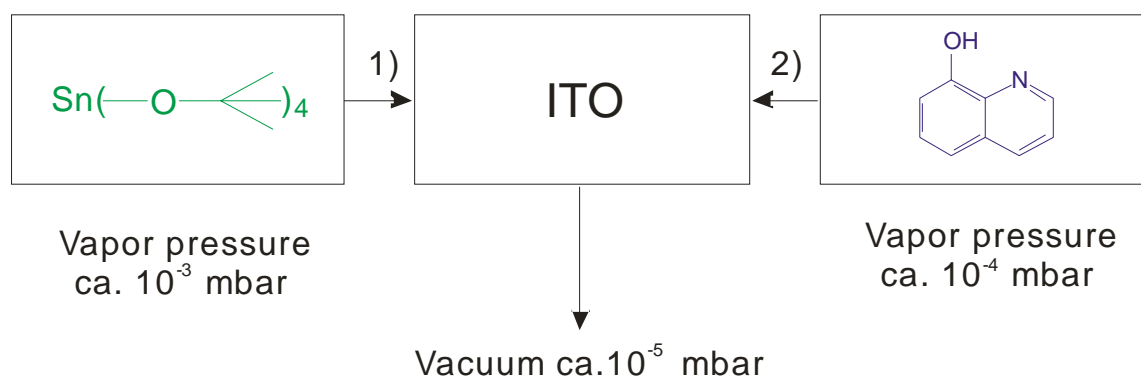
Figure 4. Schematic representation of the vacuum sublimation reaction apparatus. Reactions 1) and 2) are done one after another. Complete pumping of the chamber, between reactions, ensures no residual substance or multiple layer coverage

At moderate vacuum of about 10^{-5} mbar, a vent, connecting the precursor chamber and the substrate chamber, was opened. At room temperature, a flow of subliming Tetra(tert-butoxy)tin, reacted with the pre-cleaned ITO-glass sample. After 30 minute flow, the reaction chamber was isolated from the precursor and evacuated until no change in vacuum was to be observed, to assure the removal of excess substance, deposited on the surface, and the tert-butanol, a product of the reaction. Then the second reaction was carried out, again for 30 minutes in a flow of 8-Hydroxyquinoline. Afterwards once more the chamber was evacuated until there was no change in vacuum to ensure the evacuation of all quinoline, which is not chemically bound to the surface.

2.6.2 Zinc-Phthalocyaninetetraphosphonic acid synthesis

The synthesis of zinc-phthalocyaninetetraphosphonic acid was conducted as described elsewhere [**29**], with slight modifications. As starting material bromophthalodinitril was used. The conversion was made in three reaction stages.

3,4-Dicyanobenzophosphonic acid, diethyl ester
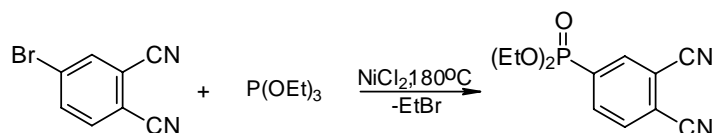
4-Bromophthalonitrile (3,1 g) is mixed with water free $NiCl_2$ (0,195 g) in a flask, fitted for direct distillation, and heated. At 180°C (and not 160 as described in the literature source) $P(OEt)_3$ (3,42 ml) is dropped to the melt. The forming EtBr distills in the same time with the weak N_2 flow. After the addition the mixture is being stirred one more hour at 180 degrees. In the end of the reaction the black reaction mixture is passed through a column of silica gel with chloroform as eluent (flash chromatography). The solvent is then distilled at a rotational evaporator. The product is vacuum distilled (0,3Torr) at about 190°C as a colorless liquid. Yield: 60%.

Zn-Phthalocyaninetetraphosphonic acid - diethyl ester,
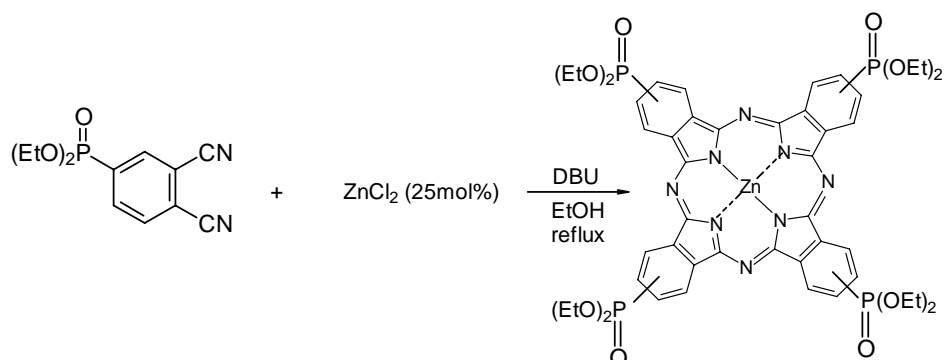
0,55 g of the precursor, 0,32 ml 1,8-Diazabicyclo[5.4.0]undec-7-ene (DBU79) and 71mg water-free ZnCl$_2$ are refluxed 40h in 35 ml abs. EtOH. After distillation of the solvent, the reaction mixture is being chromatographed on silica gel with Chloroform/Methanol (v:v=4:1). After vacuum evaporation of the solvents purple-blue powder is yielded (35% of the theoretical yield). T$_{melt}$ >300°C.

Zinc-Phthalocyaninetetraphosphonic acid
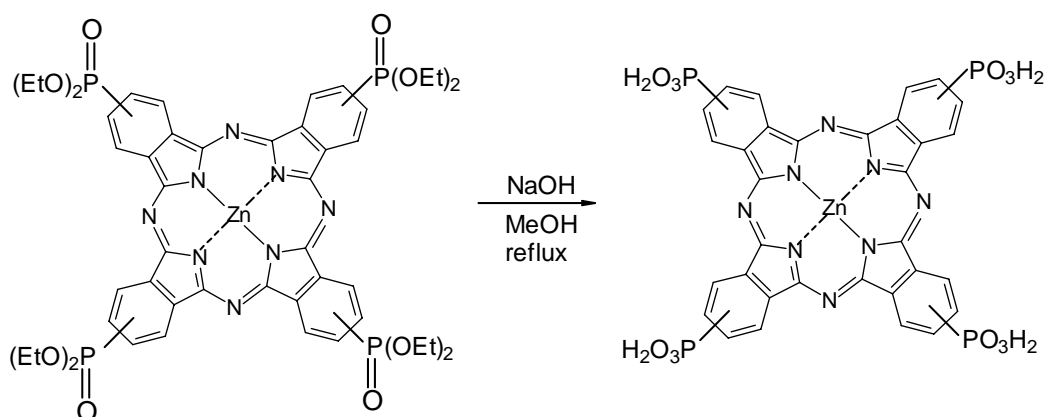
The ester is boiled with NaOH in methanol for 20h. After that the solvent is distilled at a rotation-distiller. With HCl the rest is led to a lower pH. The blue slurry is filtered. Recrystallization out of Methanol leads to blue crystals. Dimethylformamide (DMF)/Water (v:v=97:3) recommended in the literature reference as solvent for

recrystallization makes crystallization difficult, because of too high material solubility. Yield 90%.

Here it has to be mentioned, that a synthesis out of bromophthalonitril was also attempted. If the molar ratios are kept the same then the reactions can be conducted successfully and the subsequent substance is yielded. The temperature for the first substitutional reaction with bromophthalonitril is also 180°C and not 160°C, as mentioned in the literature source.

2.7 Solar cell production in UHV

The organic layers for our solar cells were vapor-deposited in an UHV chamber at $\approx 10^{-7}$ mbar vacuum. A schematic drawing of the vacuum chamber is shown on Figure 5.
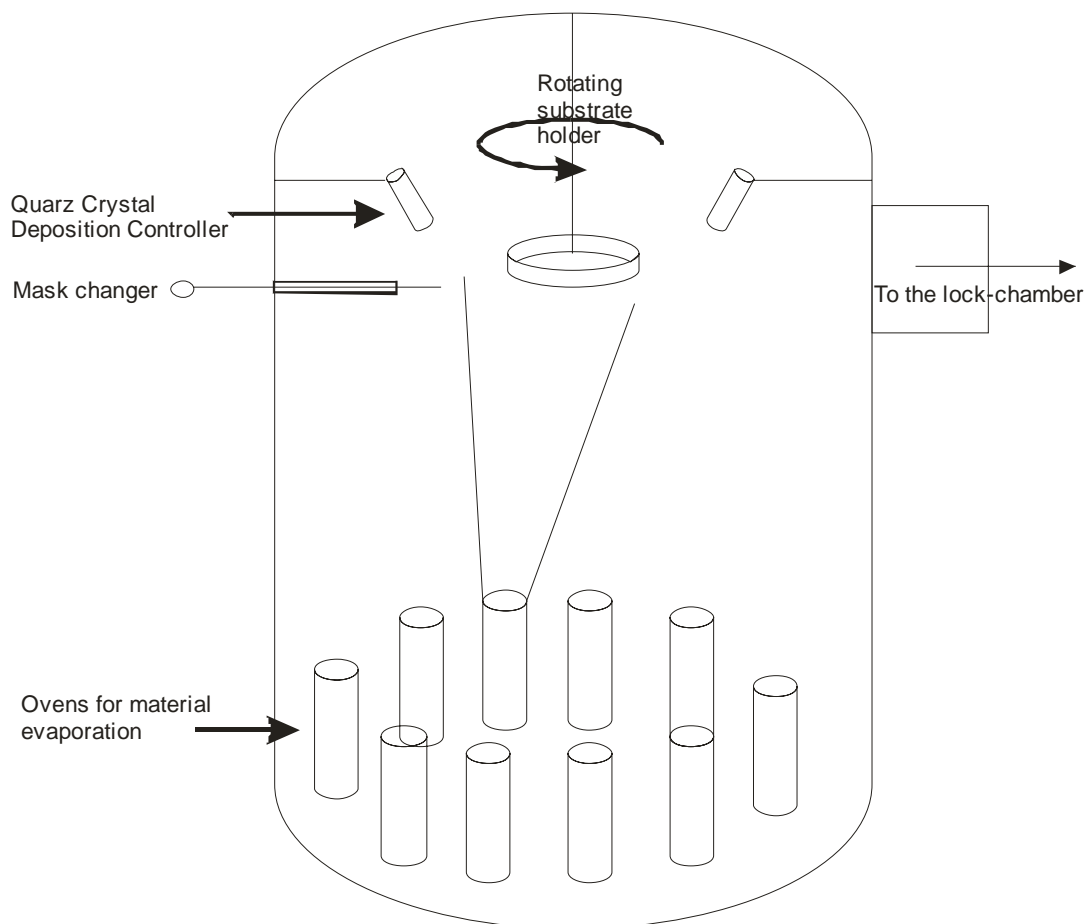
Figure 5. Schematic drawing of the UHV evaporation chamber. Material ovens are situated in the bottom part of the volume, with the opening directed to the sample holder. Rotating substrate holder and deposition controllers are near to each other in the upper part. A mask changer, perpendicular to the sample holder rotation axis, is situated at the level of the mask changing switch on the sample holder

A big cylinder with volume more than 300 liters, the vacuum chamber is kept under UHV through a system of a pre-pump and a turbo pump. The substrate holder enters the UHV chamber through a lock chamber connected to the main one with a vent.

On the side of the lock chamber is shown a manipulator, with which, after evacuation of the lock chamber, the substrate holder is transferred to the main chamber.
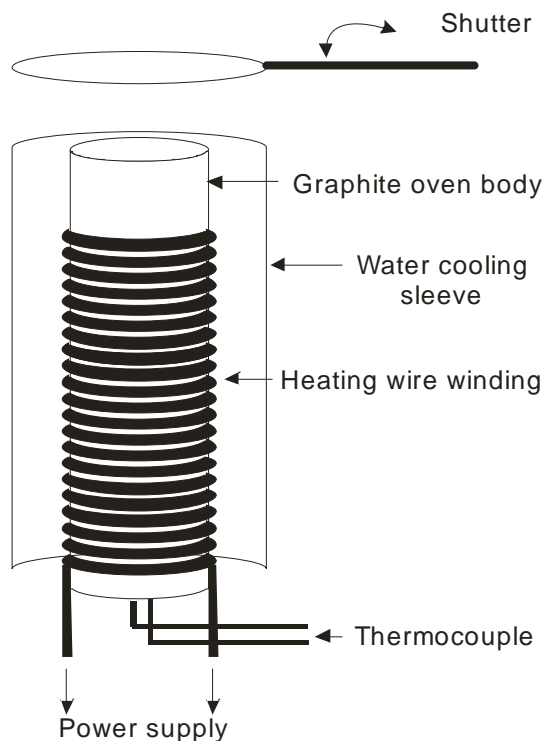
Figure 6. Evaporation oven sketch, illustrating: vertical graphite oven body, heater winding, thermocouple for temperature control and water cooling sleeve

The chemical substances undergoing evaporation are situated in 12 graphite ovens distributed in a circle on the main chamber bottom. Each oven (Figure 6) has a tantalum heater and a water cooling system, connected so, that the heater will only heat the particular oven and nothing else around itself. This way no contamination from walls or bottom can land into the substance vapor flow. The ovens are positioned vertically with the opening on top, facing directly the substrate holder. Evaporation is only possible with an open oven shutter, controlled pneumatically. For the different substances, different evaporation temperatures are used. Temperature is electronically controlled using a metallic thermocouple.

Table 1 shows the approximate evaporation temperature, needed for about 1 Å/s flow, of each substance in the cell.

	ZnPc	C_{60}	BCP	Al electrode
Temperature [°C]	480	550	200	1250

Table 1. Approximate UHV-evaporation temperatures needed for about 1 Å/s flow of the substances, used in organic solar cell production

The ITO substrates are placed in a substrate holder with evaporation mask, having space for 4 samples. The evaporation mask has two positions – for the organics and Al electrodes, between which the switching is done in-situ using a mask changer shaft. The substrate holder is then placed in a rotating head, so that it turns with a defined speed at all times during evaporation. This ensures homogenous growth of the deposited layer. The rotating head is equipped with a heater, so substrates can be heated up to 200 degrees if needed.

Next to the rotating head, quartz crystal deposition controllers (QCDC) are situated. Their function is to monitor the thickness of the layer deposited for each substance and the deposition speed. More on the calibration of QCDC will be said in 3.4.

One evaporation of a complete cell takes approximately one hour, having in mind that the ovens are being kept at parking temperatures. Only for evaporation they are heated to working temperature, which takes time if one does not want to exceed the working temperature by much and partially decompose the substance in the oven. If this happens, then the chemicals are contaminated and have to be renewed, in order to retain reproducibility of the results. For ZnPc and C_{60} the parking temperatures are 200°C, for BCP - 100°C and for Al - 700°C.

After all layer evaporation, the complete cell is transferred through the lock chamber to a glove box. There under nitrogen gas each cell is being securely protected, from atmosphere and humidity, in a specially prepared plexiglas encapsulation. In this form the cells can be taken out of the glove box and their I/V characteristics measured under a sun simulator. In encapsulated state, degradation of the cells takes place in about 5-6 hours.

2.8 Electrical characterization of solar cells

The most widely used method for solar cell characterization is the current-voltage characteristic of the cells, or the so called I/V measurement. It provides very important electrical properties of the cell, from which one can judge how the cell parameters have to be further changed, in order to achieve higher efficiency in sun-light harvesting. The I/V characteristic is influenced by the conductivity of materials and interfaces, exciton or charge carrier diffusion lengths, traps and recombination.

The most important parameter for evaluation of the performance of a solar cell is the efficiency (η). It is defined as the ratio of the maximal electrical power (P_{max}), the cell produces, to the light power received from it (P_{light}):

$$\eta = \frac{P_{max}}{P_{light}}$$

Solar cells are practically diodes, on the contacts of which, under illumination a potential difference could be detected. If the electrical circuit is closed with a resistance, current will flow. The measurement of their I/V characteristics is done the following way: during illumination, a voltage is applied on the electrodes of the cell and the flowing current is measured. The current is divided by the exact cell surface, thus normalized to $1\,cm^2$, for easier comparison of the results. After normalization the current I (in volts), is referred to, as J (in A/cm^2). A typical I/V curve is shown in Figure 7.
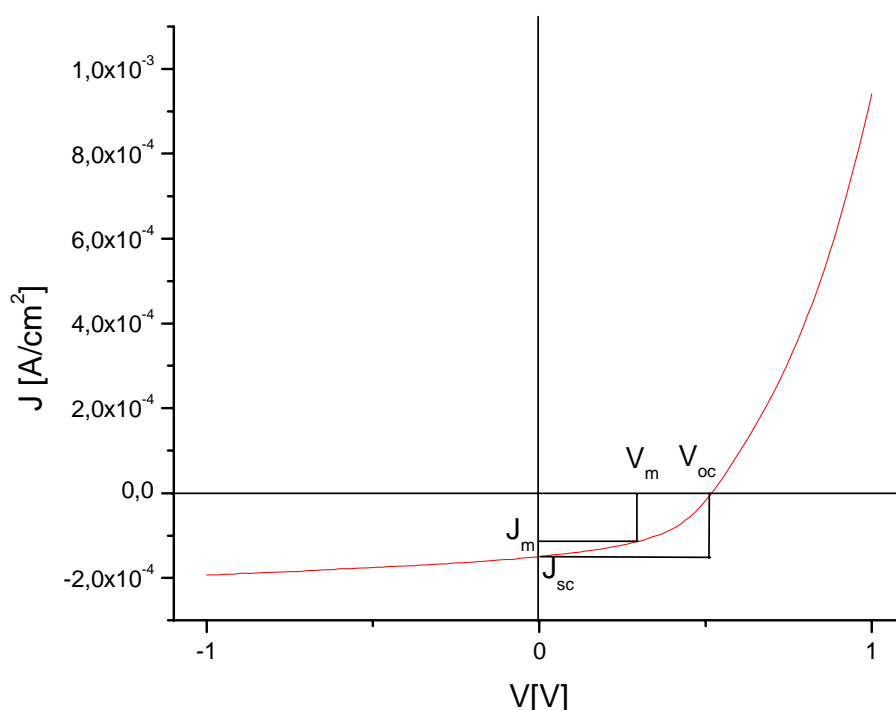
Figure 7. A typical Current/Voltage characteristic for a solar cell.
The clue points are: V_{oc} – open circuit voltage, J_{sc} – short circuit current, V_m – voltage at the point
of maximal cell power, J_m – current at the point of maximal cell power

The electrical power of the cell is the product of current and voltage. At one point of the I/V curve the electrical power has a maximum. This is the point with current and voltage marked as J_m and V_m, respectively. Exactly their product gives P_{max} of the cell.

On the I/V curve there are two other important points V_{oc} and J_{sc}. J_{sc} is called short circuit current and is the point where the curve cuts the Y axis. There the applied external voltage turns zero i.e. changes direction. In this point the measured current is entirely the current yielded by the solar cell if its electrodes were short-circuited (from there "sc").

The second clue point, the open circuit voltage (V_{oc}) is the intersection of the I/V curve with the X axis. There the applied external voltage is exactly equal to the internal voltage of the cell, so no current will flow. These points are the maximal current, respectively voltage that the cell can deliver. In the ideal diode case their product would give the maximal power of the cell, but in reality one more factor is induced: Fill Factor (FF):

$$FF = \frac{I_m . V_m}{I_{sc} . V_{oc}}$$

The fill Factor shows how strong the form of the I/V curve deflects from the curve form of an ideal diode.

The power conversion efficiency of the cell is being calculated using the following equation:

$$\eta[\%] = \frac{FF . I_{sc} V_{oc}}{P_{light}} . 100$$

If a solar cell is represented with a replacement circuit (Figure 8) [30] then the I/V curve can be fitted with the following formula [31,32]:

$$I = \frac{I_L - \dfrac{V}{R_P}}{1 + \dfrac{R_S}{R_P}} - \frac{I_0}{1 + \dfrac{R_S}{R_P}} . (e^{\frac{V - I \cdot R_S}{nkT/q}} - 1)$$

where I is the measured current; I_L – current generated from the cell under illumination; I_0 – reverse current;

This way, two more characteristics could be extracted from the I/V curve. These are the cell's parallel (R_p) and serial resistance (R_s). The parallel resistance is mainly the slope of the curve in the range around 0V (3rd and 4th quadrant). At lower R_p the open circuit voltage drops, while I_{sc} stays the same.
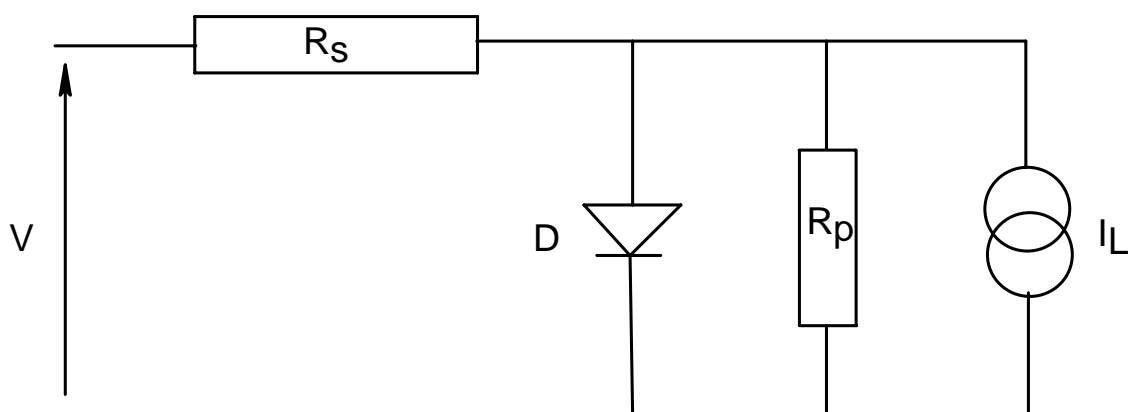
Figure 8. Simplified replacement circuit, a schematic representation of a solar cell.

The serial resistance defines the slope of the I/V curve in 1st quadrant i.e. in the range above the V_{oc} (transmitting direction of diode). Bigger R_s influences the FF and I_{sc} while the V_{oc} stays intact.

So as described the I/V measurement of a cell gives us very useful information about the cell and its internal contact interfaces. That is why every single cell modification described in the present work is accompanied by an I/V curve.

2.9 X-ray reflection [33]

With x-ray reflection, in the present work, layer thickness and structure profile measurements were conducted. A complex method with high requirements, the x-ray reflection provides almost angstrom exact layer thickness measurements. The theory, necessary for understanding the x-ray reflection measurement results in this dissertation, is described here.

In any scattering or reflectivity measurement it is important to distinguish between species of interest and the surrounding medium. This can be represented as a variation in the refractive index **n.** It can be written:

$$n = 1 - \delta + i\beta$$

where δ is the real part of the refractive index and β is the imaginary component which accounts for absorption. For x-rays:

$$\delta = \frac{\lambda^2 \rho_{el} r_0}{2\pi} \text{ and } \beta = \frac{\mu\lambda}{4\pi}$$

where λ is the x-ray wavelength ($\lambda \sim 1,5$ Å), ρ_{el} the electron density, r_0 the classical electron radius ($2,82.10^{-13}$ cm) and μ the linear absorption coefficient. β depends on the interaction of the incident photons with the electrons in the sample. Experimentally, it is the total absorption cross-section that is of importance. Therefore a strongly scattering sample or a sample with large incoherent scattering cross-section will effectively attenuate the radiation as well. In the calculation of reflectivity this has to be taken into account in β.

For x-rays, contrast or differences in the refractive index, can arise from variations in the mass density. The contrast is provided by the presence of higher atomic number elements, where the number of electrons per unit volume can be large.

In vacuum, the component of the wave vector normal to the surface is given by:

$$Q_{z,0} = \frac{2\pi}{\lambda}\sin\theta$$

where θ is the grazing incidence angle. The subscript z denotes the direction normal to the surface of the film and the subscript 0 denotes vacuum. If the reflected x-rays are measured at an angle equal to the incidence angle, the diffraction vector is oriented normal to the surface, i.e. in the z direction. In a medium with an x-ray scattering length density $\rho^s = \rho_{el} r_0$, the scattering vector in the medium is modified such that:

$$Q_{z,i} = \sqrt{Q_{z,0} - 4\pi\rho^s} = \sqrt{Q_{z,0}^2 - Q_c^2}$$

where Q_c is the critical scattering vector, which is given by $Q_c = \sqrt{2\delta}$.

It is the change of the scattering vector from one medium to another, that rises reflectivity. This may occur at an interface between two dissimilar materials or from a continuous change in the scattering length density. In either case, a gradient in the scattering length density is required to reflect the radiation. The reflection coefficient at an interface between two media, i and $i+1$ is given by:

$$r_{i,i+1} = \frac{Q_{z,i} - Q_{z,i+1}}{Q_{z,i} + Q_{z,i+1}}$$

The reflectivity is then given by: $R = r^* r$, where $r*$ is the complex conjugate for r.

In the case of a substrate with a film on it, having a thickness d and uniform scattering length density, there are two step changes in the reflection coefficients, at the air/film and film/substrate interfaces, separated by a distance d. The reflection coefficient of the sample, in terms of the reflection coefficients at the substrate/sample interface $r_{1,2}$ and at the sample/air interface, $r_{0,1}$ can be written as:

$$r = \frac{r_{0,1} + r_{1,2}\exp(2iQ_{z,1}d)}{1 + r_{0,1}r_{1,2}\exp(2iQ_{z,1}d)}$$

The reflectivity can be shown to be:

$$R(Q_{z,0}) = \frac{r_{0,1}^2 + r_{1,2}^2 + 2r_{0,1}r_{1,2}\cos(2Q_{z,1}d)}{1 + r_{0,1}^2 r_{1,2}^2 + 2r_{0,1}r_{1,2}\cos(2Q_{z,1}d)}$$

From the last equation it is seen, that for a single film, the reflectivity profile as a function of $Q_{z,0}$ will contain oscillations, that are a characteristic of the total film thickness. The "exact" film thickness is given by $\pi/\Delta Q_{z,1}$, where $\Delta Q_{z,1}$ is the distance between two oscillation peak maxima and it can be easily extracted from the R(Q) plot.

2.10 Ellipsometry [34,35,36]

Ellipsometry measures the change in polarization state of light, reflected from the surface of a sample. The measured quantities in ellipsometry are Ψ and Δ, which are related to the ratio of the Fresnel reflection coefficients r_p and r_s for parallel (index p) and perpendicular (index s) to the plane of incidence polarized light, the following way:

$$\rho = \frac{r_p}{r_s} = \tan\Psi e^{i\Delta}$$

where ρ is the complex reflectance ratio.

There are two independent parameters (Ψ and Δ) for each measurement, which can allow the determination of material properties, with the addition of tighter constraints on the results. Both terms, measured in ellipsometry, relate to a ratio of two values, which make ellipsometry measurements insensitive to fluctuating light intensity, electronic drift, or scattered light loss. In addition, the phase quantity 'Δ' provides excellent sensitivity to the presence of very thin films. For these reasons, ellipsometers can be very accurate and highly reproducible.

Since Ψ and Δ are functions of the complex refractive index: $\tilde{n} = n + ik$ (n is the refractive index and k the extinction coefficient) they do not directly provide information on the measured film. In order to extract the information contained in the ellipsometric spectra a model describing the structure of the sample and its optical response is usually applied. Only after these fit to a model, the refractive index and film thickness can then be determined.

In a fitting procedure of the experimental spectra, by a variation of the parameters contained in different models, the "Mean Square Error" (MSE) is used, as measure for the deviation between measured values and modeled data.

$$\text{MSE} = \sqrt{\frac{1}{2N-M} \sum_{i=1}^{N} \left[\left(\frac{\Psi_i^{\text{mod}} - \Psi_i^{\text{exp}}}{\sigma_{\Psi,i}^{\text{exp}}} \right)^2 + \left(\frac{\Delta_i^{\text{mod}} - \Delta_i^{\text{exp}}}{\sigma_{\Delta,i}^{\text{exp}}} \right)^2 \right]}$$

Here N is the number of experimental (Ψ, Δ) pairs, M is the number of variable parameters in the model and σ is the standard deviation on the experimental data points.

Ellipsometry measurements are typically performed at oblique angles near the Brewster condition. This provides the highest sensitivity to material properties, such as refractive index and film thickness. The Brewster condition is different for each sample and also changes over the spectral range. Thus, variable angle of incidence allows the measurement to be optimized for each data point.

Variable angle of incidence also allows measurements at multiple angles. Each new angle will change the path-length of the light traveling through the materials. This can be very beneficial for multi-layers, as different path lengths often lead to new information about the structure. Multiple angles are helpful to improve the confidence in results.

For measurement accuracy an AutoRetarder is used. The AutoRetarder consists of a computer-controlled MgF_2 Berek waveplate, which forms a compensator in the optical path. It is used to improve measurement of the phase quantity 'Δ', which can be unambiguously determined over its full range of 360°. The AutoRetarder can also distinguish unpolarized light from circularly polarized light. This is very useful for quantifying the measurement and sample effects. Depolarization of the light beam can be caused from a non-uniform film, backside reflections from a transparent substrate, spatial incoherence of a patterened film, or from the spectral resolution. A spectral measurement of depolarization can help quantify these effects.

2.11 Kelvin Probe Force Microscopy (KPFM) [37,38]

Kelvin probe force microscopy (KPFM) is a powerful technique, used to measure surface topology and contact potential variations, with an atomic force microscope (AFM), on a nanometer scale. Preparation and examination of the surfaces is done in ultrahigh vacuum (UHV). Lateral resolution of the method is ca. 10 nm and vertical resolution is 1 nm. Laser λ is 675 nm.

KPFM is a non-contact AFM operation mode in which the electrostatic interaction is minimized by application of an appropriate bias voltage during topographic imaging. For metals this voltage corresponds to the local work function difference, between sample and tip contact potential difference, whereas for insulators it gives information about the surface charge. The use of KPFM offers the advantage that not only the true topography is recorded, but also a map of the surface potential distribution is acquired.

3 Results and discussion

3.1 Studies on ITO

Transparent conducting oxides (TCOs) are materials, widely used for electrodes in photovoltaic (PV) devices [**39**]. Materials with varying properties (conductivity, work function, transparency, etc.) exist [**40**]. It is vital to understand and be able to control these properties, so that the desired functionality in a TCO-based PV device is achieved.

3.1.1 Scanning Electron Microscopy

An important approach in the research of a nano-device like the organic solar cells is to be able to actually "see" into it. Thus its structures and construction can be observed on a nano-scale. This becomes possible by using the so called Scanning Electron Microscope (**SEM**). Its functioning principle can be simplified to shooting focused electrons with defined energy on the surface of an object, collecting the back scattered and secondary ones and visualizing their intensity in a space resolved manner on a monitor. This way one gets a two dimensional monochromatic image, due to the darker-lighter coloring of different conductive spots. The information that is to be seen in a SEM image is the ability of particular spots on the examined surface to give electrons.

Our ITO was examined with SEM. The resulting images are shown on Figure 9 and Figure 10.
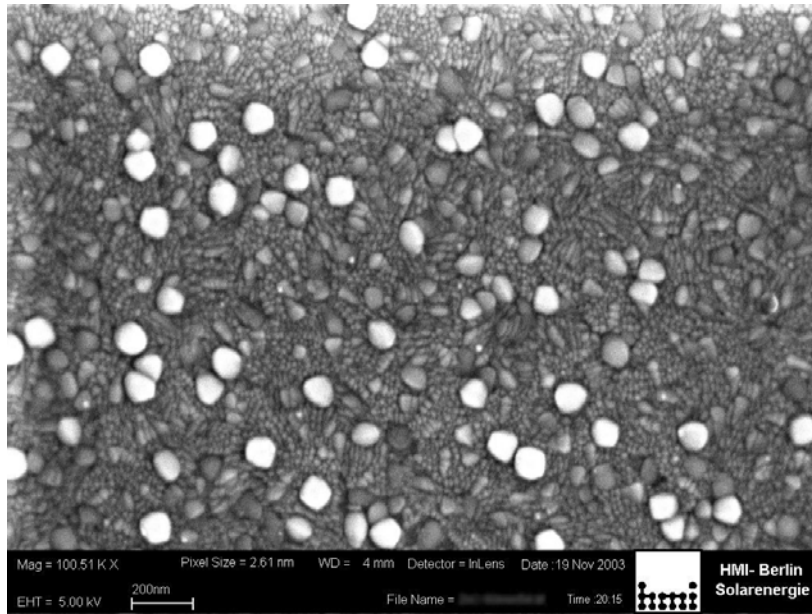
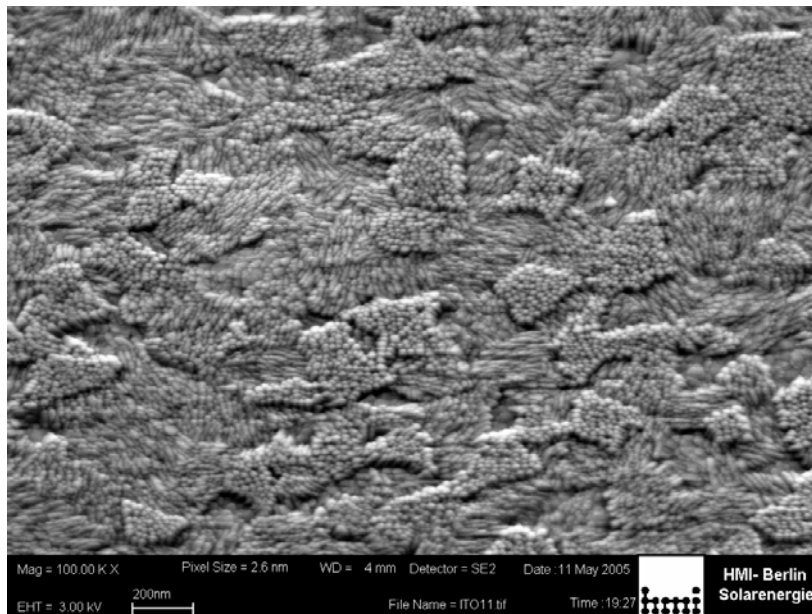**Figure 9. SEM image of our previously used ITO**

Figure 10. SEM image of our currently used 5 Ω ITO

The ITO shown on Figure 9 is a 10 Ω sample used by us in our early experiments. Here it is shown because an electrodeposition experiment in the current work was conducted exactly on such a sample. This SEM image shows that the majority of the

surface consists of smaller crystallites with size about 10-15 nm, which are relatively flat. There are also bigger islands about 70-100 nm to be seen. Exactly these big crystallites constitute the danger of getting a shortcut through the cell, when the altogether thickness between the contacts is: ZnPc + C60 + BCP = 30 + 30 + 17 = 77 nm. Using PEDOT:PSS, a thick film on the surface is created, thus making it less rough and modifying its work function (more on work function in 0) [41]. To avoid working with such rough and inhomogeneous ITO surface we started using another kind of ITO – the 5 Ω (Figure 10). Another reason is of course purely electrical – the lower the electrical resistance of the ITO layer, the higher the currents which can flow. ITO with different resistances will be discussed more detailed in 3.1.2.

The 5 Ω ITO on the contrary has only small crystallites, again about 10-15 nm, organized in bigger 200-300 nm domains. It's roughness as the figure shows is very low and homogeneous.
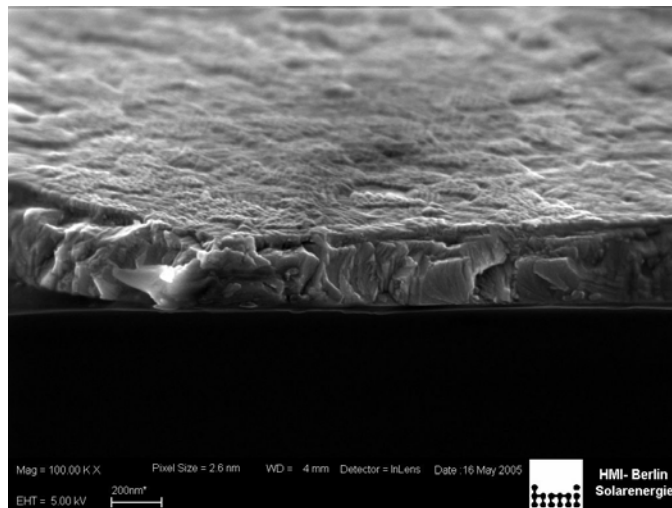
Figure 11. SEM side look at a broken edge of 5 Ω ITO

This morphology allows thinner or even monolayer passivations to be used and still have no shortcuts. A look from the side on a broken edge (Figure 11) of this 5 Ω ITO-glass sample proves this. It also shows the structure of the bulk beneath the surface. It is a homogenous material, without cavities. Interesting is that the grain structure of the surface is not the building block of the volume. On the contrary the bulk has a solid, flake-like structure, possibly due to different, from the surface material, sputtering conditions. The overall ITO thickness of this sample can be roughly estimated, from the image, to about 300 nm.

3.1.2 Different ITO types by resistance

Another parameter of a TCO layer is its sheet resistance. The resistance "R" of a semiconductor rectangular block with resistivity "ρ", length "L" and cross section "A" is given by the formula: $R = \rho.\dfrac{L}{A}$. If "B" is the width of the sample and "C" is its thickness then $A = B.C$. So the formula for the resistance could be modified: $R = \dfrac{\rho}{C}.\dfrac{L}{B}$. The sheet resistance is defined as material resistivity divided to the layer thickness $R_s = \dfrac{\rho}{C}$. Strictly speaking, the unit for sheet resistance is Ohms (since L/B is unitless), but one refers to it as being in Ohms per square to avoid confusion between R and R_s.

For TCO semiconductor layers with thicknesses less than 0,5 micron the dependence between thickness and sheet resistance is very strong. For example ITO on glass samples from our provider, the company PGO GmbH, had the following properties (Table 2):

ITO type	R_S (statistically measured) [Ω/square]	Typical thickness [nm]
CEC005	4,5	310
CEC007P	6	260
CEC010	8,5	180
CEC020	15	100
CEC030P	24	65
CEC050	40	40
CEC100	80	23
CEC120S	100	21

Table 2. Standard square resistances / ITO film thicknesses (PGO GmbH website) [42]
In the present work mainly CEC005 is used
and only the electro-codeposition study (3.5.3) is done on CEC010 ITO type

So to diminish the R_S by factor 2, one needs to about double the thickness. The problem here comes from the fact that, by increasing the overall thickness of the TCO layer one also increases the quantity of light absorbed in it. For example in four cases for the ITO-types 5s, 10p, 20s, 50s the company PGO GmbH gives the transmissions shown in Figure 12. It is obvious that in direction of increasing the resistance and decreasing the layer thickness the optical absorption also decreases.

CEC005

CEC010

CEC020

CEC050

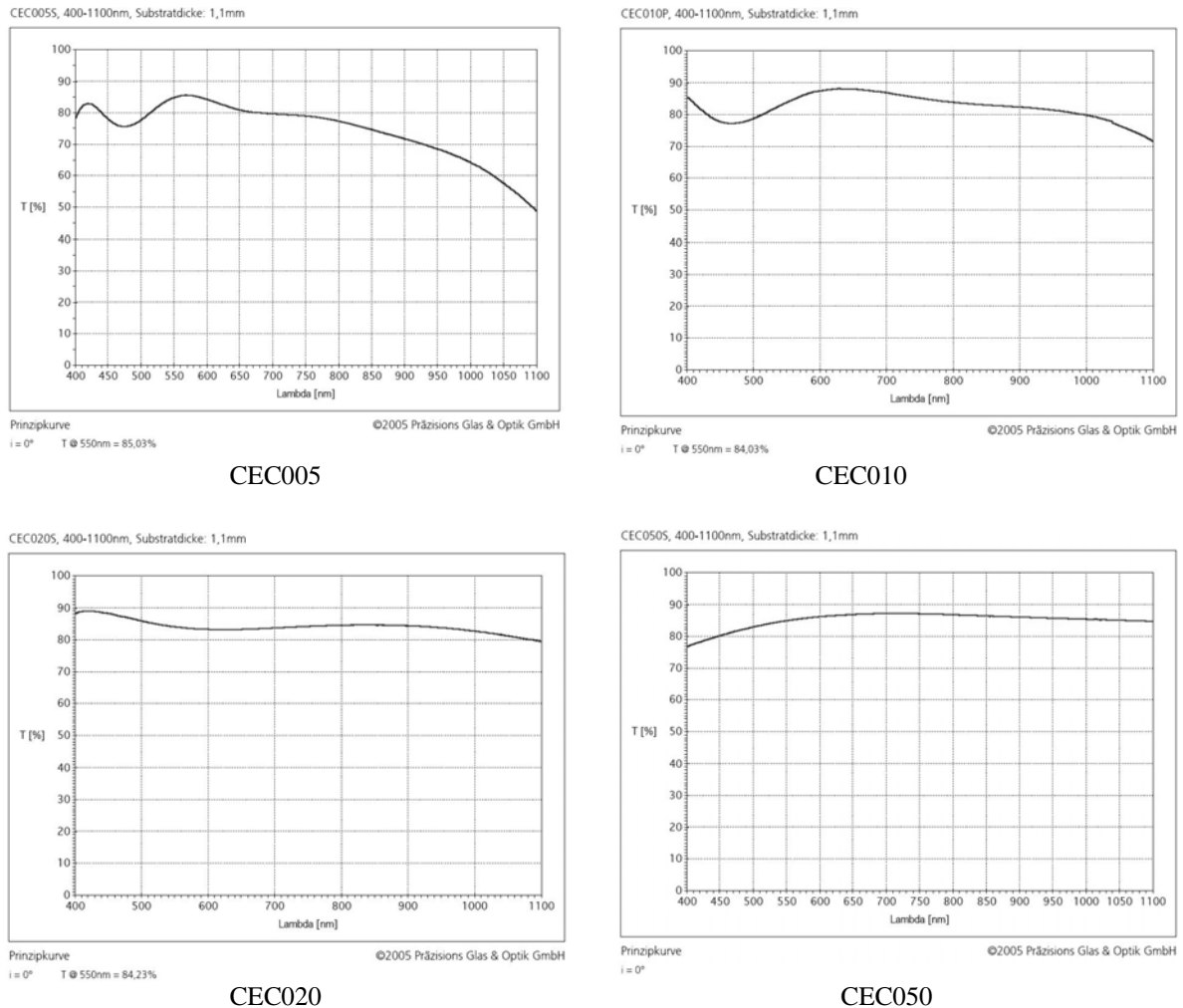**Figure 12. Optical transmissions of 5, 10, 20 and 50 Ω/□ ITO-glasses,
ordered by incrementing resistance** [42]

These four different kinds of ITO we tested in a complete solar cell. Conducting the evaporation of the active layers on these four substrates on the same sample holder assured the same conditions and layer thicknesses for all the cells. The result corresponds to what we expected and is shown on Figure 13.
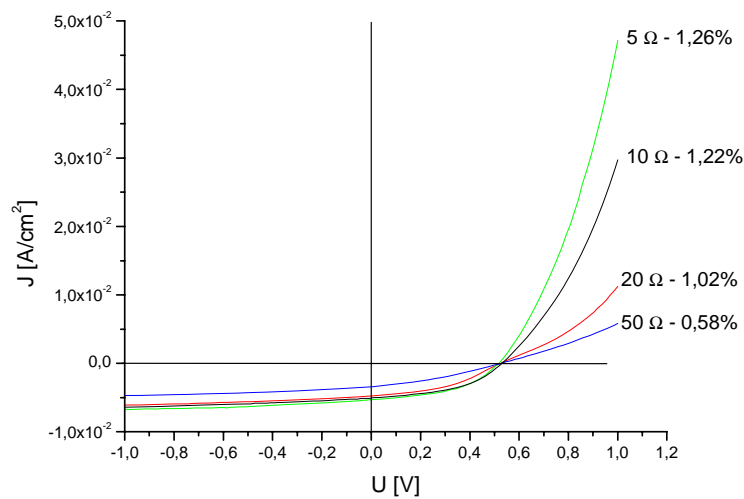
Figure 13. I/V curves of standard cell on ITO substrates with different resistances and their corresponding efficiencies in %

This result clearly shows that the effect on power conversion efficiency from conductivity gain is stronger than that of optical transmission loss.

3.1.3 Annealing/Resistance

Another factor with strong influence on the cell properties is the substrate temperature during the vacuum evaporation of the active layers [**43**]. That is why a temperature test of the TCO substrate was conducted. To see how ITO electrode behaves at higher temperatures, a sample with contacts connected to an ohm-meter, was placed in an oven and heated up to 350°C in steps of 50°C. The plotted graph of resistance vs. temperature, measured in-situ is shown in Figure 14.
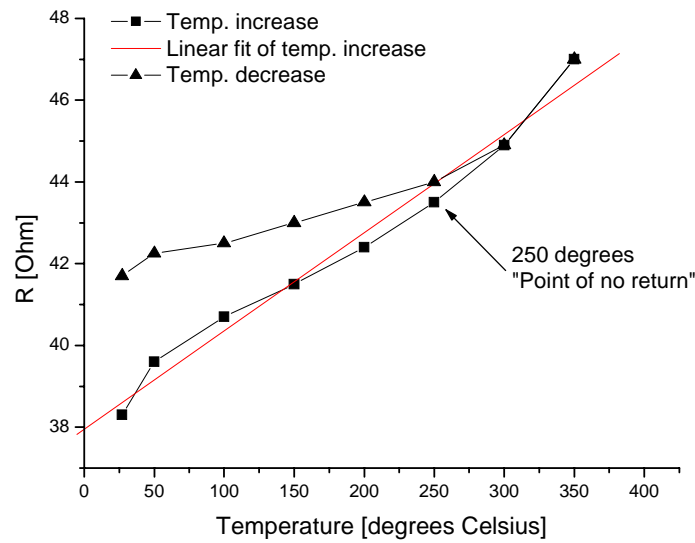
Figure 14. ITO – temperature dependence of its resistance (not sheet resistance)

The dependence of the parameters is almost linear up to 350°C, as expected. Though, the sample can be annealed only up to 250 degrees without making irreversible changes. If annealed to 250 and cooled ITO retains its initial resistance. Heated higher than 250°C there already is some obvious change, which affects the resistance also while cooling (dataset marked with triangles). At the end, already at room temperature the sample has changed and instead of its initial 38,3 Ω it shows 41,7 Ω between the contacts. From this experiment we conclude that the temperature of the substrate should never exceed 250°C [43].

3.1.4 Work function - KPFM, XPS

One of the most important properties of a TCO, which also influences the choice when starting new device architecture, is its surface work function. A crucial point in an organic PV device is the interface between the inorganic TCO and the first organic layer [**44**]. Schottky barrier, bad charge transfer, recombination at defects are some of the problems which might occur. That is why, studying the surface work function is important, if one wants to fit the TCO to the needs of the specific task.

As already mentioned (in 1.3) in the scientific literature there are very different opinions concerning the ITO work function value. We measured it using Kelvin Probe Force Microscopy (KPFM) and X-Ray Photoelectron Spectroscopy (XPS) and the results were in good agreement. KPFM as a method could be simply described as an Atomic Force Microscope (AFM), which can also measure the contact potential of the monitored surface. From the contact potential the work function is calculated using the formula: $\Phi = \left(4,5 - CP_{CL}\right) + CP_{Sub}$, where CP_{CL} is the contact potential of the KPFM cantilever and CP_{Sub} is the contact potential of the substrate. The value 4,5 comes from the calibration of the cantilever.

The KPFM image is shown on Figure 15. As standard the sample was heated up to 130°C in high vacuum to remove water adsorbed on the surface and measured after that. If some change in ITO during this heat treatment happened this method cannot tell.
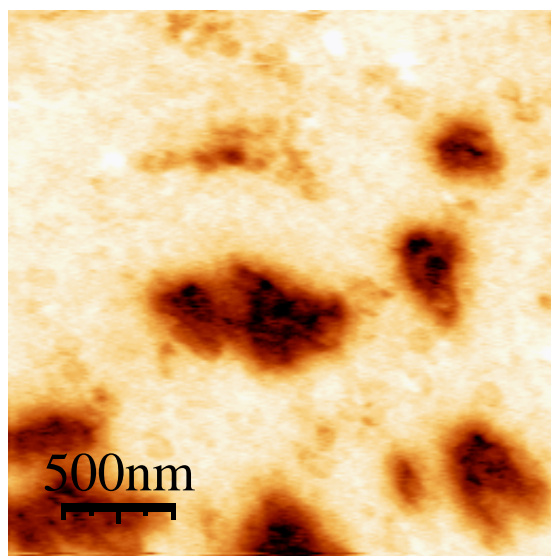
Figure 15. KPFM image of the work function distribution on the clean ITO surface[1];
measured in dark, after annealing in UHV at 130°C, 30min;
darker spots indicate lower values, brighter areas – higher values

The minimal value measured is 3,56 eV and the maximal 4,48 eV. The mean work function value is found at 4,3 eV. What one also sees, is that the distribution is very uneven and big spots of low work function areas are present.

The other method for measuring surface work function, namely XPS, determines the value on a bigger scale thus the result is a mean value of the entire measured area. The work function value calculated from the XPS measurement is 4,2, which is in good agreement with the one measured by KPFM. We now assume this value for a clean and untreated ITO in all our further comparisons and diagrams.

---

[1] Measurement: N. Barreau, HMI

3.2 Active layers stability tests – FTIR

The problem with the degradation of organic photovoltaic devices was already discussed in 1.4. There it was also mentioned that one hypothetical route to degradation is the UV activation of the substance of the active layers, thus allowing diffusing oxygen to chemically destroy them and their initial properties. We studied this possible way of degradation with Fourier Transform Infra-Red spectroscopy (FTIR). Measurements were conducted on a BRUKER FTIR spectrometer.

At first IR spectra of the pure ZnPc and C_{60} in a KBr pill were recorded. Then powder samples of the pure substances were exposed to UV light under a 150 W Xenon-Arc lamp (ORIEL Instruments) for 12 hours. After this the IR spectra in KBr were measured again and compared with the ones before UV exposure. Differences in the spectra, before and after UV treatment, were expected, because of changed chemistry. All substances were exposed to air all the time. The spectrum of BCP was taken basically to be compared with a reference spectrum from literature, to verify if the substance is identical and free from contaminants. The results are shown on the following figures (Figure 16 to Figure 19):

Figure 16. FTIR spectra of ZnPc in KBr before (black) and after (red) 12h UV light treatment of the substance in powder form. Shown is only the fingerprint range. Absorbance of both spectra is normalized for comparison purpose. Differences are observed only in absorbance, but not in peak position. Peak disappearance around 500 cm^{-1} is attributed to compensation problem
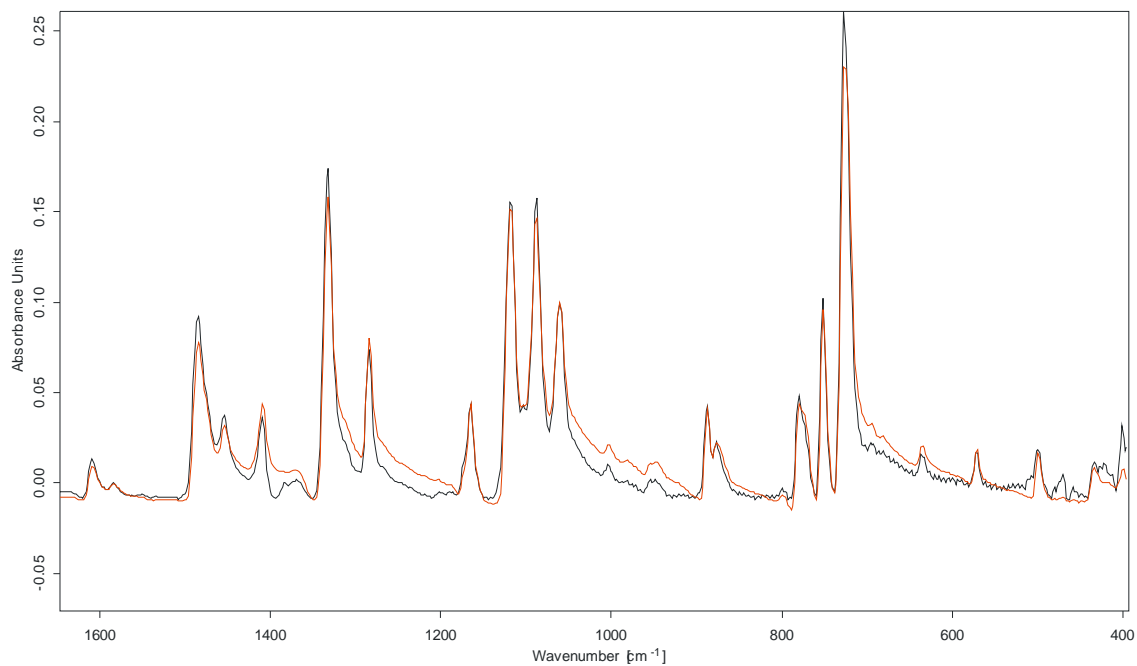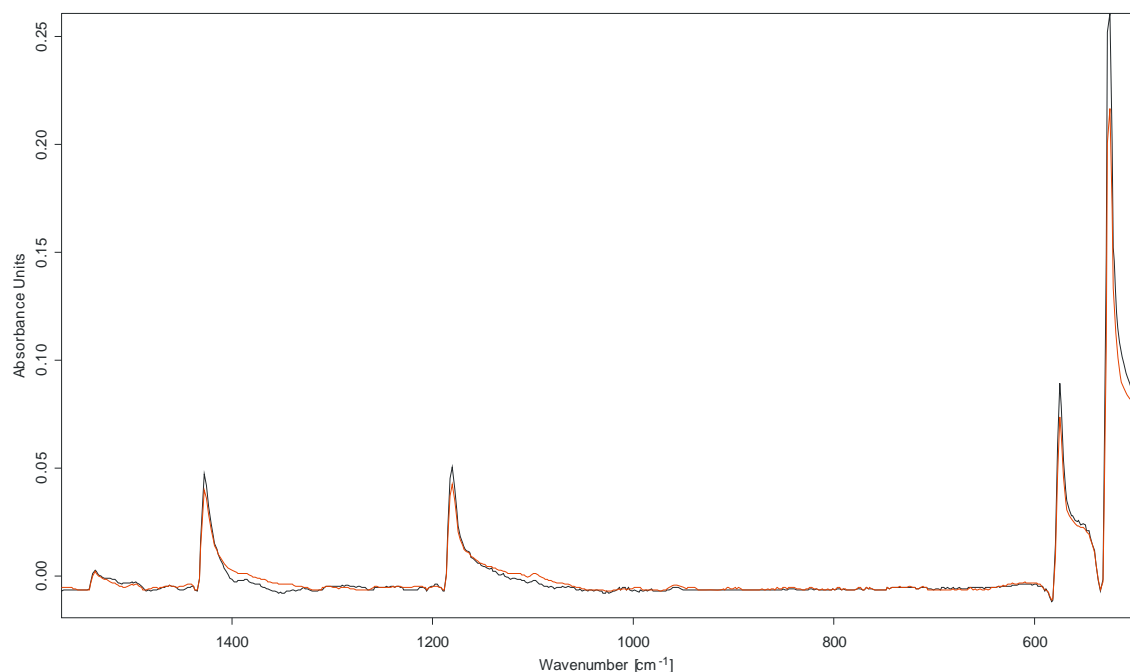

Figure 17. FTIR spectra of C_{60} in KBr before (black) and after (red) 12h UV light treatment of the substance in powder form. Absorbance of both spectra is normalized for comparison purpose. As with ZnPc, differences in C_{60} spectra are observed only in absorbance, but not in peak position or number of peaks. This is a hint for stable chemistry
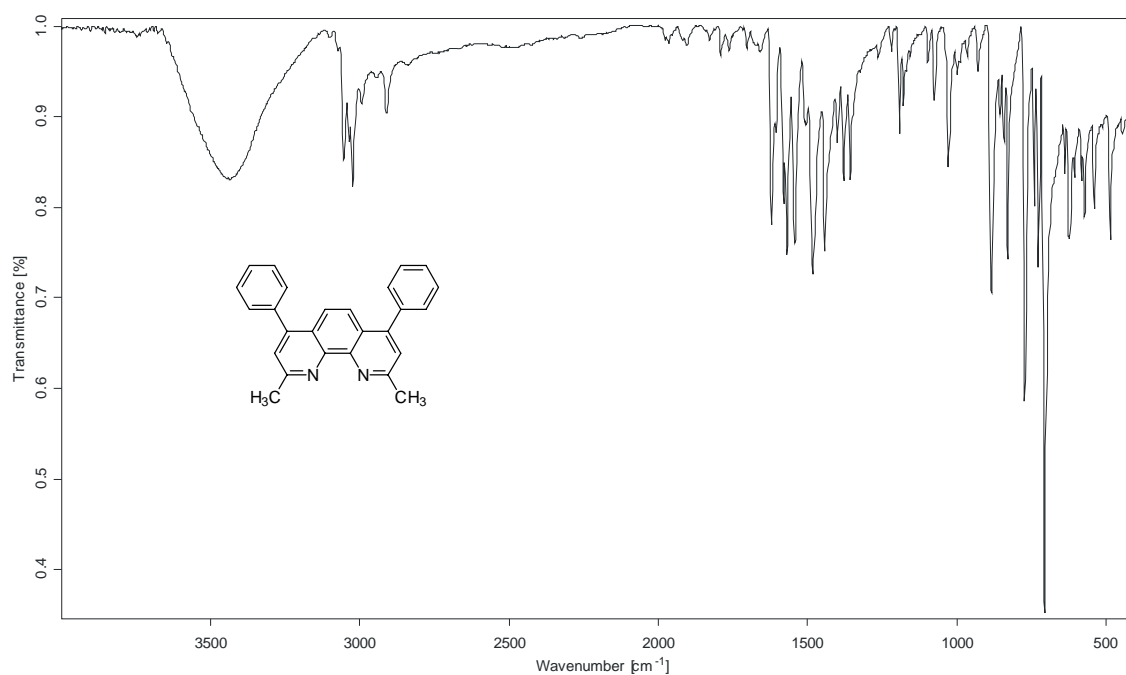
Figure 18. FTIR transmittance Spectrum of BCP in KBr

HIT-NO=5888 | SCORE= ( ) | SDBS-NO=11056 | IR-NIDA-51573 : KBR DISC
2,9-DIMETHYL-4,7-DIPHENYL-1,10-PHENANTHROLINE

$C_{26}H_{20}N_2$

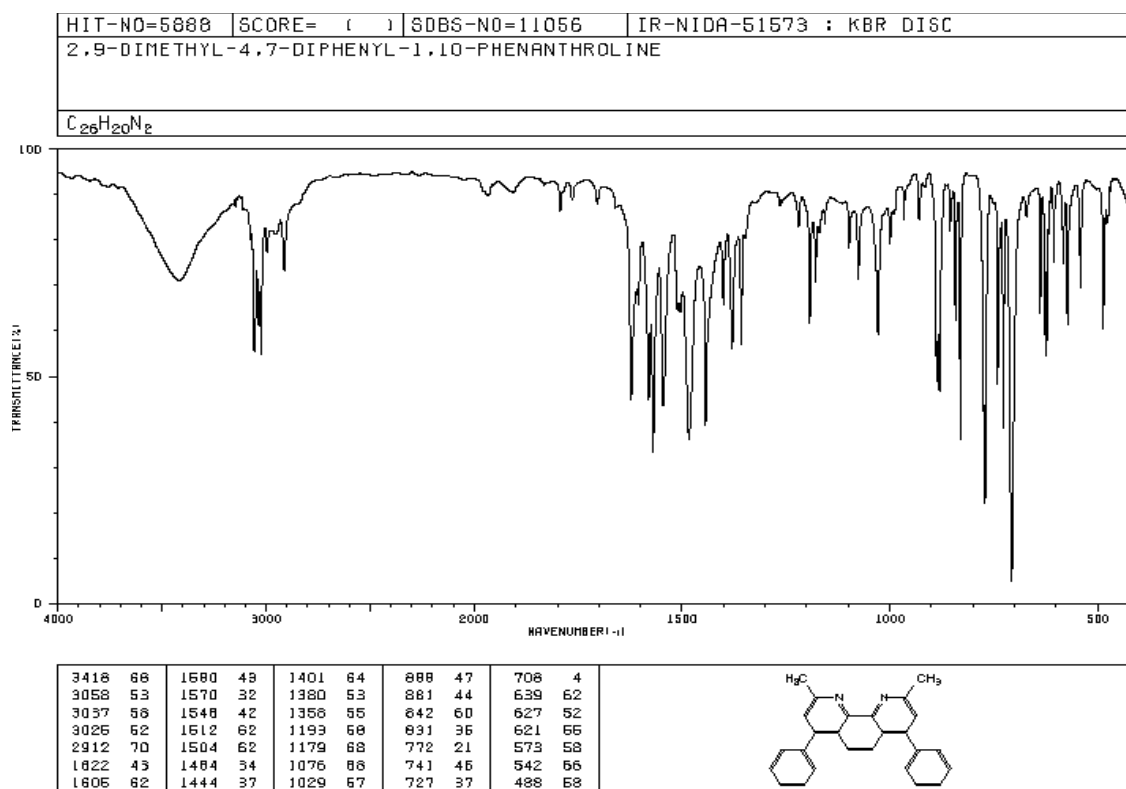|									
3418	68	1580	49	1401	64	888	47	708	4
3058	53	1570	32	1380	53	881	44	639	62
3037	56	1548	42	1358	55	842	60	627	52
3026	62	1512	62	1193	68	831	36	621	55
2912	70	1504	62	1179	68	772	21	573	58
1622	43	1484	34	1076	68	741	46	542	66
1606	62	1444	37	1029	57	727	37	488	68

Figure 19. FTIR transmittance spectrum of BCP from Spectral Database for Organic Compounds SDBS; x-axis has two different scales, before and after 2000 cm^{-1}

It is astonishing that on the spectra of both ZnPc and C60, before and after UV light treatment in air, there is no noticeable new peaks to observe. The only dissimilarities between the spectra are compensation problems (water contents in sample, different vacuum quality during measurements). The reason, for these matching spectra, may lie in the fact that the substances were in powder form during the UV treatment. Possibly the chemistry could have changed only on the surface of the powder particles. This would be a very small quantity of material and its IR signal could be easily suppressed by the peaks of the bulk material. The method sensitivity lies beyond one percent, but since the initial material purity is ca. 99%, it can be concluded that no additional impurity was detected.

The IR spectrum of BCP is in good agreement with the reference one from literature.

The material stability shown by this study does not explain the cause of cell degradation. It can only be hypothesized about the degradation background and cause. It is possible that the separate substances show stability, which after bringing them in contact changes. Probably in contact the reaching of thermodynamic equilibrium destabilizes the molecules, thus making them vulnerable to aggressive gas radicals, created by the UV irradiation. The cell degradation in encapsulated state is a suggestion that the radicals could be emitted from the ITO, which is a non-stoichiometric metal oxide and can contain excessive amounts of oxygen.

3.3 *UV-VIS Spectroscopy of cell layers and computer simulation*

In 1.2 our cell architecture was described, as practically optimized i.e. the thickness of the active layers in the cells was changed, until an optimum in efficiency was reached, using the trial and error principle. This way a good starting efficiency was reached, from where all optimizations of these organic PV devices began.

Although these devices worked fine, a theoretical backbone was somewhat missing. One did not know if the thickness of every layer was really the optimal or whether there could be a better optimized one. That is why a theoretical simulation of this PV device was required. More exactly, the phase distribution of different wavelengths of light in the cell was of interest. That means, where exactly the different wavelengths have their phase maxima in the cell.

A simulation of a multilayer solar cell is a complicated task. It is done by a computer program, where one feeds in data about every single layer's material – its refraction index "**n**" and extinction coefficient "**k**" over the interval of utilizable light wavelengths i.e. 350-850 nm (mostly visible light). **n** and **k** can not be obtained by any direct measurement. They have to be calculated from other spectroscopic data (see **Appendix A** for theoretical basis).

3.3.1 Practical measurement of R and T; n and k calculation

In order to determine the optical constants of Zn-phthalocyanine, C60 and Bathocuproine 50nm layers have been evaporated separately on a quartz substrate. The ITO was already sputtered on a glass substrate. According to the provider, PGO, the ITO had a layer thickness of 180 nm but the value, measured and used by us was 150 nm.

The reflection and transmittance of the samples have been determined with a "Cary 500Scan UV-Vis-NIR Spectrophotometer" in dependence of the wavelength. At first the clean substrate was measured and then the film evaporated on the substrate.

To make the data compatible to the "Optik"-program[2] and perform Kramer-Kronig calculations they must be formatted in a special way. At the beginning the optical constants **n** and **k** for the substrate must be calculated by the program. These constants must be written in a file used for determination of the constants of the thin films. Calculating the n- and k-values of the film follows in a second step.

From our measurements we obtained the data, shown on the following diagrams:
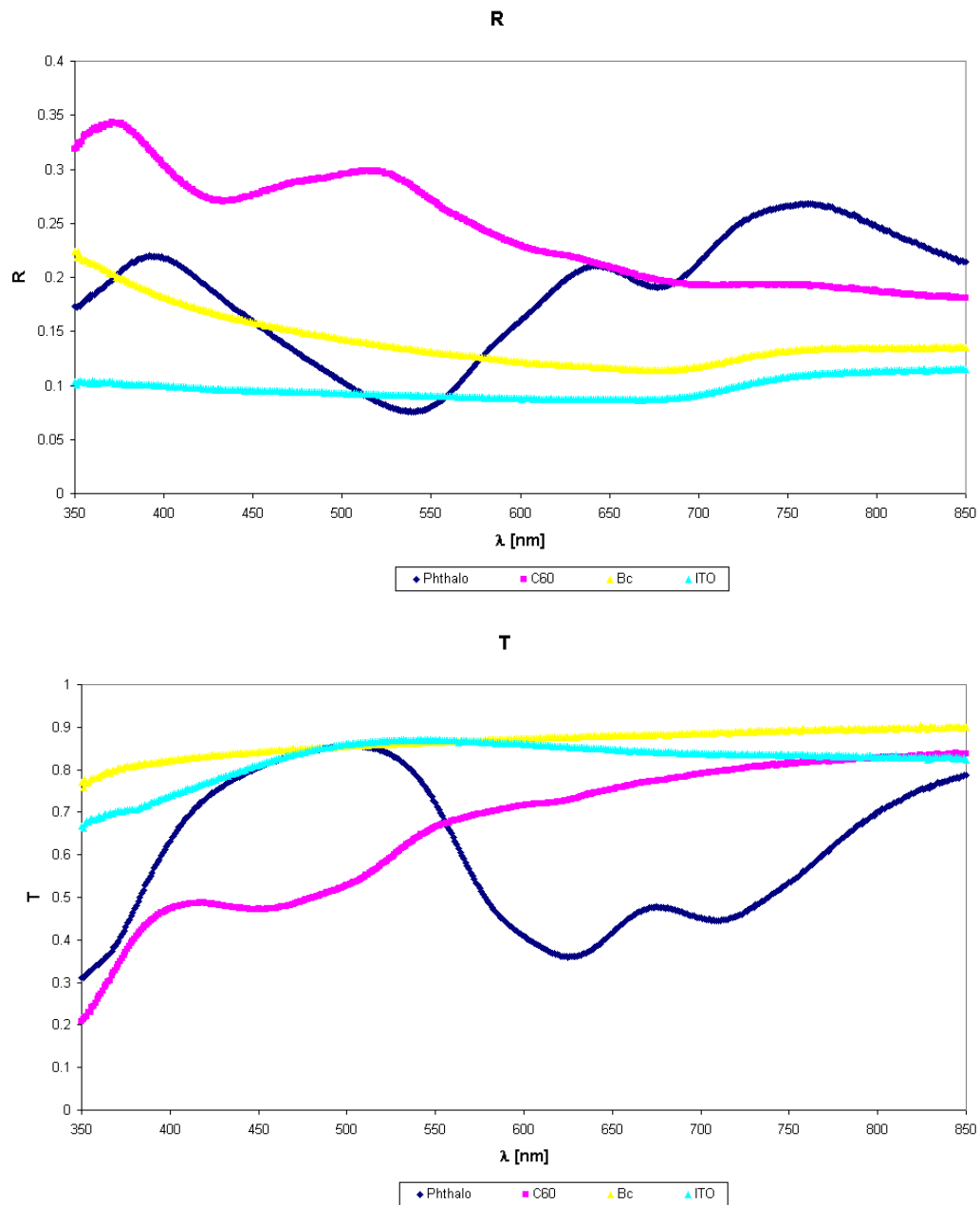

Figure 20. Reflection and transmission data, obtained from the spectroscopic measurements in reflectance (upper plot) and transmission (lower plot) geometry, in absorption units

---

[2] The program "Optik" is written by Kristian Peter

Calculations with the program "Optik" yielded the following results:
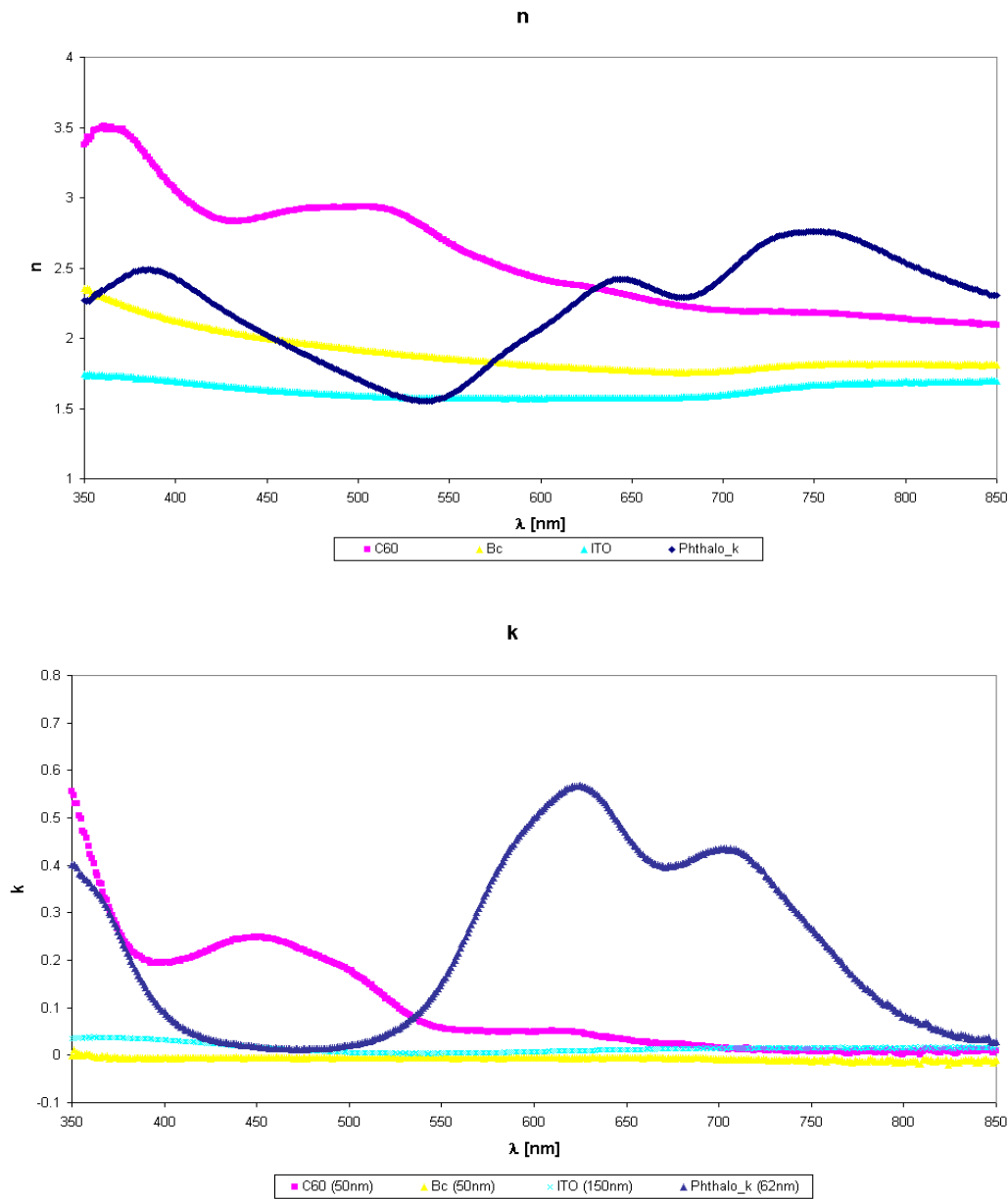
Figure 21. Plots of the calculated (with the "Optik" program) data for refraction index (upper plot) and extinction coefficient (lower plot). The values in brackets show the layer thicknesses evaporated on the substrate, measured with CARY and used for the calculation in the "Optik" program

For application in a solar cell it is especially important to know what optical absorption each material has. The absorption coefficient α is connected with the

extinction coefficient in the following relation: $\alpha = \dfrac{4\pi k}{\lambda}$. From this relation one can estimate the absorption from the diagram for k.

So in the k/λ diagram it is to observe that C_{60} has a relative absorption maximum at about 450 nm and at wavelengths bigger than 550 nm there is almost no absorption. ZnPc has two characteristic absorption maxima. One is around 625 nm and the second, not so intensive just above 700 nm. The absorptions of Bathocuproine and ITO are, as desired, very low. This way the absorption of the solar cell consists mainly of the absorption sum of the active layers ZnPc and C_{60} which almost do not overlap, but complement each other (see Figure 21; pink curve stays for C_{60} extinction and dark blue for ZnPc extinction; extinction is proportional to absorption). The combination of these two substances in a solar cell covers a big part of the solar spectrum (shown on Figure 22).
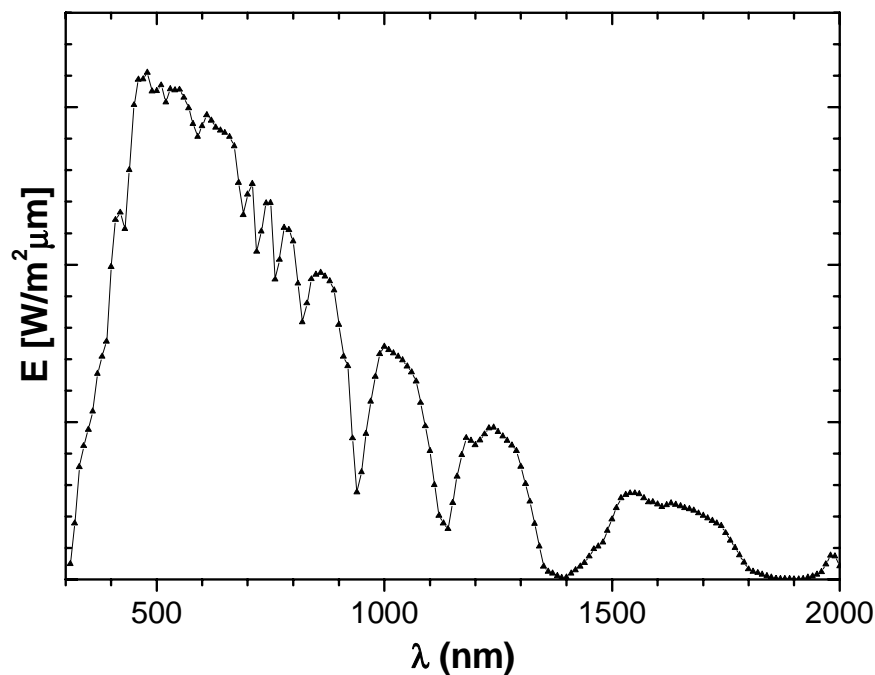
Figure 22. The AM 1.5 G solar energy spectrum [45]**.**
Its maximum lies at about 500 nm, where our cell has an absorption gap (above 550 nm)

The maximum of the solar spectrum lies at about 500 nm. There our cell has a gap in absorption. This value is just between the maxima of the absorptions of C_{60} and ZnPc, so there the cell absorbs very weak. There could be a possible improvement in

efficiency, if by any means, by chemical modifications or additional absorber material, the wavelengths around 500 nm are better absorbed.

To estimate the accuracy of our calculations the resulting data was compared with the literature. For ZnPc a comparison with the data obtained by [46] in 1992 showed a good agreement between the results.

For C_{60} the result comparison with P. Milani et al. 1994 [47] and A. Richter et al. 1995 [48] showed a mismatch in the initial layer thickness value given to the "Optik" program for the calculation. A corrected layer thickness value was found, which brought the results to a good agreement with the ones from literature. That is why for the further simulation of the cell, the calculations for C_{60} **n** and **k** were repeated with the corrected layer thickness.

For ITO and Bathocuproine as colorless materials the data on the diagrams are in good agreement with the expected ones.

3.3.2 Optical simulation and result discussion

With the assumption, that our calculations were right and that we had the right datasets for all the layers of our cell, an optical simulation of the distribution of light intensity in our cell was made. This simulation makes sense only for the thin organic solar cells as their overall thickness is less than light wavelength and knowing the distribution of light intensity is an important precondition to their optimal construction. The thicknesses of the separate layers are set to the typical values for our standard cell: ITO – 180 nm; ZnPc – 30 nm; C_{60} – 30 nm; BCP – 17 nm. The result of the optical simulation is a distribution of the electrical field square in the cell. Because of the aluminum electrode, acting as a mirror for the incoming light, for every wavelength a standing wave arises. For all standing waves there is a common knot on the aluminum surface. The resulting distribution is shown on Figure 23:

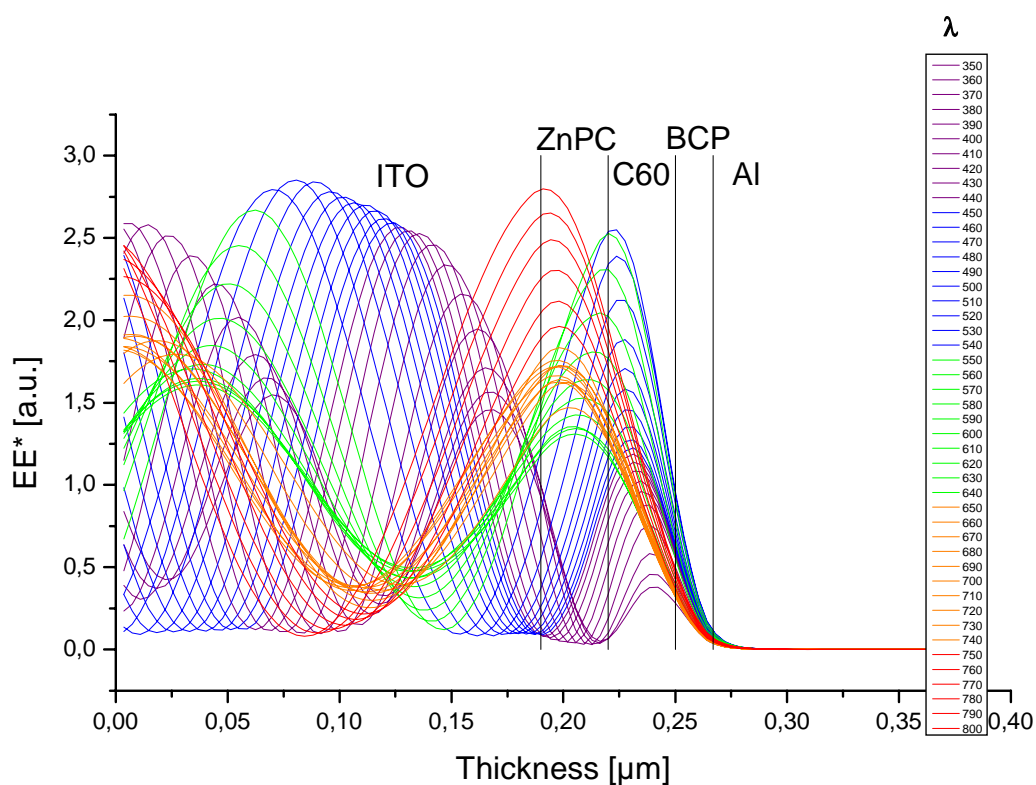**Figure 23. Computer simulated distribution of the electrical field square
in the multilayer system ITO/ZnPc/C$_{60}$/BCP/Al. Color corresponds roughly to wavelength color**

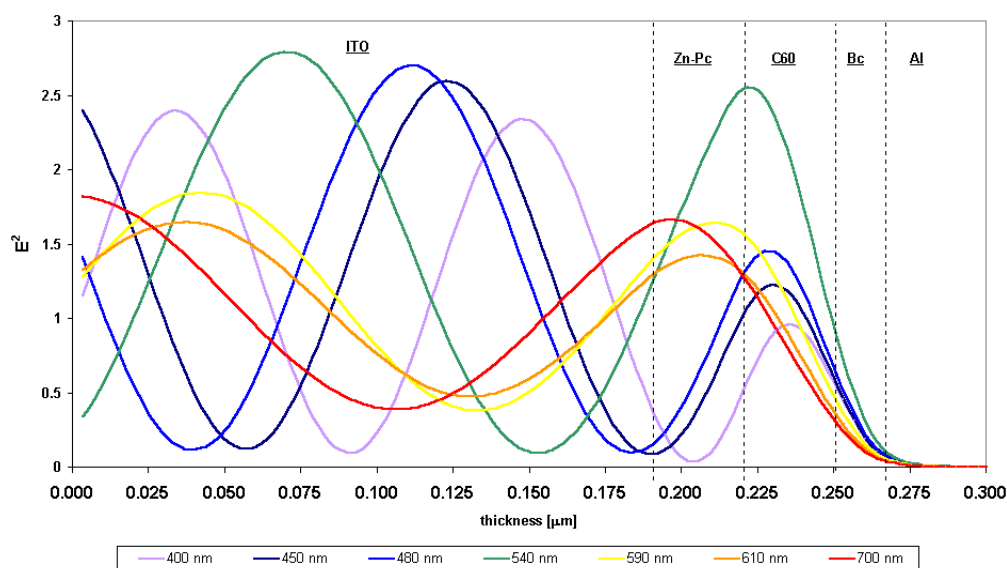For clarity, also a simplified diagram is provided on Figure 24.

**Figure 24. Simplified distribution of the electrical field square [a.u.] in our solar cell.
Green light (around 550nm) is almost unabsorbed due to absorption gap in the cell**

An important note should be added here, that for the simulation, the interfaces between the material layers in the cell are assumed flat and it is also assumed that no mixing occurs at those interfaces!

The distribution of the square of the electrical field is proportional to the energy density distribution. So from the optical simulation results, the light intensity distribution in the cell can be estimated.

From the graph, it can clearly be seen, that after passing through ITO only a small part of the UV-light is being absorbed. All other wavelengths reach the active layers intact.

The absorption maximum of C_{60} lies at about 450 nm. Apparently the maximum of this wavelength lies aside from the C_{60} layer midpoint. For a full absorption the layer could be made 5-10 nm thicker.

The maxima of ZnPc absorption peaks are ca. 620 nm and 720 nm. The maxima, of the distribution of these wavelengths in the cell, lie displaced from the ZnPc layer middle. For moving these into the middle of the ZnPc layer the thickness of ZnPc can not be increased [14]. Due to the limited charge transport properties of this material (explained in 1.3) this is impossible.

BCP could also not be made thicker, so that the corresponding maxima are set in their right places, because of its insulating properties. In this case a spacer layer is recommended, directly before the aluminum contact, i.e. a layer of a substance which does not absorb in the region 350-800 nm and which is a good electrical conductor.
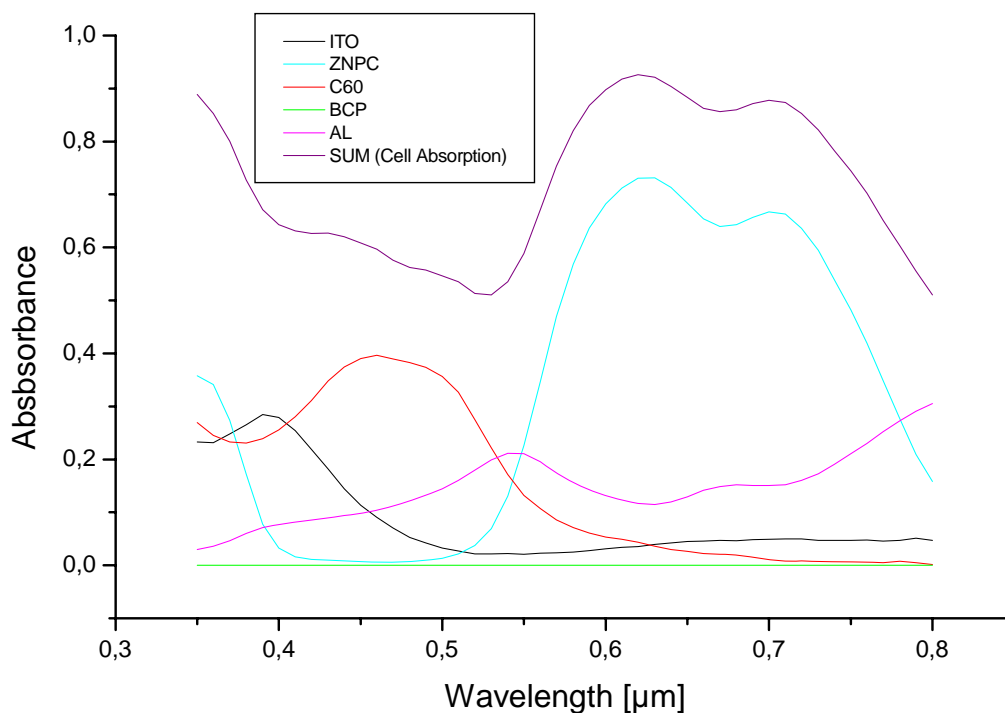
Figure 25. Theoretically calculated absorptions of the different materials in our solar cell, and their sum, the complete cell absorption. The weak absorption in the region around 540 nm does not match the sun spectrum maximum, lying around 500 nm

From the theoretically calculated absorptions (Figure 25) it appears that the wavelengths around 540 nm are absorbed very weak from the active layers. Unfortunately the maximum intensity of the sun spectrum lies at 500 nm. A solution to that would be to extend the cell absorption by either incorporating a second absorber material, absorbing in this region, or by chemically modifying ZnPc in such a way that it covers a wider part of the spectrum.

3.4 Layer thickness measurements

In the previous chapter the importance of exact layer thickness determination was emphasized on for result reproducibility, calculation and/or estimation accuracy. As it was mentioned in 2.7, during the solar cell layer evaporation in UHV, the layer thickness is being monitored by quartz crystal deposition controllers (QCDC), situated next to the rotating ITO substrates. By the producer company Inficon it is claimed, that after correct calibration, these deposition controllers can measure accurate, even tenths of an angstrom deposited layer thickness. It is only required one absolute thickness measurement to calibrate them. But calibration on nanometer scale is not an easy task. As it will be seen further, many different thickness measurement methods had to be employed, and their results compared, in order to accomplish this task.

3.4.1 Profilometer measurement

At first a very fast and easy method was tried – DekTak profilometer. With roughly calibrated deposition controllers, a defined layer thickness of each cell material were deposited on plain glass. Then a sharp scratch with a scalpel, through the layer was inflicted. Thus a step, with sharp edges was created, reaching from the surface of the organics to the glass substrate and having the height of the deposited material. Perpendicular to this scratch, the surface profile was then measured with profilometer. An example of the resulting measurement printout for 200 nm C_{60} layer can be seen on Figure 26.
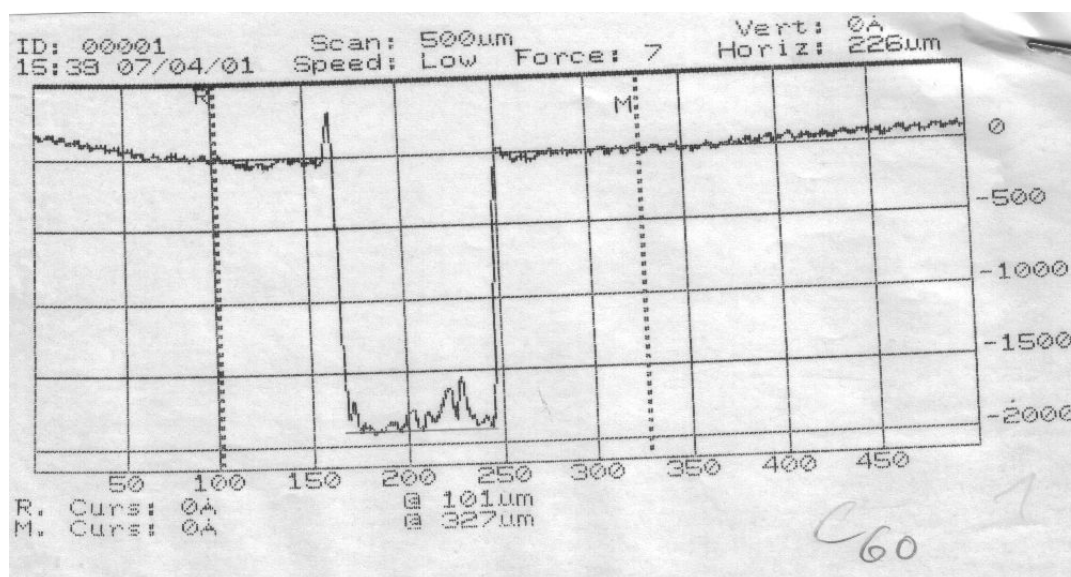
**Figure 26. Profilometer printout for a measurement, perpendicular to a scratch
in a 200 nm C$_{60}$ layer. Horizontal scale – distance [μm], vertical scale – height (film thickness) [Å].
Method accuracy is not better than 10%, for this thickness scale and soft material surface.**

The image shows the profile of a scratch in a 200 nm layer of C$_{60}$. The mean value of the surface height is set as zero, and the value of the scratch bottom is chosen as layer thickness. From the figure, it is clear how big the error on the nanometer scale can be, having in mind that the bottom of the scratch can never be made flat and even enough to diminish the mistake. Also the soft nature of the organic materials, whose thickness is being measured, allows the cantilever of the profilometer to penetrate the layer, thus additionally distorting the measurement result. So with this, more than 10% error, the method proves as unreliable, but a good approximation, concerning simplicity and low time-consuming measurement.

3.4.2 X-ray reflection[3]

The x-ray reflection provides angstrom exact layer thickness measurements. It requires very flat surfaces and also layers not thicker than 30-40 nm [**49**]. Its principle could be summarized, as Bragg-reflection of x-rays from parallel surfaces – layer and

---

[3] X-ray reflection measurements conducted by R. Steitz, SF1, HMI

substrate surface, at constantly changing angle. As a result a plot of reflectivity against the angle can be constructed, where the layer thickness can be calculated from the peak position.

For a substrate with low roughness, pre-cut, polished silicon wafers were used (100 Si crystal side). On the substrates 30 nm ZnPc, C60 and BCP were vacuum evaporated. These thicknesses were measured by our quartz crystal deposition controllers. An x-ray reflection measurement of all samples was made. The resulting plot reflectivity/angle for ZnPc is shown on Figure 27.
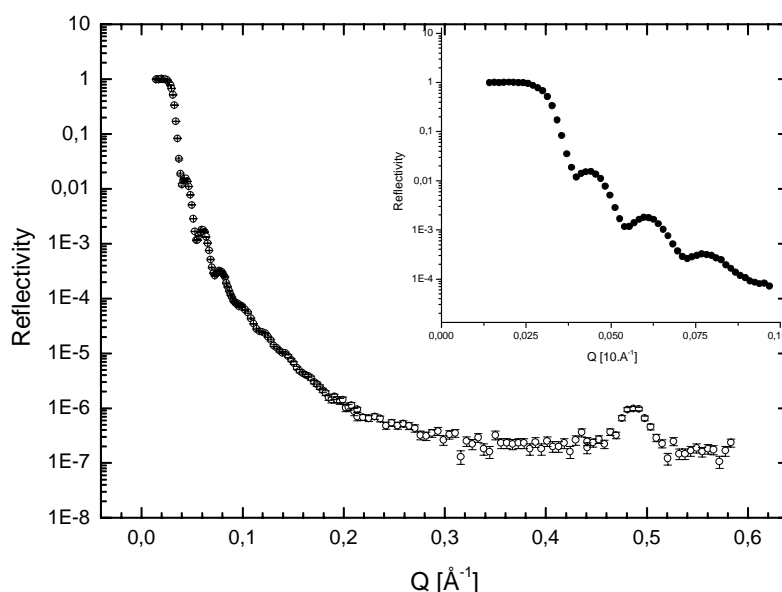
Figure 27. X-ray reflection measurement of 30 nm ZnPc (measured with QCDC) on silicon substrate. Calculations show 36 nm ZnPc layer thickness. The peak with maximum at 0,48 on the Q/Å^{-1} axis corresponds to a layer with thickness 1,3 nm. This can be interpreted as ZnPc molecular sub-layer structure in the main layer

The figure shows a well defined, cascade-like peak structure, where the peaks have a gradually fading intensity. The distance between two peak maxima allows to calculate the layer thickness ($d = \dfrac{\pi}{\Delta Q}$ [33]), which in this case is 36 nm. So 6 nm too much have been evaporated. The figure shows, also a peak with maximum at 0,48 on the Q/Å^{-1} axis. It corresponds to a layer thickness of 1,3 nm. Since the molecule of a ZnPc has a similar size, this can be interpreted as ZnPc molecular sub-layer structure in the main layer. Fitting of the data to a theoretical model revealed the following ZnPc layer configuration (Figure 28).

Figure 28. X-ray reflection data fit, layer scheme and an SEM image of a 30 nm ZnPc layer, evaporated on Si (100). The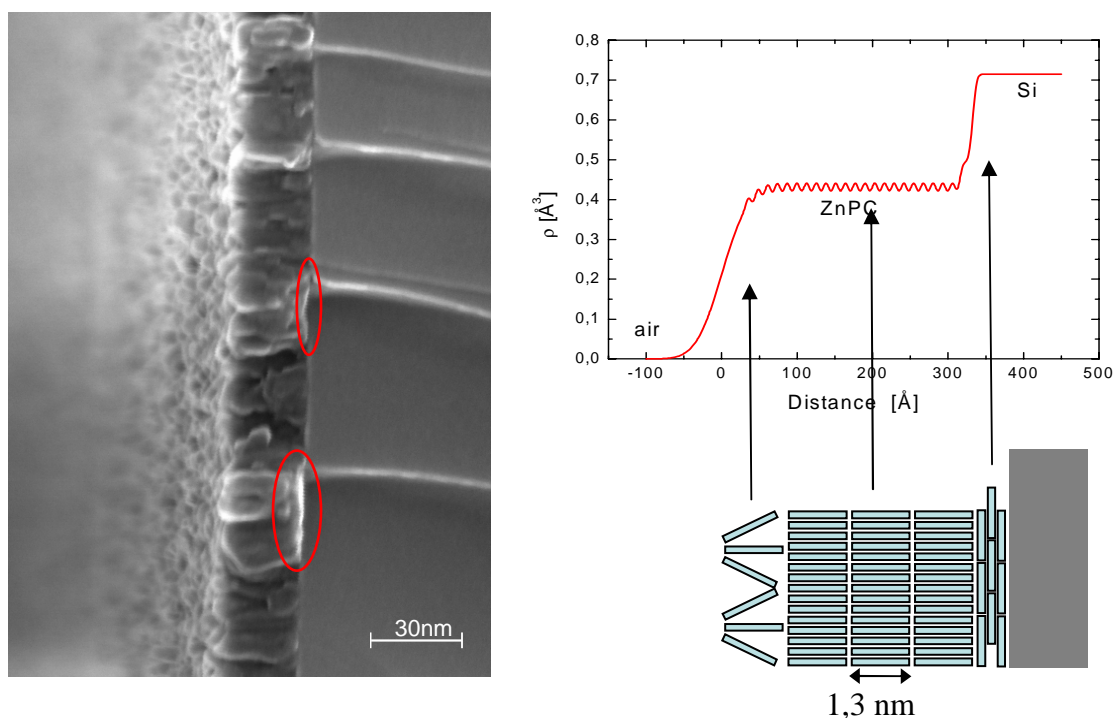 fit reveals 3 different sub-layers. First evaporated nanometers lie horizontally on the Si surface. Then sub-layers with 1,3 nm thickness are evidence for perpendicular to substrate surface molecules. Surface roughness is referred as third layer. The SEM image also shows some regions of ZnPc, near ITO, where some differences to the bulk areas are observed

Figure 28 shows an X-ray reflection data fitted to a multilayer model, layer scheme and an SEM image of a 30 nm ZnPc layer, evaporated on silicon. It should be mentioned here, that the scheme is not absolute and the molecules do not definitely arrange that way. It is only intended to show, that three different sub-layers are discovered. In the model fit the different electron density steps stand for different substances. The slope between Si and ZnPc has a shoulder, near the ZnPc density level, showing a different ordering of this same substance. The model attributes that to the first evaporated nanometers of material, which lie quasi-horizontal on the Si surface. The sub-layers with 1,3 nm thickness are evidence for almost perpendicular to substrate surface ZnPc molecules, since this size is comparable to the size of a single ZnPc molecule. The slope from ZnPc electron density to zero density is attributed to surface roughness and is referred as third layer. The middle of this slope is chosen as zero point, i.e. this is where air and organic material have equal presence.

The SEM image illustrates the ZnPc layer on Si, where some regions, different from the bulk are observed, near ITO. Also the surface roughness, predicted from the model fit, can be seen.

This structural analysis leads to the conclusion, that ZnPc layers consist of molecular sub-layers, with two different molecular orientations and structures contributing to surface roughness. Here it has to be mentioned that this x-ray measurement of ZnPc was made immediately after the evaporation of the organics, thus avoiding any recrystallization and change of surface roughness. A measurement of the same sample a week later showed almost 50% roughness, which resulted in a reflectivity/angle plot, having no peaks at all. This, of course, makes determination of the layer thickness impossible, and is an evidence of rapid recrystallization of the ZnPc even at room temperature.

The x-ray reflection measurement of a 30 nm C60 layer, yielded the following result (Figure 29).
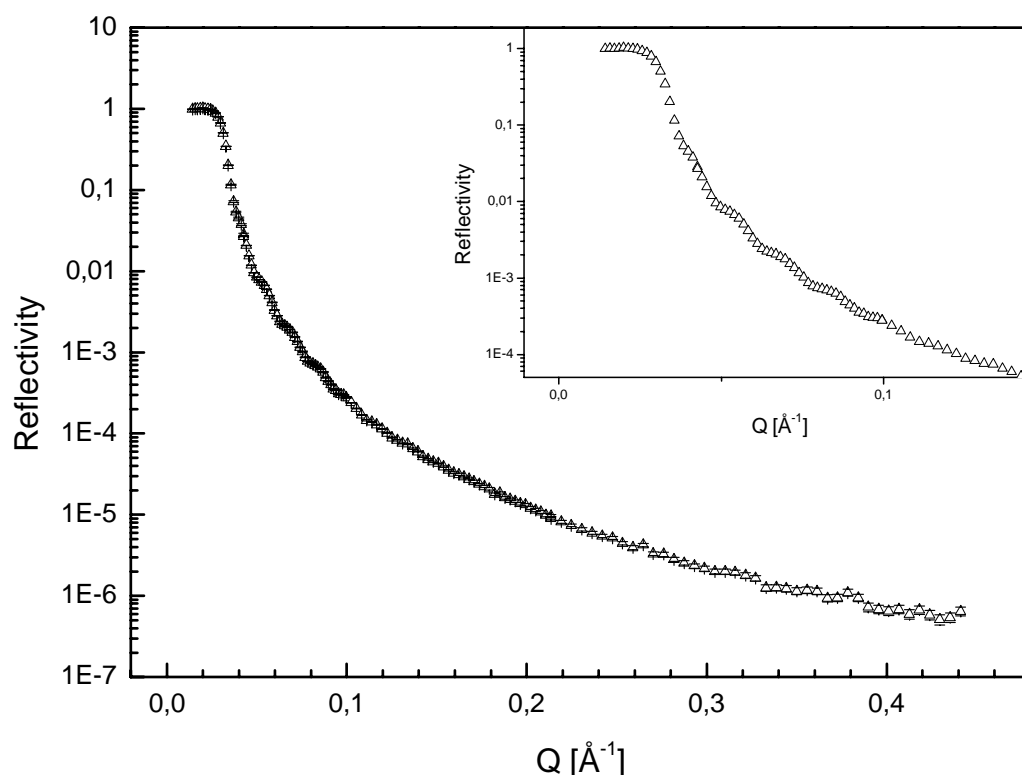

Figure 29 X-ray reflection measurement of 30 nm C$_{60}$ (measured with QCDC) on silicon substrate. Calculations reveal a C$_{60}$ film thickness of 32 nm. High surface roughness influences measurement accuracy

For C_{60} the Bragg reflection oscillations in the R/Q curve are not so well defined, even if that region is zoomed. This is an indication of high roughness, although the sample has been measured directly after evaporation of the organic substance. This result for a C_{60} layer is not unexpected. Literature sources [50] show that, during evaporation, after being distributed in a monolayer on the substrate, further C60 molecules start piling up on each other, thus creating clusters and opening free space on the substrate surface. Only after growing big enough, these fullerene clusters cover the surface with a closed layer (Figure 30), consisting of 100-400 nm domains. This explains the behavior observed by us, after evaporating C_{60} on silicon.
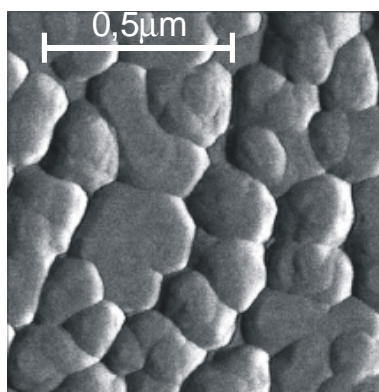
Figure 30. AFM image of 10 nm thick C_{60} film on glass, from [50].

The high surface roughness smudges the peaks and lowers their intensity. Nevertheless the peak positions on the figure can still be located. Calculations show that this fullerene layer has 32 nm thickness. Again a little more than measured by the profilometer calibrated, quartz crystal deposition controllers, but the deviation is not as high as with ZnPc.

For 30 nm BCP (measured with QCDC) the image on Figure 31 was obtained.
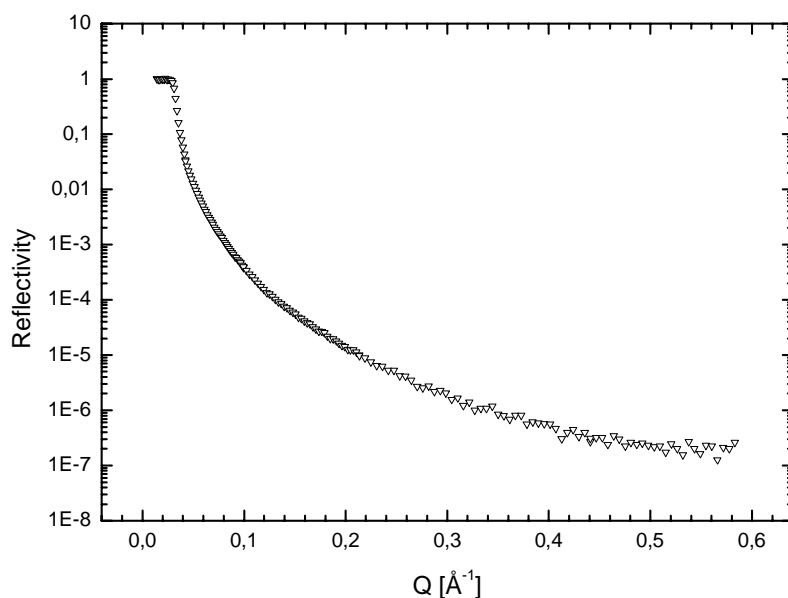
Figure 31. X-ray reflection measurement of 30 nm BCP (measured with QCDC) on silicon substrate. No oscillation peaks for thickness calculation can be obtained, due to high surface roughness, i.e. impossible reflection measurement, due to scattering

The x-ray reflection measurement of BCP showed no distinguishable peaks at all. Here the possible explanations are, that either the very high surface roughness prevents an accurate measurement, or some epitactical growth effect creates organic structures and not a layer, thus leaving the x-ray reflection meaningless.

As a conclusion it can be said that x-ray reflection is a powerful method, concerning layer thickness measurement. Results with angstrom accuracy could be obtained for ZnPc and C_{60} layers, where a well defined layer was present. For BCP the measurement yielded a result which did not allow layer thickness calculation, due to sample incompatibility with the method.

3.4.3 Ellipsometry[4]

For layer thickness determination with ellipsometry, three samples were prepared – ZnPc, C_{60} and BCP, each 100 nm (measured with QCDC). The measurement has been

---

[4] Ellipsometry measurements conducted at TU Chemnitz

conducted at three angles for each sample: 65°, 70° and 75°, in the range between 0,73 eV and 5 eV. For sensitivity enhancement an autoretarder has been used. The results of the measurement of the layer thicknesses for the three samples are shown in Table 3. It has to be mentioned, that the measurement for ZnPc had to be repeated with fresh samples in order to obtain a reasonable value. First measurement was made on an aged sample, which showed a thickness of 51±48 nm and a roughness of 68±49 nm. Obviously, with this high roughness, our assumption for recristalization of this substance at room temperature is confirmed. The formed crystals make the surface so uneven, that half of the layer thickness is lost into roughness.

Material	Thickness [nm]	Roughness [nm]
ZnPc	113,7±0,4	1,659±0,007
C_{60}	116,8±0,2	3,2±0,3
BCP	82,4±0,7	16±1

Table 3. Layer thicknesses, determined by ellipsometry ZnPc, C60 and BCP.
Results are in good agreement with the ones obtained with x-ray reflection.
Bathocuproine roughness explains the lack of peaks in the x-ray measurement

In the ellipsometry measurement the result for the roughness of the layers follows the same trend as shown by x-ray. ZnPc with the smallest roughness precedes C_{60}. For the fullerene this value is almost double and clarifies the reason for the worse x-ray reflection peak separation. The 16 nm surface roughness of BCP (≈20%) explains why with x-ray reflection no meaningful layer thickness measurement could be achieved. Simply the method does not function for surfaces, rougher than 10 nm.

The results of the ellipsometry measurement confirm the results from x-ray reflection, that the quartz crystal deposition controllers measure a bit less material, than is actually being evaporated. At this point a correction to the QCDC was made, but the obstacle with unrealistic thickness measurement of the QCDC remains, because of their sensitive nature. Even after small interventions leading to QCDC position change, like maintenance operations inside the UHV chamber, a new absolute thickness calibration has to be done.

As a comparison of the three thickness measurement methods Table 4 can be put together. For ZnPc x-ray shows 20% and ellipsometry shows 14% more than

profilometer measurement. For C_{60} the corresponding values are 7% and 17%, respectively.

Thickness, relative to profilometer	X-ray reflection	Ellipsometry	Profilometer
ZnPc	120%±1,7%	114%±0,4%	100%±10%
C_{60}	107%±1,9%	117%±0,2%	100%±10%
BCP	–	82%±1%	100%±10%

Table 4. Comparison of the film thickness measured by x-ray reflection and ellipsometry, relative to profilometer. Profilometer error is at the lower limit of the real one

As an explanation of the differences it can be said, that on one side the profilometer calibration is inaccurate, but also the density setting in the deposition controller computer might be incorrect. The QCDC measures the layer thickness through mass of deposited material. If the density of the evaporated films is lower than the one of the bulk material, then the layer will be measured thinner than in reality. The mass density of the ZnPc layer can be calculated from the x-ray reflection model fit, using the following formula:

$$\rho_{mass} = \frac{M}{N_A.Z} \rho_{el}$$

where ρ_{mass} is the mass density, M is the substance molar mass, N_A is the Avogadro constant, Z is the number of electrons in one molecule and ρ_{el} is the electron density value from the x-ray reflection model fit. The calculation for ZnPc mass density of the film is 1,41 g/cm^3, compared to a bulk density of 1,65 g/cm^3. This amounts to a 15% difference, roughly as much, as measured with x-ray and ellipsometry.

3.5 Different ITO passivations and their I/V results

There are many known ways to manipulate the surface properties of a TCO – plasma treatment, acid/base treatment, annealing etc [**51**,**52**,56,57]. These treatments usually influence the surface work function of the TCO by modifying the surface chemistry, thus raising or lowering the potential, needed to inject or extract an electron from the TCO electrode [27]. Being able to control and modify the surface electronic properties, makes it possible to fine-tune its parameters for better performance in a PV device. By influencing the surface chemistry, exciton and charge carrier traps could be possibly removed and also a better electrical conductivity through the organic-inorganic interface could be achieved, thus increasing the possible currents which can flow.

In order to find the surface treatment which works for our cells, we have tried several TCO surface chemical modification techniques, each of them including one or more substances tested. The aim of these chemical modifications of the ITO surface is the alignment of the energy bands at the organic-inorganic interface, as well as the variation of the contact resistance. The I/V characteristics of each cell with modified ITO electrode have been measured and presented in the next sections of the current work. Additional measurements and analysis of the chemical TCO treatments will be presented separately in 0, together with the analysis method for clarity and easier result comparison.

3.5.1 Spin coating

The "standard" and mostly used way to modify the surface of an ITO electrode, to be used in a PV device, is the introduction of an additional buffer layer – PEDOT:PSS [**53**]. Through spincoating of this material the whole ITO surface is covered with an extended organic layer having a defined work function.

As a commercial product PEDOT:PSS has a formula which is not very well known to the public. Known is only that it consists of a block-copolymer PEDOT:PSS (Poly-Ethylene DioxyThiophene : Poly-Styrene Sulphonate) with a bad water solubility and polymer-chain length not more than 50-60 units. Thus it comes not as a solution, but as an emulsion in water, sometimes containing some 2-propanole. So, many of its

ingredients are only to be guessed – adhesives and resins, emulsifier agents, inorganic counter-ions like Na$^+$, etc.

Spin coating allows only limited ways of controlling the deposited layer thickness. Either by varying the emulsion concentration or by controlling the spin coater turning speed one can achieve some well defined surface coverage. Then after applying the PEDOT:PSS, the substrate must be heated for 10 min 100°C in air, to allow the organics to melt and bind the surface in a polymer net. An I/V characteristic of a standard cell whose ITO is covered with PEDOT:PSS can be seen on Figure 32 in comparison with a non PEDOT:PSS cell:
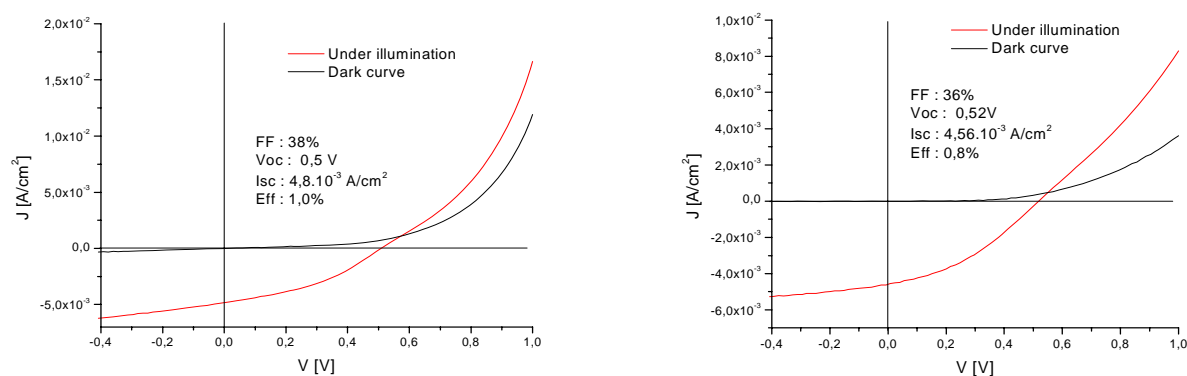

Figure 32. I/V curve of a cell with PEDOT:PSS (left) and without PEDOT:PSS (right)

In the figure it is clearly comparable that a cell with PEDOT:PSS has an improved serial resistance and by the same V_{oc} higher currents are able to flow (J_{sc}). From there the fill factor gets a little higher and the power conversion efficiency of the cell improves. The influence of PEDOT:PSS use is obvious. Chemically designed as a better hole conductor, this layer is also believed to block electrons coming from the bulk and only allow the holes travel to the ITO.

Although PEDOT:PSS improves the overall performance of the cell, it also has drawbacks. Its unknown composition makes it difficult to optimize anything in it except its concentration, so it must be used as delivered. Another drawback of PEDOT:PSS is that the spin coating is a separate process between the substrate washing and vacuum evaporation. An interruption like this could make the industrial production process very complicated and therefore expensive. Further more PEDOT:PSS has a blue colour which means it has an optical absorption. This way it diminishes the quantity of

red light left for absorption in the ZnPc layer. PEDOT:PSS also leads to reproducibility problems due to formulation and quality changes from the supplier. But with all these drawbacks, PEDOT:PSS stays the mostly used TCO treatment for PV devices.

3.5.2 Monolayer sublimation-deposition

With the monolayer sublimation-deposition method we tried to eliminate the cell production step of spin coating and immediately after the wet cleaning procedure proceed in vacuum. There a single layer of 8-OH Quinoline is deposited on the surface of ITO using the already described in (2.6.1) two step procedure. The choice of this specific substance was made from a literature source [26] where it was used as an ITO passivation for OLEDs and gave good results. The ITO surface after the reaction should be covered with a chemically bound organic monolayer, making the transfer of electrons between bulk organics and inorganic TCO easier, and hopefully remove any Schottky barrier or interface defects.
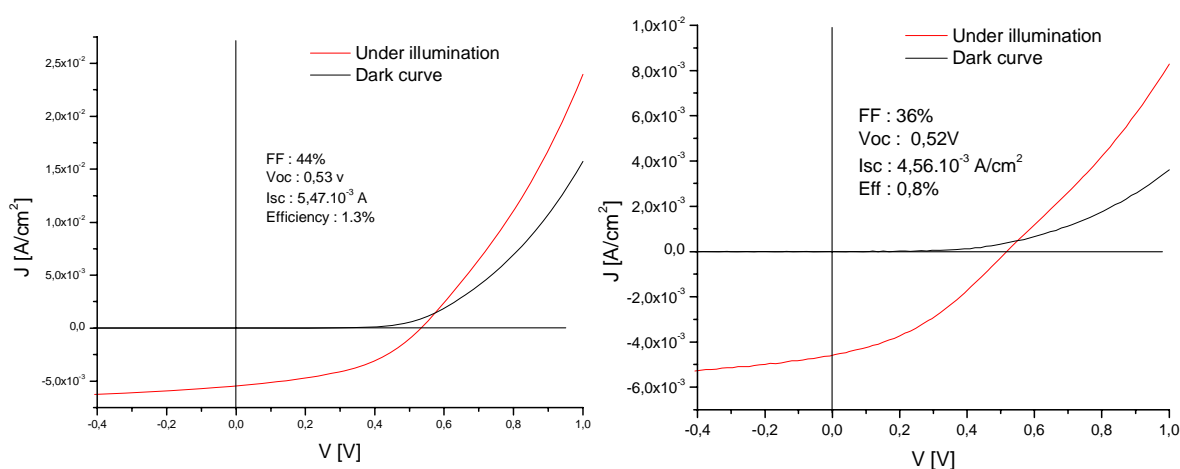
Figure 33. I/V curve of a cell with 8-OH Quinoline passivated ITO (left)
and ITO with no treatment (right)

Figure 33 shows a cell with 8-OH Quinoline compared to one with untreated ITO. The organic, although a thin monolayer on the surface [27], helps improve the serial resistance and higher currents are yielded (J_{sc}). The fill factor increases and although V_{oc} stays almost unchanged, the efficiency of the cell is improved.

The possible reason for these improvements is more likely to be the covalently bonded aromatic molecules on the ITO, than a favourable change in the surface work function of the TCO, as we will see in the further analysis of the treatments in 0.

3.5.3 Electro-codeposition

Electro-codeposition of a conducting metal oxide with a dye as a method to produce light absorbing layers is known and has already been used for production of solar cells [**54**]. Although the latter have a low efficiency, the concept of passivating the ITO surface with a thin layer of electro-codeposited ZnO/water-soluble-Pc seems acceptable, mainly because one would expect a coverage preferably at better conducting spots of the TCO, thus creating a conductive nano-wire net. Moreover, the so deposited ZnO is expected to be covered with the water soluble phthalocyanine (tetrasulfophthalocyanine), which happens to be also acidic, thus reacting with the surface of the newly formed ZnO (having an alkaline reaction).

Electro-codeposition was conducted as described in [54] at -1,1 V and 70°C for 15 min, from a solution with concentrations: $0,1M$ $Zn(NO_3)_2$ and $5.10^{-4}M$ $CuPc(SO_3H)_4$.

The I/V characteristic of the resulting solar cell is presented on Figure 34.
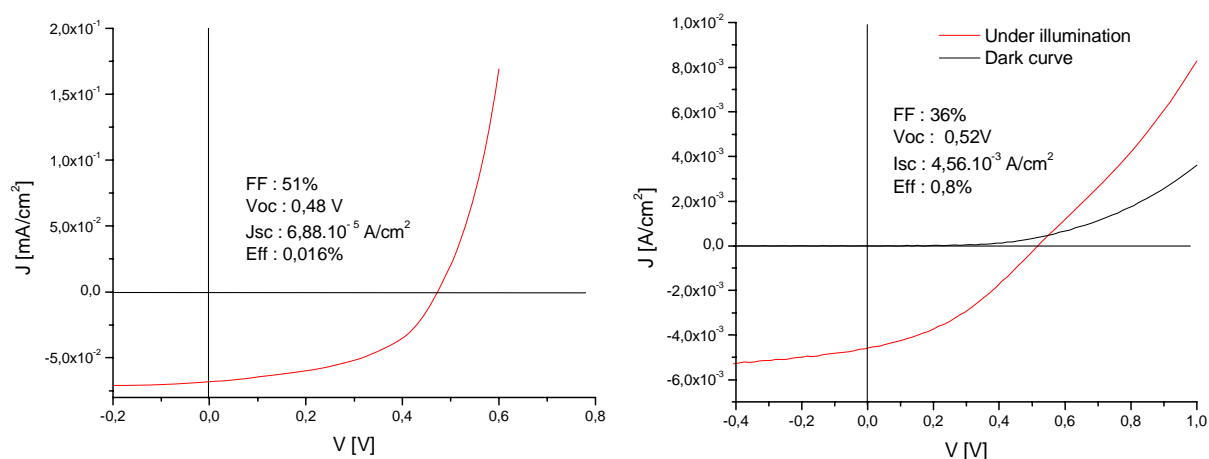

Figure 34. I/V curve of a cell with a thin layer of electro-codeposited ZnO/water-soluble-Pc on the ITO (left; under illumination curve only) and ITO with no treatment (right)

In this cell an interesting effect is to be observed. Having almost unchanged Voc, compared to bare ITO, the fill factor improves as much as with other passivations. Here the low efficiency is due to the very low current flow. Possible reasons include recombination or bad ZnO conductivity, due to lack of dopant (usually Al).

A big drawback of this passivation is that it not only involves an additional procedure in the cell production, but also electricity, which could interfere with a cheap industrial production.

Despite the unexpected outcome, further analysis of this ITO treatment is done in 0 for better understanding of the result.

3.5.4 Dipping

This ITO surface modification technique is a well studied field of TCO science. It has become a favorite because of its simplicity and eventual cost effectiveness. Shortly described, the method consists in dipping the washed and prepared ITO substrates in a solution of the corresponding passivating substance, for a defined time, and then rinsing with plenty of water. This way the passivation becomes a last step in the wet-cleaning procedure. Only the strongly adsorbed species remain on the TCO surface, creating a passivation monolayer. About the coverage one is for sure – it can never be 100%. Anyway, it will be shown that some dip-passivations, even without full coverage of the surface, can provide pretty amazing results in solar cell performance.

3.5.4.1 HCl

Hydrochloric acid was the first substance we tested as a dip-passivation. We tried to influence the work function of the TCO by modifying its surface acidity, as already described in literature [55]. ITO was dipped in 1M HCl for 5 min, then washed with plenty of water and dried with nitrogen flow. Thus it was intended to create a surface dipole, charging the inner ITO surface positive and the outer surface negative [56]. This would change the surface work function and stimulate electron injection from the TCO electrode into the organic.
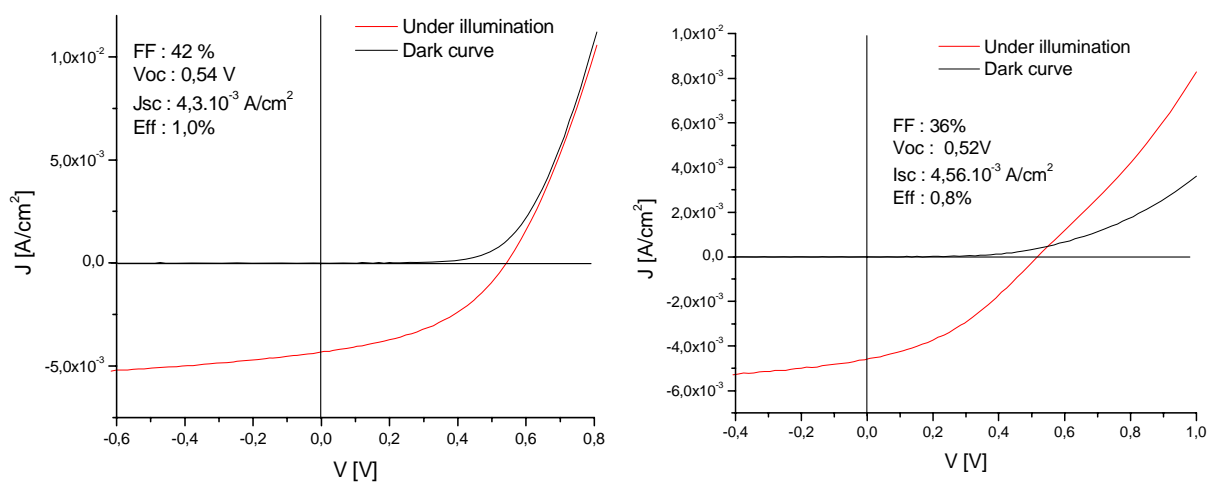
**Figure 35. I/V curve of a cell with HCl passivated ITO (left)
and ITO with no treatment (right)**

On Figure 35 a solar cell, whose ITO was treated with HCl can be compared to a cell with untreated TCO. V_{oc} of both cells shows a minor difference, which can be neglected. As can also be seen from the figure, a higher V_{oc} does not definitely mean a higher short circuit current. An obvious improvement in the serial resistance is observed in the voltage region above V_{oc} for the cell with HCl treated ITO. This improves its fill factor and is the reason of the efficiency increase.

An XPS study of HCl treated ITO substrates showed no presence of Cl⁻ on the surface though [59]. This led to the conclusion that a strong acid like HCl does not get adsorbed on the surface but only etches the substrate, so a really clean surface is obtained. It is possible that a protonation of the surface occurs, but the effect on cell performance is not that big. That is why we looked for some weaker acid molecule which would get attached to the ITO.

3.5.4.2 H₃PO₄

A surface dipole created by chemi-sorbed acid molecules on the surface of TCOs change their work function [**56,57**]. From electrostatics it is also known that a dipole moment equals the charge times the distance between charge centers: $\vec{\mu} = q.\vec{r}$. That is

why phosphoric acid was an apparent choice for an ITO passivation. Phosphate anion has a diameter of 0,26 nm [**58**] (2,6 times bigger than the 0,099 nm ionic radii of chlorine anion) and can have a charge from -1 in dihydrogenphosphate to -3 in phosphate, which could generate a serious dipole on the ITO surface.

Better sticking to metal oxides [**59**] than HCl makes it the perfect surface work function modifying agent. 1M H_3PO_4 treatment of ITO for 5 min yields a cell with I/V characteristics, shown on Figure 36 (left).
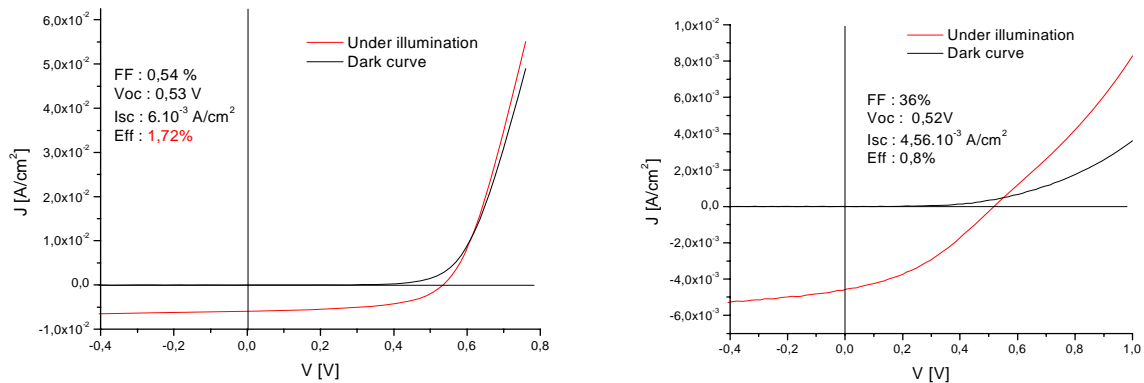
Figure 36. I/V curve of a cell with H_3PO_4 passivated ITO (left)
and ITO with no passivation (right)

An exciting record result, concerning the simplicity of the treatment and the method as a whole. In 0 a full surface work function characterization of this ITO passivation is done.

With phosphoric acid passivation a concentration variation was also tried out. The I/V characteristics of solar cells with 10^{-2}M and concentrated (85%) H_3PO_4 passivated ITO are shown on the next figure.
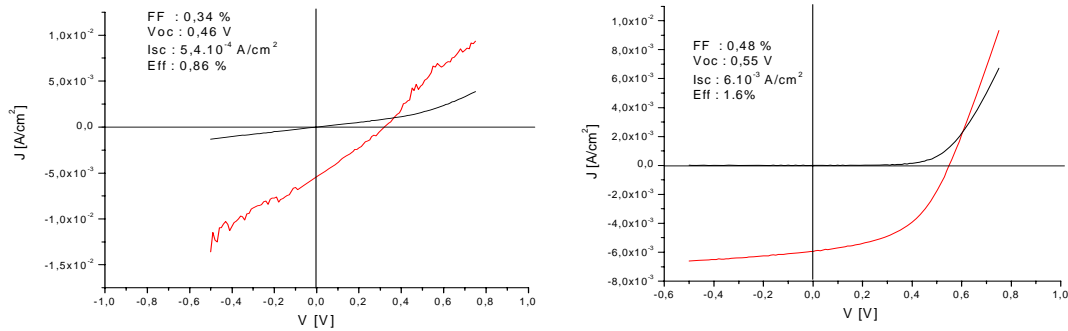
Figure 37. I/V curves of solar cells with 10^{-2}M and ~15M (concentrated 85%) H3PO4 passivated ITO

The cell passivated with 10^{-2}M acid and its measured parameters behave almost as a non-treated ITO cell. On the contrary the cell treated with concentrated acid shows a similar to the 1M H_3PO_4 parameter values. In this case obviously a saturation of the surface is reached even with 1M acid, and higher concentrations do not yield a higher coverage.

3.5.4.3 HIO$_4$

Per-iodic acid passivation was another try to push the surface work function of ITO even further, by modifying the surface acidity. A per-iodate anion would not have the charge of a phosphate one, but its diameter of 0,33 nm (calculated from literature data [**60**]) is a promise for a big dipole moment, thus a strong change in work function.

In Figure 38 the I/V curve of a cell with HIO$_4$ treated electrode is shown.

**Figure 38. I/V curve of a cell with HIO$_4$ passivated ITO (left)
compared to ITO with no passivation (right)**

Per-iodic acid did not yield a record cell, but still a good one. Compared with the 1M phosphoric acid the difference in eff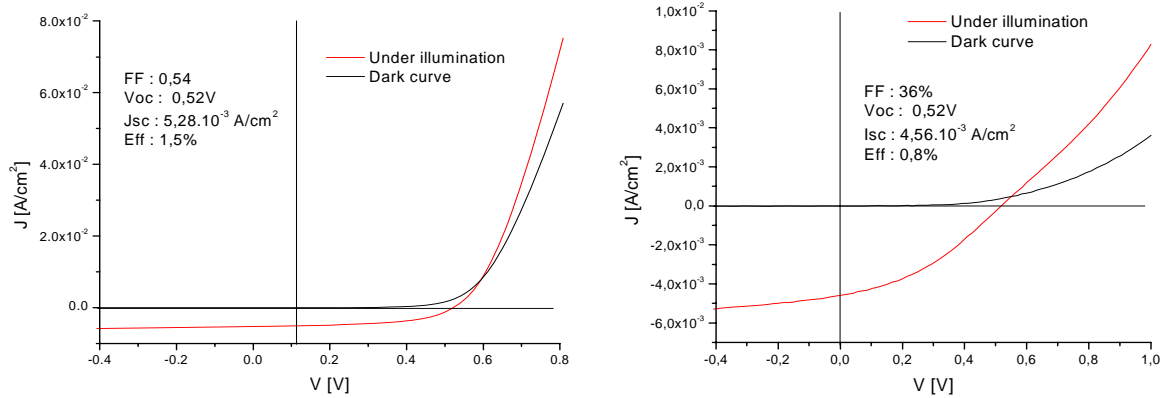iciency comes mainly from less current flow. V_{oc} and FF are about the same. If we compare the serial and parallel resistances (R_s and R_p are described in 2.8) of the non-passivated, H$_3$PO$_4$ and HIO$_4$ cells (Table 5) also other differences are found:

ITO passivation	none	H$_3$PO$_4$	HIO$_4$
R_s [Ω.cm^2]	$63,2 \pm 0,8$	$3,06 \pm 0,025$	$2,82 \pm 0,039$
R_p [Ω.cm^2]	709 ± 29	671 ± 12	704 ± 13

**Table 5. Non statistical comparison of Rs and Rp for cells with untreated and H$_3$PO$_4$, HIO$_4$
passivated ITO. Values are calculated from I/V curve fits**

The parallel resistance is more or less in the same range for all three samples. The passivation influences much stronger the series resistance. Apparently a big part of the series resistance of the cell comes from the ITO-organic interface. Table 5 is a proof that acid passivation improves the contact between ITO and organics, although the measurement in the first quadrant, during the I/V characterization, is not the extraction of charges from the cell, but their injection. The increase in cell efficiency shows that this improved resistance also influences the cell performance.

3.5.4.4 NH$_3$

Literature sources [56,57] show that basic treatments of the TCO electrode decrease its work function. This should be critical for the solar cell performance. To obtain better understanding of the TCO work function influence on the solar cell, 1M ammonia solution was tried as a passivation, to observe how a basic treatment would manipulate the cell properties. The I/V characteristic of such a cell did not look like a diode curve at all, so it will not be presented here. The solar cell had practically no photocurrent and efficiency.

3.5.5 Further analysis of ITO passivations

In this chapter a comparative analysis of three differently passivated ITO types will be made. PEDOT:PSS, H_3PO_4 and HIO_4 treated ITO will be compared to untreated ITO. Some additional measurements on ITO passivated with 8-OH Quinoline, co-electrodeposited ZnO/soluble Pc and HCl will be shown. In the search for a better passivation, the advantages of each single treatment have to be considered and the disadvantages overtaken. Only after that, a passivation molecule can be designed, to incorporate all the needed properties and have the advantages of the best treatments.

3.5.5.1 SEM

The electro-codeposition of a conducting metal oxide with a soluble phthalocyanine was unfortunately conducted in the early times of the current research, thus on old samples of 10Ω ITO glass. The surface of this TCO "looked" like the one shown on Figure 39 (upper left).
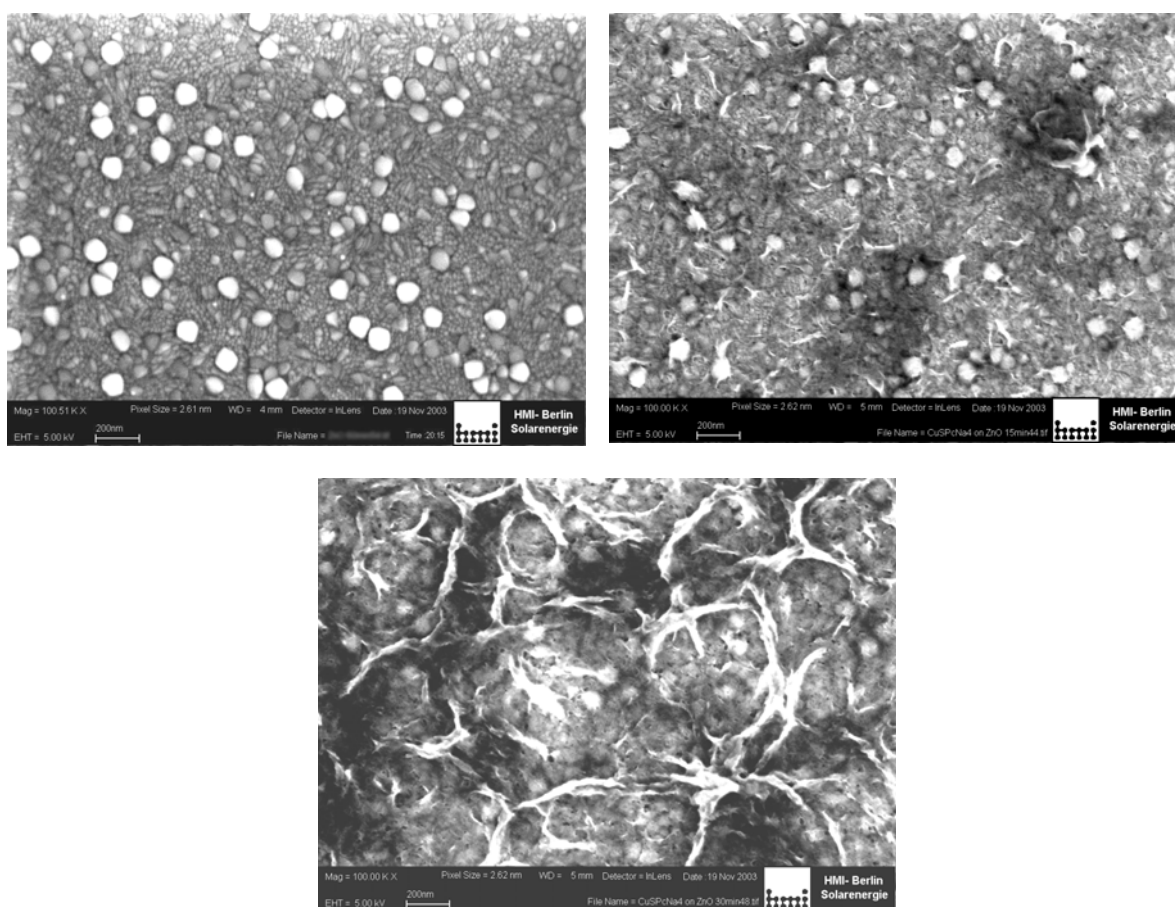
Figure 39. SEM illustration of ITO surface (upper left) covered with co-electrodeposited ZnO/soluble Pc for 15min (upper right) and 30 min (lower image)

Fifteen minutes of electrodeposition with the parameters described in 3.5.3 yielded the surface shown in the upper right of the figure. A ZnO web is created, starting from better conductive places on the surface. There is no homogenous coverage but scattered fibres without preferred direction. The I/V characteristic of a cell produced on such a substrate (Figure 34) showed almost no efficiency due to low photo-current flow, but not only. The explanation here is not simple. The serial resistance of this sample calculated from the I/V curve is $52,44 \pm 1,39$ $\Omega.cm^2$, still lower than the one of bare untreated ITO ($63,25 \pm 0,76$ $\Omega.cm^2$). So there must be a second reason for the low current. Possibly the ZnO web created defects where excitons recombine before they get separated. If the recombination would happen to already separated charges, the voltage would not be the same, but lower.

This passation technique gave us precious information concerning the possibility of creating traps through ITO treatment. This should be avoided in order to get more efficient in light harvesting process.

3.5.5.2 KPFM

With KPFM the topology of ITO, passivated with different treatments was monitored and its work function was measured, space resolved. The work function strongly depends on the treatment applied [56, 57]. As we will see, the homogeneity of the work function distribution is also affected with the passivation applied.

The results from the KPFM study of bare, untreated ITO surface are shown on Figure 40.
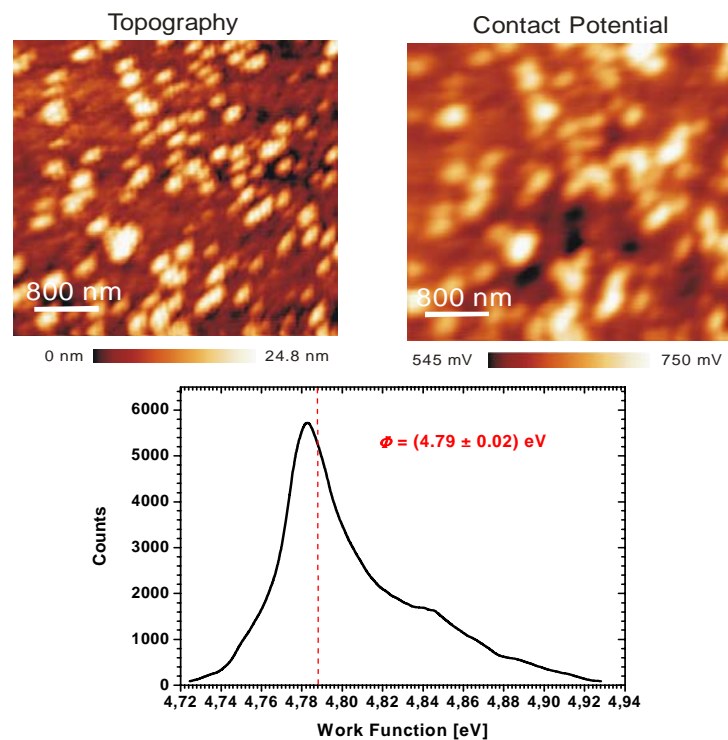

Figure 40. KPFM study of bare, untreated ITO surface[5]. Upper left and right images show the surface topography and contact potential, respectively. Lower graph presents the statistical distribution of the calculated work function, where the mean value is the weighted average

---

[5] KPFM measurements: Marin Rusu, HMI

The topography image shows a more or less homogenous surface with single peaks of up to 25 nm height. Their origin could be found in the ITO SEM image on Figure 10 and Figure 11. The domain structure of the surface is not completely flat. These domains are situated at a certain angle to the substrate plane, and their highest place could be those peaks in the KPFM image.

When comparing the image of topography and that of the contact potential, one sees certain similarity. Of course the two images are taken on the same area spot. This means that the higher peaks of ITO (shown in a brighter color) correspond to a higher contact potential (also brighter, see legend under images).

This overall inhomogeneous surface shows also inhomogeneity in its contact potential. The mean value for the bare untreated ITO surface work function lies at 4,79±0,02 eV (value is the middle of the half width of the distribution graph). This value lies much higher than the one measured by Nikolas Barreau, mentioned earlier in the current work. The reason is that the first measurement has been done at room temperature without annealing and the measurements of M. Rusu have been conducted after annealing at 130°C in vacuum and cooling to room temperature in order to remove adsorbed water species on the surface, which obviously also changes the work function. At least all the measurements in this KPFM series are conducted the same way, so they are comparable between themselves.

The KPFM illustration of the surface of ITO covered with a monolayer of 8-OH Quinoline (Figure 41) shows completely different electrical properties as compared with untreated ITO.
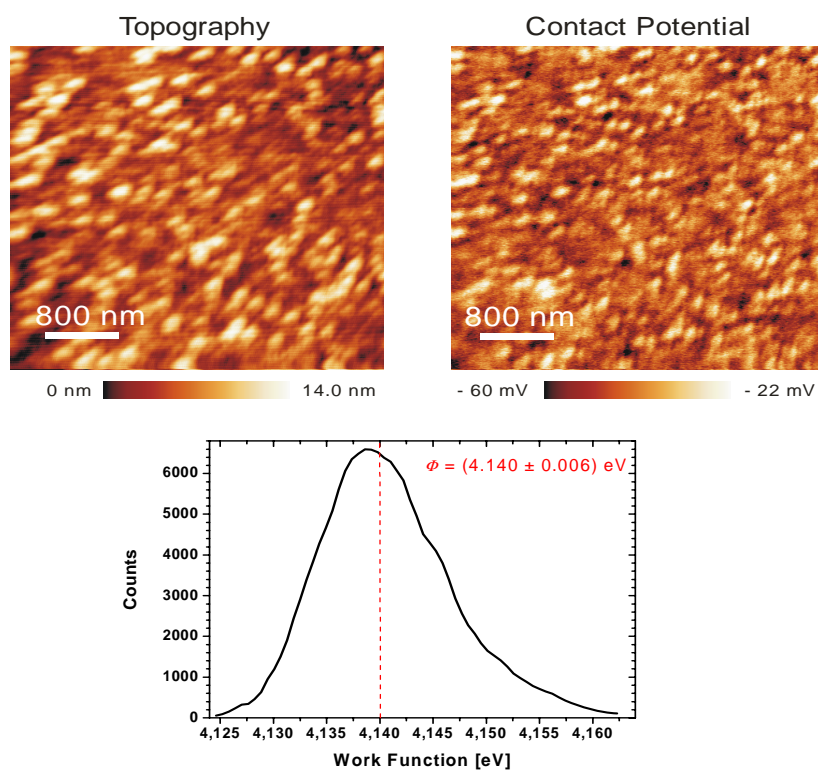
Figure 41. KPFM illustration of the surface of ITO covered with a monolayer of 8-OH Quinoline. Upper left and right images show the surface topography and contact potential, respectively. Lower graph presents the statistical distribution of the work function, where the mean value is the weighted average

Although the topography seems unchanged, the surface work function is in a narrower range compared to untreated ITO. Obviously the covering of ITO with a single, well defined chemical substance smoothens significantly the electrical properties of the surface.

A surprising result of this study is the work function value. For a cell with efficiency 1,3 % where nothing but the ITO passivation is changed one would expect the TCO work function to lie high above the usual one for bare ITO, because this is usual for the better cells. Here this is not the case. A work function of $4,140 \pm 0.006$ eV was measured. Lower than any other measured value it is even less than the one for untreated ITO. This is a hint that as an ITO passivation 8-OH Quinoline lowers the absolute value of the surface work function of this TCO.

Used as an electrode for a solar cell it yields a cell who's I/V characteristic was already shown on Figure 33. The parameters, fitted from this curve are as follows: $R_s = 23,6 \pm 0,3$ $\Omega.cm^2$ and $R_p = 471 \pm 15$ $\Omega.cm^2$. R_s is lowered in comparison with untreated

ITO, but still higher than PEDOT:PSS or the dipping passivations. R_p is surprisingly low compared to the other dippings and even untreated ITO (usually around 700 $\Omega.cm^2$). This is a precedent, since it is the only passivation that changed R_p of a cell to such extent ($> \approx 30\ \%$).

In our scientific discussions there were different opinions concerning the reason for this cell's efficient performance regardless the low work function of the TCO electrode. The dipole created on a surface passivated this way is a weak one, because of the lack of actual charges. Apparently the covalent bond to the ITO surface is responsible for the good connection between the inorganic electrode and the organics. A schematic illustration of an adsorbed/chemi-sorbed acid passivation compared to a covalently bound passivation is shown on Figure 42.
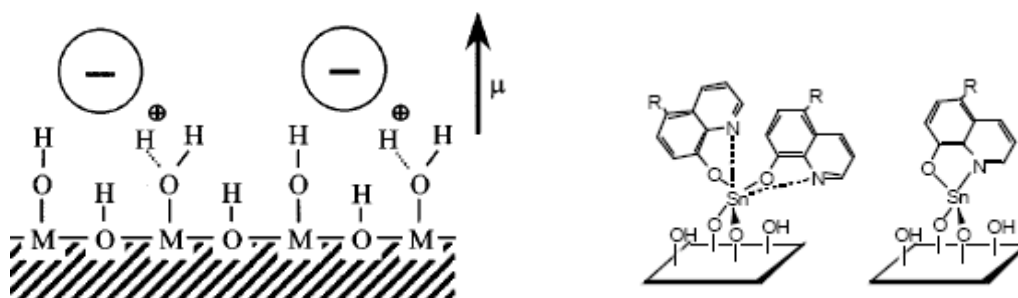

Figure 42. Two different ways of TCO monolayer passivation.
"Weak acid" adsorbed on TCO surface (left) [56] and
covalently bound 8-OH Quinoline on TCO surface (right) [26]

A strong surface dipole is created only with the adsorption of charged particles (acids/bases). It should ease the charge transfer the following way (Figure 43):
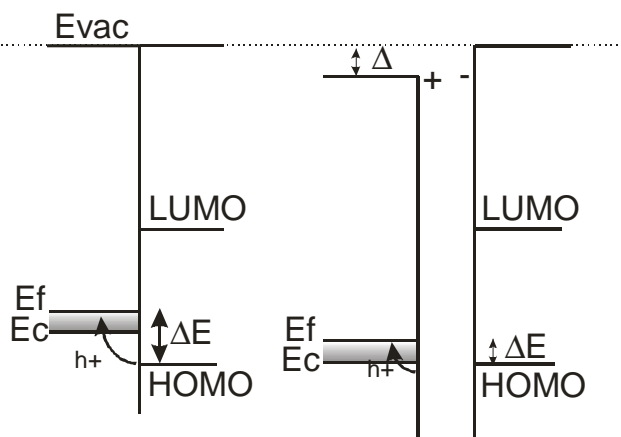
Figure 43. (left) Energy level diagram of the ITO/organic interface. The energy gap between the vacuum and Fermi levels represents the ITO work function. ΔE represents the thermodynamic barrier to hole extraction. (right) Producing a dipole on ITO surface shifts the energy levels of ITO by Δ, increasing ITO work function and lowering the barrier to hole injection.

Holes extracted from the HOMO ZnPc to the E_{Fermi} of ITO need to pass the barrier ΔE. By creating a dipole on the TCO surface, the work function of ITO increases and the thermodynamic barrier for the holes is lowered, thus easing their way to the TCO, through the forbidden zone under the conduction band of ITO. An example of this phenomenon is illustrated on Figure 44 for phosphoric acid passivated ITO.
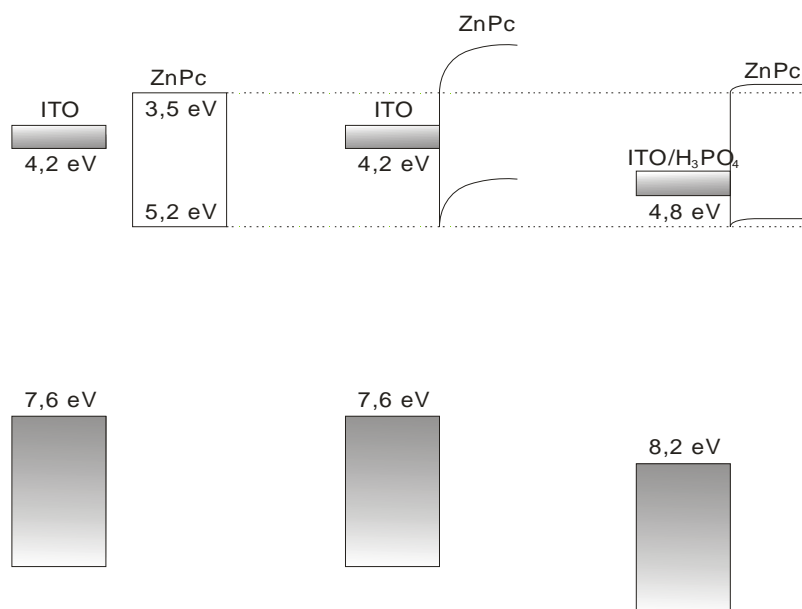
Figure 44. Energy band diagram, showing three possible relations between ITO and ZnPc. Left is shown the case when the two layers are not in contact. The middle case illustrates the ZnPc energy levels upon contact. On the right, an ITO with modified energy levels (H₃PO₄) is shown in contact with ZnPc. It can easily be seen that the thermodynamic barrier from the second case is diminished by the passivation

In the illustration three possible cases of energy band alignment are shown. First, ITO and ZnPc are shown as separate layers. The second case shown is the two layers in contact. A big energetic barrier is created, blocking charge transport. In the third case ITO, passivated with H_3PO_4 with higher work function is shown in contact with ZnPc. There the thermodynamic barrier is much lower, allowing also charge carriers with less energy through.

For a covalently bound passivation this can not be the case. The lack of a real dipole is enough to abandon this theory. A possible explanation of the cell improvement in this case is that the organic molecule bound to the inorganic surface creates a bridge for charges, thus eliminating all surface interface defects and allowing high currents to flow with no option for charge carrier recombination. And really, if J_{sc} for such a cell (Figure 33) is compared to J_{sc} of all the other passivations it becomes clear that only the best cells like 1M H_3PO_4 and 1M HIO_4 passivated have their J_{sc} in the same range.

For H_3PO_4 passivated ITO the KPFM snapshot looks a bit different - Figure 45
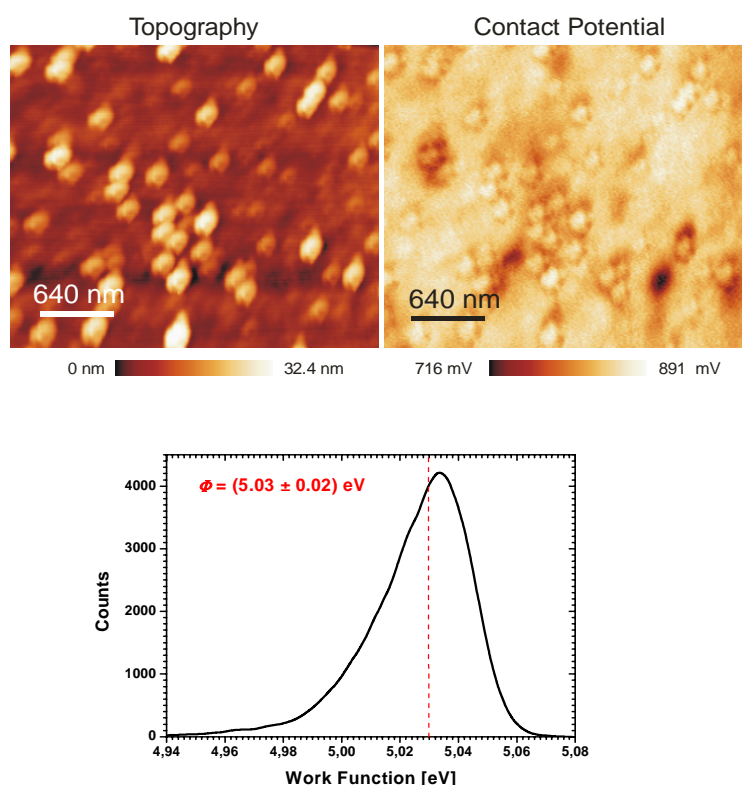

Figure 45. KPFM illustration of the surface of ITO covered with a monolayer of H_3PO_4. Upper left and right images show the surface topography and contact potential, respectively. Lower graph presents the statistical distribution of the work function, where the mean value is the weighted average

Here the topography stays, as expected, unchanged, because a weak acid like phosphoric one does not etch the ITO surface. But this time the contact potential resides in real narrow range, except for some very low potential spot (marked in very dark color on the image). Due to dipole building, the whole surface has almost identical electrical properties. The distribution of the small acid molecule on the surface, as the homogeneity of the contact potential image shows, is amazing. Obviously it reaches even the smallest crack or opening and passivates there also.

The work function of ITO for this passivation, measured with KPFM, is as expected very high: 5 eV we never measured before. And this huge change is induced with such a simple procedure as dipping the sample in a passivating solution and rinsing it thoroughly with water after this. No additional vacuum depositions, no spin coating. And more, this coverage, as proven by XPS (Figure 46) is temperature and vacuum stable up to $\approx 300°C$.
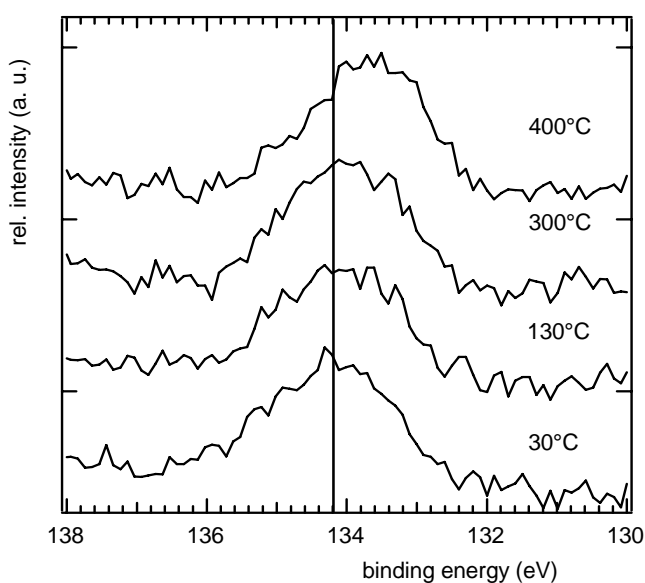
Figure 46. Phosphorus 2p electron peak corresponding to $H_2PO_4^-$ species in a XPS spectrum of H_3PO_4 passivated ITO. Measurement: M. Vogel [59]. Adsorbed species are stable up to 300°C in vacuum, with slight shift to lower energies at higher temperatures (means chemical change)

The phosphorus 2p electron peak corresponding to $H_2PO_4^-$ species, seen in the XPS spectrum of phosphoric acid passivated ITO changes position only after approximately 300°C. For comparison, adsorbed on ITO surface species of per-iodic acid, as measured in [59] are stable, without decomposition, only up to 130°C.

Per-iodic acid (HIO_4) also has a similar behavior to phosphoric acid concerning ITO passivation.

Topography

Contact Potential

800 nm

800 nm

0 nm   20.3 nm

778 mV   828 mV

$\Phi = (4.991 \pm 0.007)$ eV
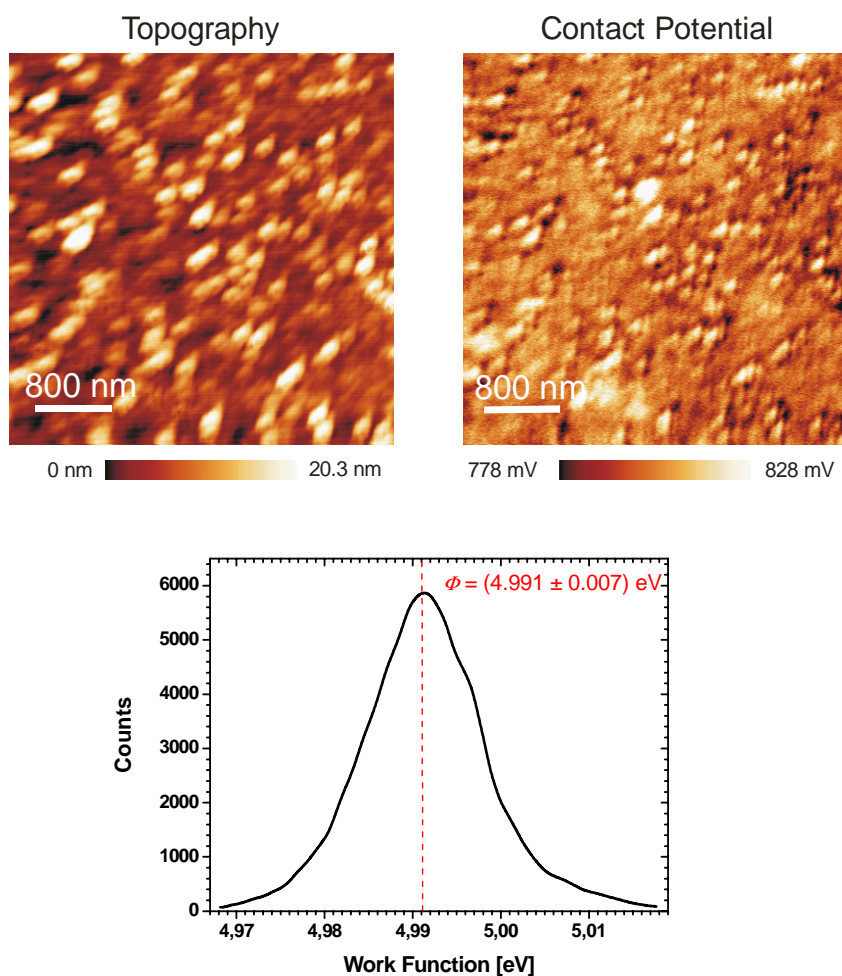
Figure 47. KPFM image of ITO covered with a monolayer of HIO_4. Upper left and right images show the surface topography and contact potential, respectively. Lower graph presents the statistical distribution of the work function and the mean value is the weighted average. Narrow distribution of the surface work function is a hint for surface homogeneity

The surface dipole also keeps surface topology unchanged. Contact potential is again in a narrow range, similar to phosphoric acid. The well defined Gauss distribution of the ITO work function is also to be observed here. The work function value of ≈5 eV is not surprising for this passivation, knowing the I/V characteristic of the cell made with such passivated ITO.

Obviously an optimum has been reached for this kind of passivation and even bigger dipole moment from bigger anion diameter or charge does not affect the work function much more.

3.5.5.3 XPS

A second method we used to measure surface work function and compare the results with KPFM is XPS. The method analyzes the kinetic energy of electrons, emitted from a surface, under irradiation. The binding energy of the electrons in the solid can be calculated using the formula: $E_k = E_X - \left(E_{bind} + \Phi_{mat} \right)$, where E_k is the kinetic energy of the emitted electron, E_x the energy of the exciting irradiation, E_{bind} the binding energy of the electron and Φ_{mat} is the work function of the material. From the electron binding energy, information on the surrounding of the electron is obtained. Thus, core electron analysis (element and chemical analysis; emission excited with x-rays), or analysis of the outer electron's ionization energies (valence band analysis; emission excited with UV irradiation), can be done.

The XPS values of ITO work function for the different treatments are shown in Table 6, compared with the ones obtained from KPFM.

Work function [eV]						
	Untreated ITO	PEDOT:PSS	8-OH Quinoline	HCl	H_3PO_4	HIO_4
XPS	4,2±0,2	4,6±0,1	3,5±0,1	4,6±0,1	4,8±0,1	4,8±0,1
KPFM	4,3	4,759±0,008	4,140±0,006	–	5,03±0,02	4,991±0,007

Table 6. Surface work function of different treated ITO, measured with XPS[6] and KPFM.

The values measured by XPS and the mean values received from KPFM show a poor agreement. As explained before in 3.5.5.2 the samples are differently pretreated for the two different measurement methods after the passivation. XPS is measured directly after passivation without any further treatment, but samples for KPFM had to be heated to 130°C and cooled down before the measurement to assure the removal of any surface adsorbed water. That should be the reason for the differences in the measured values.

---

[6] Measurement: M. Vogel [59]

More important in our case, is that the results for both methods are arranged in the same order so they are comparable in terms of ranking.

3.5.6 Short review and estimation of the passivations

In the previous chapters it was made clear that the acid passivations have reached an optimum (H_3PO_4) and further increase of the dipole moment (HIO_4 for example) of the dipole created on the ITO surface contributes almost nothing to the work function raise and to the cell efficiency.

It was also shown that an organic passivation of ITO (8-OH Quinoline) could improve the current flow to the TCO electrode and exclude recombination on traps situated on the TCO surface.

A water soluble passivation could be good enough to substitute PEDOT:PSS – a commercial mixture with little known parameters.

A passivation which shifts the work function of ITO in the desired for solar cells direction should be acidous and not basic.

The ITO treatment should not create, but eliminate TCO surface recombination sites, thus promoting undisturbed charge transfer on the organic-inorganic interface in the solar cell.

If we order the tested passivations in incrementing order of different TCO and cell parameters the following rows can be listed:

- Efficiency:

    ITO<PEDOT:PSS<8-OH Quinoline<Acids

- ITO work function:

    8-OH Quinoline<ITO<PEDOT:PSS<Acids

- Short circuit current:

    ITO<PEDOT:PSS<8-OH Quinoline<Acids

Obviously organic and acid passivation do the biggest favor to the organic solar cell, built on an ITO electrode.

3.6 ZnPc4P – a chemically engineered passivation material

In the search for a state-of-the-art passivation material many simple substances were tested and their efficiency for solar cell production analyzed. Summarizing our studies yielded several properties, that a material should possess, in order to serve as a high-end TCO passivation for solar cells. These properties include:

- Organic compound, with conjugated double bonds in the molecule, in order to achieve a good contact with the first organic layer of the cell, by possible π-orbital overlapping;

- Anionic (acidic). After chemisorption on the surface a dipole will be created, thus shifting the TCO work function to higher absolute values;

- Its acid group(s) should possibly be phosphoric, because of their better sticking to the surface and high stability of the chemisorbed species (proved in 3.5.5.2);

- Water solubility, the easiest way to passivate the TCO electrode and the most cost effective treatment is the dipping procedure

The modification of the surface of the TCO contact also influences the way, the first organic layer in the solar cell grows. The structure of ZnPc, at least in the first several nanometers, depends on the properties of the substrate (epitaxy). On non-polar surfaces ZnPc lays its molecules horizontally, parallel to the surface. On highly polar media the molecules tend to be deposited almost perpendicular to the surface [61].

ZnPc, itself possesses some interesting architectural properties. As sketched in Figure 48, ZnPc molecule has anisotropic conductivity 3:1, and its better conductivity is in the direction perpendicular to its molecular plane [62].
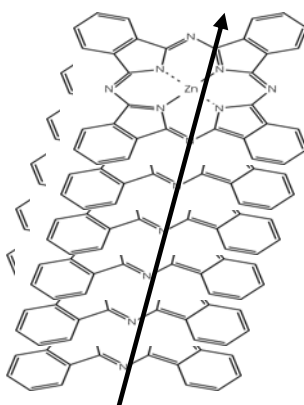

Figure 48. Electrical conductivity axis of the ZnPc molecule and molecular crystal

Also known is that ZnPc crystals consist of slightly shifted in one direction, stacked-overlapping molecules [**62**]. Evaporated on polar surfaces as TCOs, ZnPc creates its crystals parallel to the surface, thus having its molecule plane perpendicular to it [62]. This way the conductivity direction of this layer is almost entirely parallel to the TCO surface. In consequence the current flow is limited by the organic layer resistance. The same is the case with amorphous layers (evaporated on cold substrate) where the conductivity is in all directions, but worse than in crystals, due to the lack of order of the Pc molecules. So if a passivation could help to order the first evaporated layer of this flat molecule parallel to the surface, then all other molecular layers might follow the growth order and the conductivity would be in the right direction - perpendicular to the TCO.

All these requirements for a TCO passivation could be combined in a single molecule, having all the properties needed for a good solar cell. After consideration and revision of all passivation requirements, finally a substance was "born", incorporating the majority of the properties required (Figure 49).
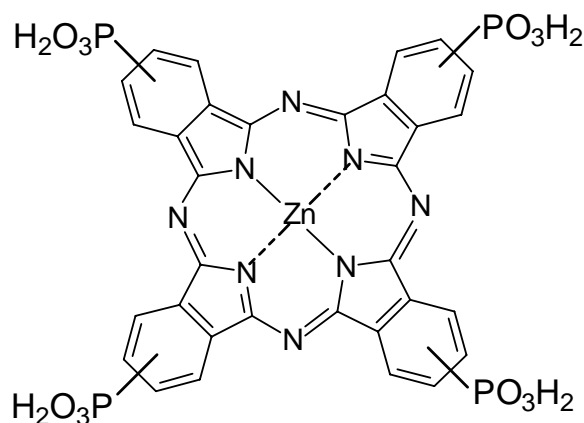

Figure 49. Zinc-Phthalocyaninetetraphosphonic acid (ZnPc4P)

An anionic, water soluble dye molecule, the Zinc-Phthalocyaninetetraphosphonic acid (ZnPc4P) incorporates the phosphate groups and is an organic molecule as a whole. It is similar to ZnPc which ensures the "epitactical" compatibility between passivation and first organic layer.

The synthesis of this substance was conducted as described in 2.6.2. As a passivation it was applied using the dipping procedure, out of a 10^{-4} M aqueous solution. An astonishing fact about this passivation came up after the first passivation test. The ITO substrate turned bluish after only 5 minutes spent in that solution and even huge amounts of distilled water did not wash it away from the surface. This was a hint of the adsorption strength of this substance on the ITO surface.

Of course much could be speculated on the topic why the bluish color could be seen. One possible explanation, is that this phthalocyanine molecule has such a strong light absorption, that even a monolayer can be visible to naked eye. Another possible explanation is the creation of molecule dimers or polymers. As described in [63], organic molecules with an acid group, like our substance are capable of creating intermolecular H-bonds (Figure 50).
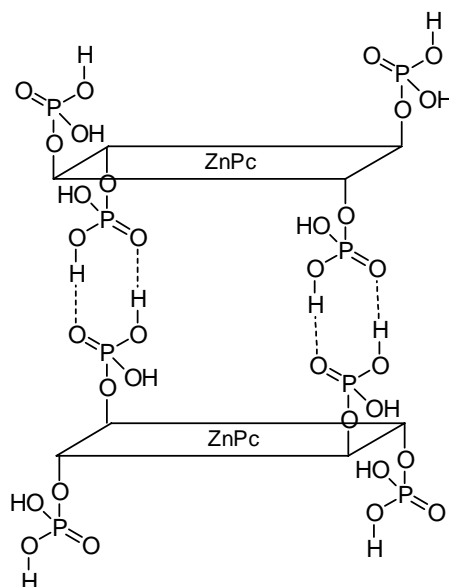
Figure 50. A possible ZnPc4P dimer

So not just a monolayer, but a dimer or even polymer layer could be present on the ITO surface. Although a polymer is very improbable, because the H-bonds are weak ones and by washing with excess of water they would eventually break and substance would get washed away. After all, dimers should only exist in concentrated solutions [64].

3.6.1 I/V characterization

After applying the Zinc-Phthalocyaninetetraphosphonic acid as a passivation on ITO a solar cell was produced. Its I/V curve is shown on Figure 51.
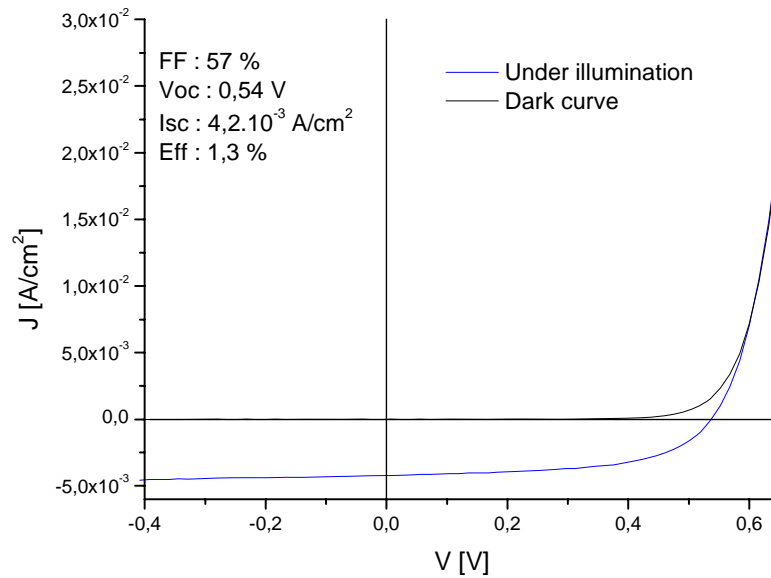
Figure 51. Current voltage characteristic of a solar cell with ZnPc4P passivated ITO

Apart from the not so high efficiency, this cell has the highest fill factor we ever measured. This is due to the improved serial and parallel resistance. R_s: 2.5 ± 0.1 $\Omega.cm^2$ – a hint for an excellent, low barrier contact on the ITO-ZnPc interface. R_p: 1351 ± 62 $\Omega.cm^2$ is almost the double resistance compared to the other passivations. This high parallel resistance stands for extremely low recombination rate of charge carriers at the ITO interface and almost no leakage current [65].
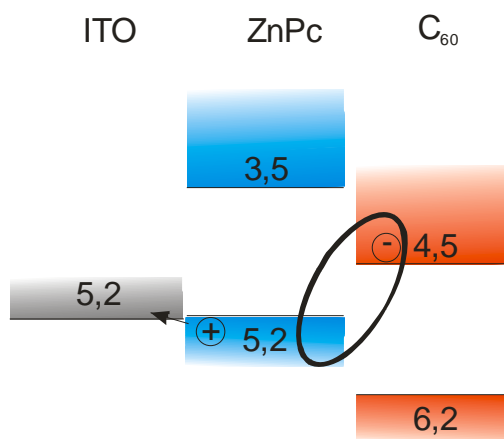
Figure 52. Energy band diagram showing the only possible place in the ZnPc/C$_{60}$ solar cell where recombination could occur (black circle). Having the work function of ITO tuned to 5,2 there remains no forbidden zone for holes under the ITO conduction band, so hole extraction should be the more favored process, than recombination

In Figure 52 the only possible recombination place for the ZnPc/C$_{60}$ solar cells is shown. Tuning the ITO work function to 5,2, the forbidden zone between the conduction band of ITO and the HOMO of ZnPc is no longer a barrier for the hole transport. That is why hole extraction is favored instead of recombination to occur.

Another interesting fact observed in this I/V curve is the perfect matching between the bright and dark measurement in the region above V_{oc}. The reason lies in the electric properties of the ITO. Some TCOs, have almost no charge carriers in the conduction band. When kept in the dark these materials are insulators. As soon as light falls on the electrode charge carriers are excited from the valence to the conduction band and the material turns into a conductor. With ITO the difference in the slope of dark and bright curves (the crossing of the curves) is due exactly to this effect. More charge carriers are created when under illumination, thus the steeper slope. In the case with ZnPc4P as passivation this does not happen, because obviously all possible carriers are already in the conduction band, near the dipole on the electrode surface. So what one observes is matching of the two curves at higher voltages. So the resistance at ITO-ZnPc interface is already not a barrier for transferring even higher currents.

3.6.2 SEM

With SEM we studied the ways of growing the 30 nm ZnPc layer on ITO surface, passivated with ZnPc4P and not passivated. Here it is important to mention that all images of ZnPc on untreated ITO were much harder to focus and to obtain a decent image in comparison to ZnPc4P treated ITO. The reason is that the treated ITO has a much better surface conductivity, thus its interaction with the electrons shot from the SEM electron-gun is much stronger. In SEM better conducting surfaces are easier to see and focus.

The next figure shows a SEM image of the Phthalocyanine layer on untreated ITO.
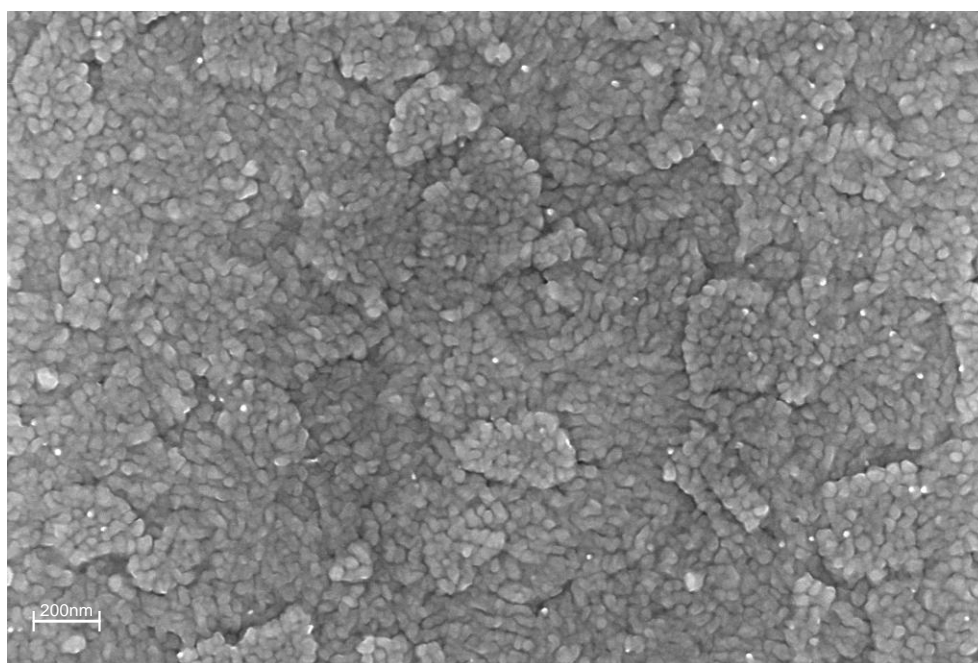
Figure 53. SEM image of 30nm ZnPc on ITO

The original domain structure of ITO is clearly observable. Obviously the layer of ZnPc is thin enough to preserve this structure. On this image the phthalocyanine has some very small "white" spots. These spots are not observed on ITO. So they are some local structure of the organics. Much smaller than the single ITO crystals in a surface domain, these "white" spots have either a very good conductivity and look brighter, or the contrary – they do not conduct but accumulate charge which makes them seem so bright. Usually a surface which accumulates charge drifts in the electron microscope

(glass for example). It is difficult to focus and moves constantly, which makes it impossible to snapshot. Here this was not the case so we assumed the other possibility – highly crystalline and very conductive spots of phthalocyanine.

If we now compare the ZnPc on untreated ITO with the one evaporated on ITO passivated with ZnPc4P, we see the same domain structure of the TCO, but the bright spots of conductive ZnPc have multiplied many times (Figure 54).
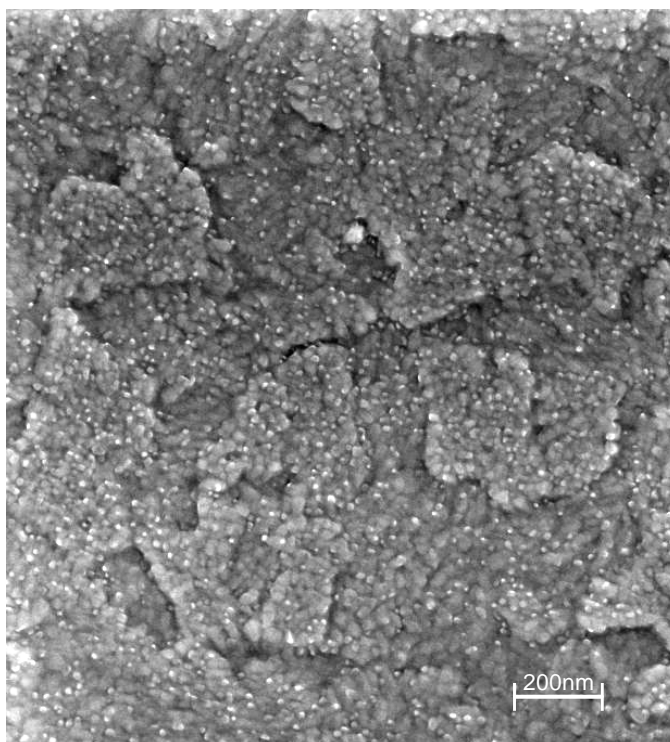
Figure 54. SEM image of 30nm ZnPc on ZnPc4P passivated ITO

If zoomed at some 45° angle to the surface these bright conductive spots look the following way (Figure 55).
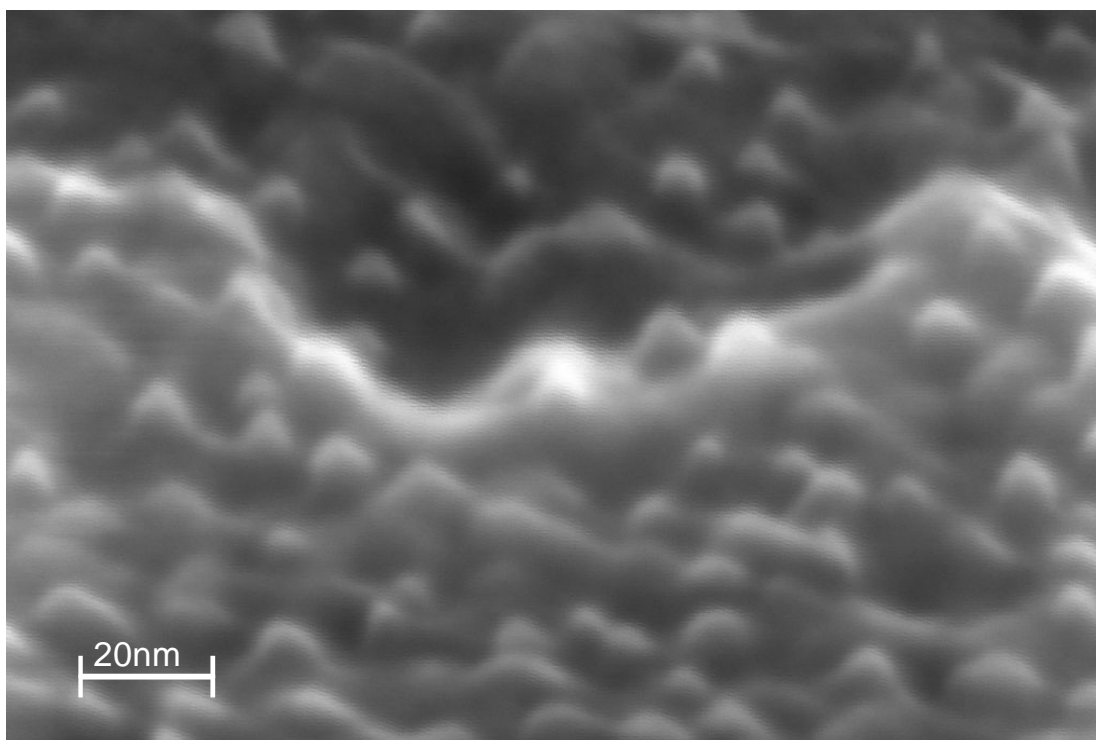
Figure 55. Highly zoomed ZnPc on ZnPc4P passivated ITO

ZnPc4P applied on ITO as passivation helps create multiple highly conductive centers in the layer of evaporated ZnPc. When zoomed in, these conductive centers reveal to be small crystallites in the otherwise amorphous organic layer. So it can be concluded that this passivation manages to cover and prepare the ITO surface on certain spots for probably epitactical crystalline growth. It is well known that evaporated layers of phthalocyanines could be made highly crystalline by increasing the substrate temperature [43]. At room temperature, though, not much can be done about the crystallinity of a vacuum evaporated organic layer. This is where ZnPc4P passivation could help.

To see the effect of this passivation on ZnPc crystallinity, we also conducted a study of evaporating the 30 nm ZnPc layer on ITO at different substrate temperatures. Three layer depositions were carried out on substrates preheated at 60, 90 and 120°C. For those three temperatures both ZnPc4P treated and untreated ITO samples were used. The results are shown for comparison next to each other in two columns in the following Figure 56.
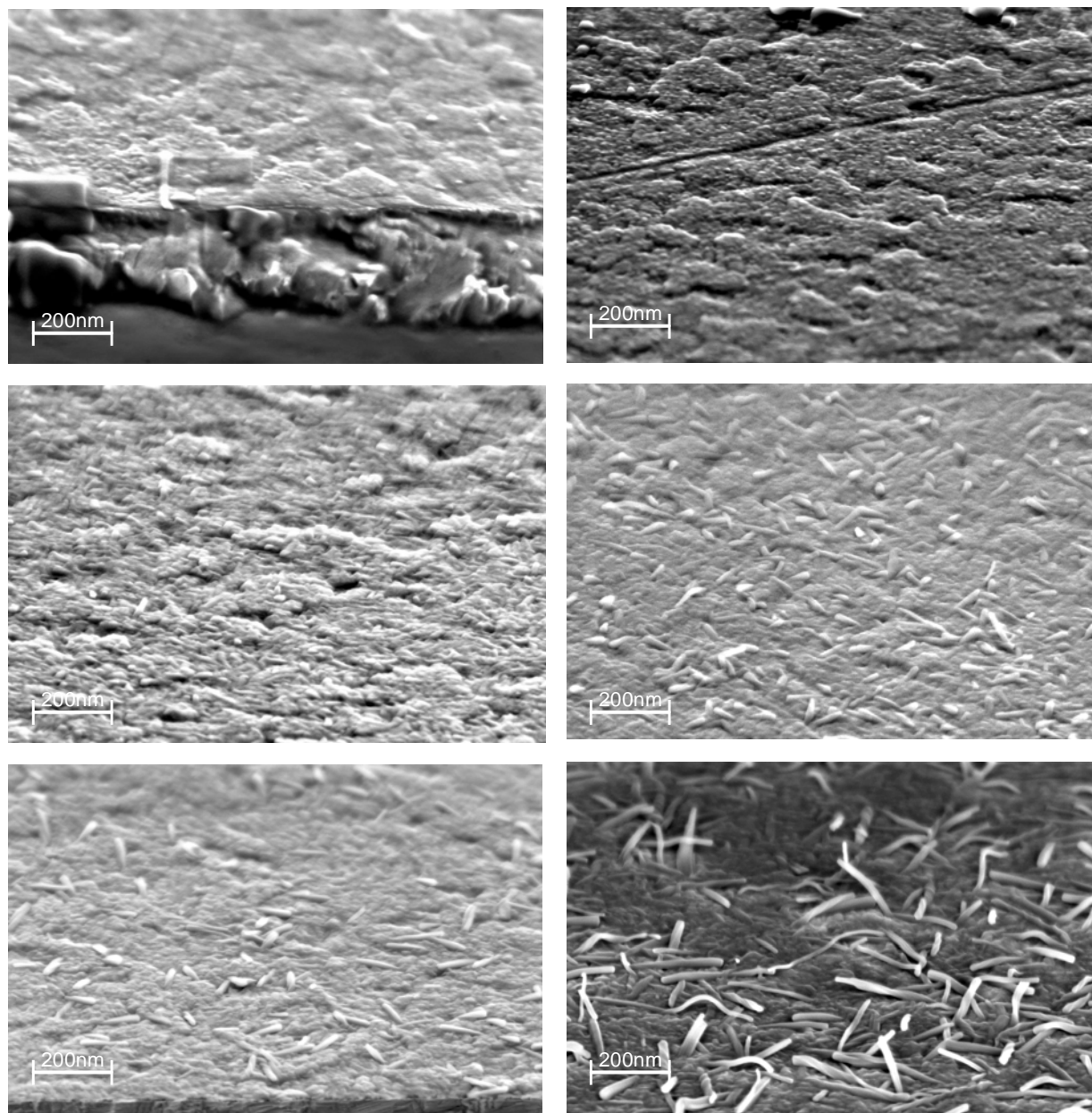
**Figure 56. Study of the 30 nm ZnPc layer crystallinity
in dependence of substrate temperature and ITO passivation.
Left column non-passivated ITO, in descending direcction: 60, 90 and 120°C.
Right column ZnPc4P passivated ITO, in descending direction: 60, 90 and 120°C**

At 60°C ZnPc on untreated ITO shows the same behavior as at room temperature - homogenous coverage with no particularly expressed structures. Compared to this, at the same temperature ZnPc4P passivated ITO gives a prepared substrate on which the ZnPc creates the small crystallite bumps already known to us from the room temperature deposition.

With 90°C the influence on the crystal growth is stronger. The ZnPc molecules are more mobile, thus creating crystalline bumps even on untreated ITO. For the ZnPc4P treated ITO the image shows clearly observable stick-like crystals, along with the otherwise homogenous coverage.

Heating the untreated ITO to 120°C creates a ZnPc layer, whose topology looks like 60°C ZnPc4P treated surface. In comparison to that the 120°C passivated ITO creates so long crystals, that they already bend, as worm-like structure. Those crystals are also too long to be used in a solar cell, because of shortcut danger.

So to summarize, ZnPc4P as ITO passivation leads to a desired crystallinity in the ZnPc layer of the cell, thus enhancing this layer's electrical conductivity. For the same crystallinity to be obtained on a non-passivated ITO surface, one needs to raise the substrate temperature during evaporation with about 30 degrees higher than for a passivated sample.

3.6.3 KPFM

A work function study of ITO passivated with ZnPc4P was made with KPFM. The results are shown on Figure 57.

Topography   Work Function

0 nm   20.0 nm   5.01 eV   5.05 eV

$\Phi = (5.031 \pm 0.005)$ eV
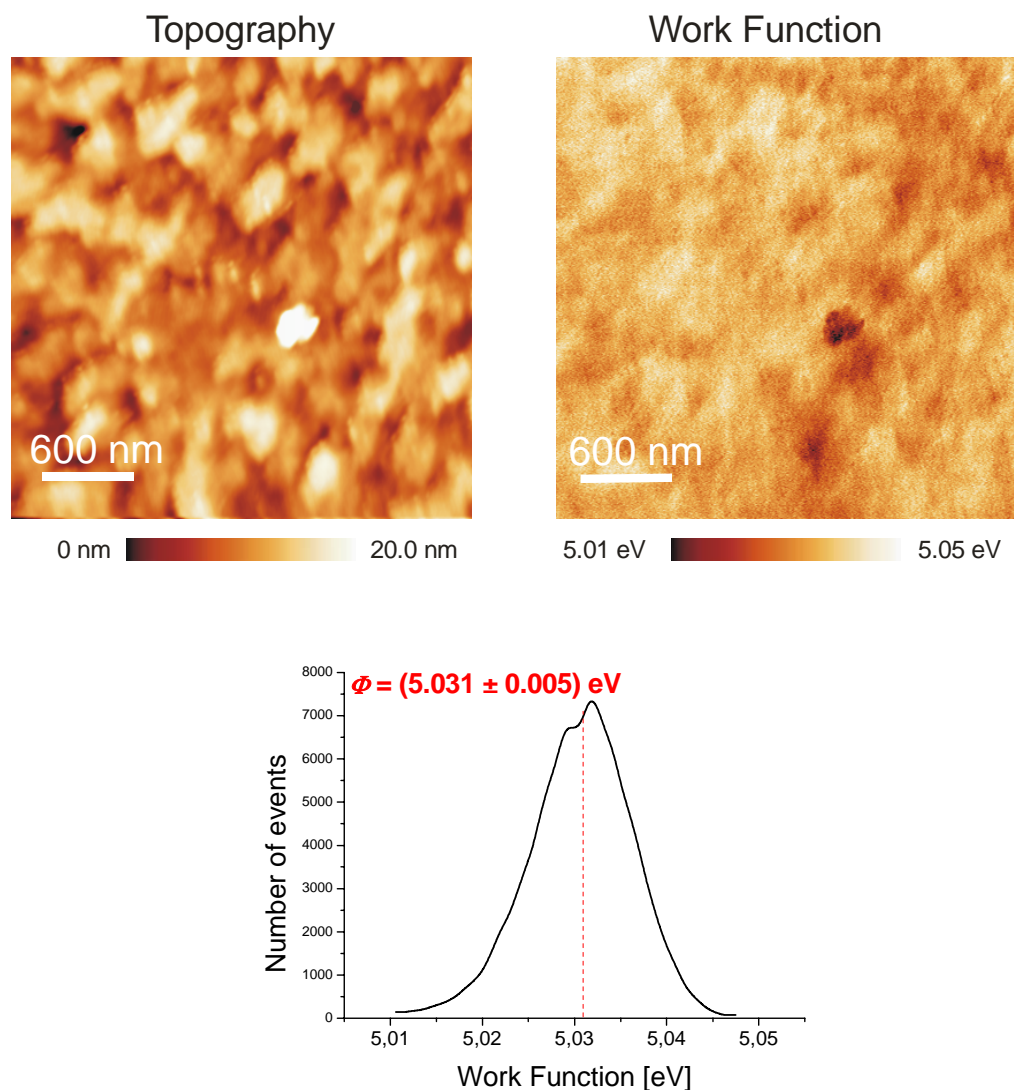
Figure 57. KPFM image of ITO passivated with ZnPc4P. Upper left and right images show the surface topography and work function, respectively. Lower graph presents the statistical distribution of the work function, where the mean value is the weighted average

The topology of ITO stays intact. The work function could not be driven further compared to H_3PO_4, but the value of 5,03 eV is satisfying. Possibly when ZnPc4P dissociates, its first proton the molecule becomes a very weak acid, thus incapable of dissociating a second proton. After all, a strong base as NaOH, for example, is required

to dissociate more protons and get the anion to higher oxidation state. With a weak base like ITO this is not possible. So the charge of the anion stays -1. Eventually this might be also the case with H_3PO_4, which possibly also dissociates only one proton as surface passivation of the weak base ITO. If the two substances create a dipole with the same moment on ITO surface (both dipoles are localized between the phosphoric group and the surface) it is also to expect the same work function value.

3.6.4 XPS

The work function value, measured with XPS, for an ITO sample passivated with ZnPc4P, is 5,2±0,1 eV. The corresponding value for H_3PO_4 (from Table 6) is 4,8 eV. For the KPFM measurement the values for ZnPc4P and H_3PO_4 are the same, but for XPS they differ with 0,4 eV. Having in mind that the error of XPS is 0,1 eV we could not assume that the values measured with XPS are the same even in the error interval. Possibly again the difference comes from the preheating procedure in KPFM.

3.6.5 FTIR of ZnPc4P on TiO$_2$ P25

In the search of more information on the surface adsorption species created by passivating ITO with ZnPc4P we made an FTIR study. Although we finally obtained a spectrum, we had some difficulties on the way.

The first complication was that we could not measure our ITO samples in transmission, because of the glass substrate (not IR transparent). So we tried attenuated reflection FTIR (ATR-FTIR). With this modification of the method we did not receive any signal from the adsorbed organics. Obviously the adsorbed material quantity is very low, so its interaction with the light was very weak. We also tried transmission FTIR spectroscopy on a single crystal, but there was also no trace of organics in the spectrum.

Finally we decided to try FTIR on a powder sample. It would have enough surface area to adsorb a descent quantity of material and provide a better signal. The only problem we met is that no company had powdered ITO to deliver. So it was decided to work with P25 TiO_2 because of the similarity of the two materials. Although not the

same material, P25 could give us precious information about the adsorbed species on its surface.

So a small quantity of TiO$_2$ P25 in powder form was stirred in a 10^{-4}M solution of ZnPc4P and centrifuged. Then the liquid decanted and the rest was again dispersed in deionized water to wash the excess of adsorbed material. After a centrifugation, a second wash was performed with deionized water again, and once more centrifuged. The material left was dried in an excicator. Then two KBr pills were prepared, one containing only P25 as a reference and one with ZnPc4P on P25 as a sample. The FTIR spectrum was then measured and compared to one of the clean ZnPc4P material in KBr (Figure 58).
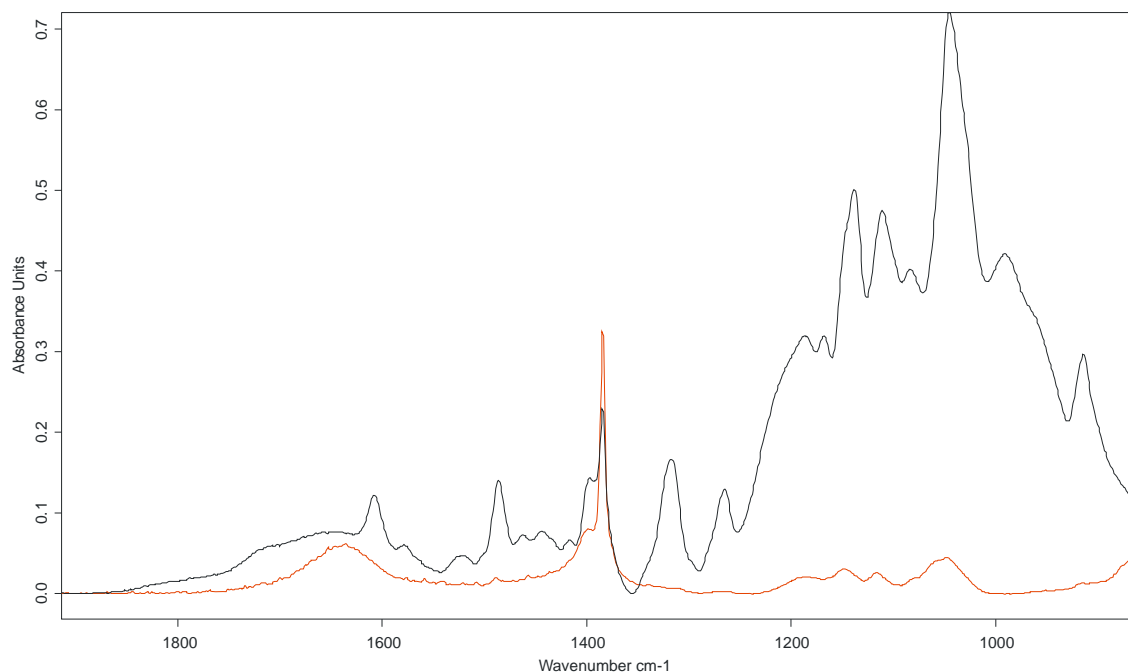
Figure 58. FTIR spectra of ZnPc4P (black) and ZnPc4P on TiO$_2$ P25 (red), both in KBr. In the spectrum of the passivation, adsorbed on the metal oxide, some of its characteristic peaks are found. No additional information on the adsorption species was obtained, due to weak IR absorption of the adsorbed molecules

The comparison of the adsorbed on TiO$_2$ ZnPc$_4$P spectrum to the spectrum of the clean organic material showed, that some characteristic lines match in position in both spectra. This proves that on the metal oxide, even after the two washing steps in the sample preparation, adsorbed ZnPc4P is present. None of the bigger distinguishable characteristic lines has a frequency shift. The most intensive peak in the spectrum of the adsorbed material is the phosphoric group peak (around 1400 cm^{-1}), unlike the original

spectrum of the substance. The intensity increase of this peak could be a clue for ordered structures of the organic substance having the same orientation on the adsorbing surface [66,67]. Nevertheless the result is unclear and suggests further analysis of the adsorption of this organic molecule on TCO surfaces.

As a conclusion, it can be said that by designing ad applying this new TCO passivation material ZnPc4P, the solar cell parameters, except I_{sc} and therefore η, were improved. Improved were also the cell serial and parallel resistances. It was shown that ITO treated with this material offers impressive substrate for ZnPc crystal growth. The positive contribution to the cell is obvious. Further analysis of this material should be done, to learn more about its TCO surface adsorption species and its part in the interface resistance adjustment. This concept of combining organic and acid passivation in one substance was never reported before, so it is a novel approach. ZnPc4P was never used for a TCO passivation in organic solar cells before.

3.7 Cell up scaling and space resolved I/V measurements

Space resolved I/V measurements on solar cells are helpful to visualize the cell electrical properties, resolved in a way, which shows their distribution on the cell surface. The measurement consists of a focused laser beam, scanning the cell surface pixel by pixel and an I/V measurement unit connected to the cell electrodes, to register the photo-current and voltage. Depending on the electrical properties of the particular spot, being illuminated by the laser, the local current and voltage are registered. Then all the data is displayed in color scale, in dependence of the current strength.

For space resolved I/V measurements our current solar cells are too small. With their 0,032 cm^2 and round form, they are difficult to be found and the laser focused on them. That is why for the needs of space resolved measurements, the cells needed to be up-scaled. Also the form had to change from round to rectangular, because the apparatus scans only rectangular areas. So the sample holder for UHV evaporation and the evaporation masks had to be newly designed and reengineered. The cell encapsulation also had to be completely changed to fit and protect the new, rectangular cell from atmosphere. The blueprints of all newly built parts for the up-scaled solar cells can be seen in **Appendix B**.

With the up-scaled solar cell, which had an area of $\approx$1cm^2 (11x9 mm), space resolved I/V measurements can now be conducted. An example of a measurement result for a cell with untreated ITO is shown on Figure 59.
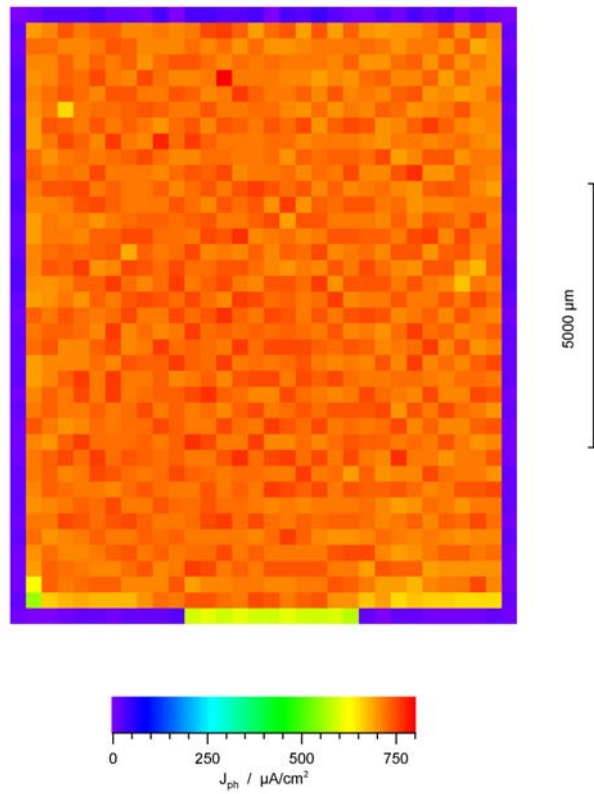
Figure 59. Space resolved I/V measurement of an up-scaled organic solar cell, without ITO passivation or PEDOT:PSS. The blue regions show low currents and the red high current areas. J_{ph} - photocurrent in $\mu A/cm^2$
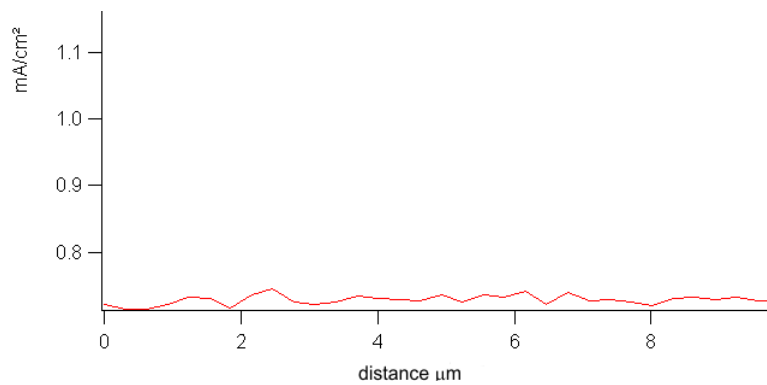
Figure 60. Line scan of the current across the sample. The even distribution of the values is an indication for a homogenous solar cell

Degradation remains a big problem with space resolved measurements. The measurement itself takes minimum 30-40 minutes, in which time the cell degrades, thus showing a space gradient of the measured current. This is not the real picture which should be observed, but degradation with time creates this effect. That is why the measurement shown on Figure 59 had to be conducted with a very large laser spot, which of course does not allow a fine resolution. Also the scanning speed was set to maximum, so that the degradation effect does not affect the measurement.

On the next Figure 61, the I/V characteristic of an up-scaled cell is shown, produced on H_3PO_4 passivated ITO.
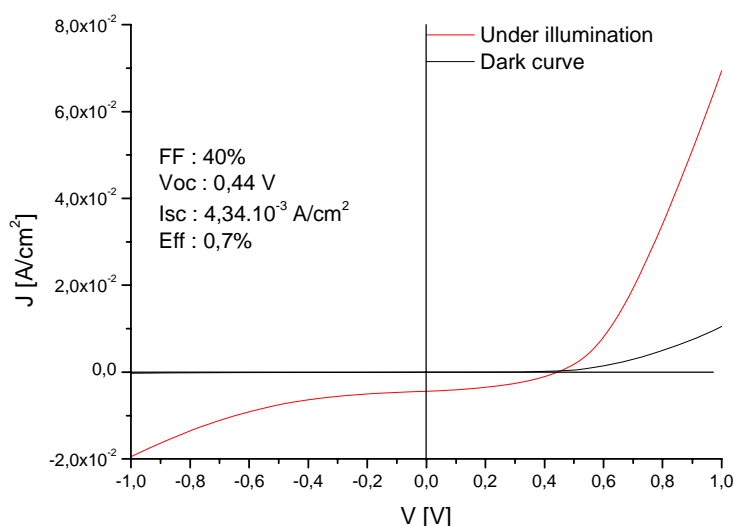
Figure 61. I/V characteristic of an up-scaled (1cm^2) solar cell, on H$_3$PO$_4$ passivated ITO. The increasing R$_p$ in the negative voltage region and the low J$_{sc}$ value are an indication for pinholes and increased leakage currents. The efficiency is as expected lower, than for the H$_3$PO$_4$ passivated ITO cell with 0,032 cm^2 area

As expected the cell efficiency is lower than the corresponding H_3PO_4 passivated 0,032 cm^2 cell. In the negative voltage region a gradual increasing of the R_p is observed. Together with the low Jsc value for this cell, this is an indication for leakage currents and pinholes through the cell. Possible reasons for this include particle contamination of the TCO surface, high structures of the transparent contact interpenetrating the cell or inhomogeneous cell thickness over this "big" area.

4 Ca and Mg as counter electrode materials

Although the current work is concentrated on the interface TCO-organics, an additional experiment was made in order to observe the effect of change in the work function of the metal back-electrode. Changing the material of the metal electrode with one possessing different work function should change V_{oc} of the cell [68]. We produced standard cells with untreated ITO where instead of Al as metal electrode Ca and Mg were used. The resulting I/V characteristics are plotted on Figure 62.
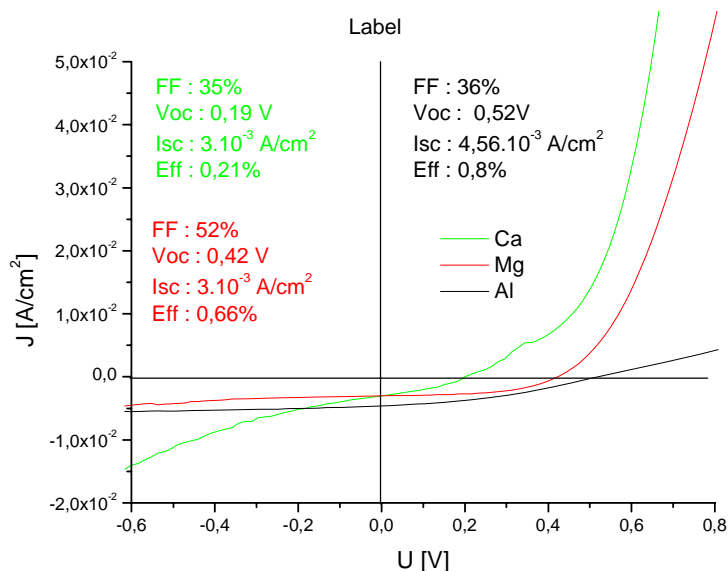
Figure 62. I/V curves of standard cells, with only difference the metal back-electrodes. All cells are produced on untreated ITO.

An interesting result, since by changing the work function of ITO with surface passivations we did not observe such significant change of the cell V_{oc}. A possible explanation is that the ITO work function change was not in that big range. We also changed the ITO work function to higher values and not to lower, as in the case with Ca and Mg. Figure 63 shows the values of work function for the three different metals Ca, Mg and Al [69,70].
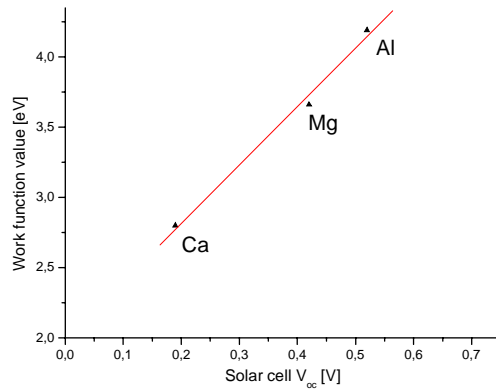
Figure 63. Plot of the work function of the metals Ca, Mg and Al against the corresponding solar cell V$_{oc}$ achieved with these metals as back electrodes

The work function values of the three metals seem to be in the same order as the corresponding cell V$_{oc}$ values. Moreover, the almost linear dependence of V$_{oc}$ from the work function was not observed while changing the work function of ITO.

An explanation of the lower cell efficiency, with lowering the back-electrode work function can be sought in the band energy diagram of the interface, responsible for electron collection at that electrode (Figure 64).
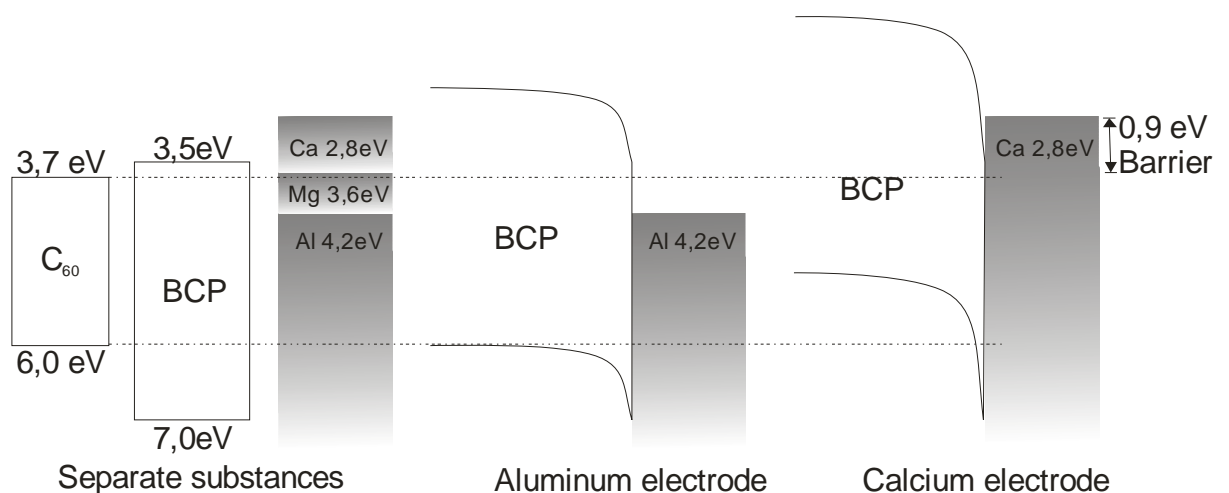
Figure 64. Band diagram section, visualizing the interface between back contact and C60, through the BCP buffer. Bending of the bands of BCP favors electron transport to Al, but creates an energetic barrier with Ca, as a back-contact (similar to Mg, not shown on the figure). Values for C60 are obtained from [59] as measured by us, and differ from the ones shown on the general cell energy band diagram from literature, shown in 1.3

The energy band diagram illustrates the bending of the energy bands of the organic buffer in contact with the back-electrode. In the case of aluminum as a back-electrode, a smooth passage for electrons coming from the acceptor layer is possible. Changing the electrode to a metal with lower work function, creates an energy barrier (of 0,9 eV, in the case of Ca), which suspends the electron transport to the Fermi level of the metal electrode.

5 Summary

In this work, organic solar cells consisting of Zinc Phthalocyanine (ZnPc), Fullerene (C_{60}) and Bathocuproine (BCP), with an overall thickness of about 70 nm, were studied. In this layer system, interface processes dominate over their bulk properties. The most challenging interfaces in these cells are between inorganic electrodes and organic photoactive layers, where an ohmic contact is difficult to achieve. In the present dissertation, a comprehensive study of the Indium-Tin Oxide (ITO)-organics interface was carried out. The main topic of this work is to improve the contact resistance by chemical passivation of ITO surface and enhance charge carrier transport through this interface.

The surface of the ITO electrode, as the main focus of the current dissertation, was thoroughly examined, before any modifications were undertaken. To establish an understanding of the commercial ITO substrates, a comparison between different ITO types, offered by the industry was made. On the basis of optical transmission, electrical resistance and surface homogeneity, 5 ohm ITO was chosen as a solar cell substrate.

Annealing of the ITO electrode and measuring its resistance in situ, showed that up to 250°C this TCO can be reversibly heated and cooled. Irreversible change in resistance appears to happen above this temperature. The work function of ITO, as an important parameter and a reference value, was measured using X-ray Photoelectron Spectroscopy (XPS) and Kelvin Probe Force Microscope (KPFM). The resultant values were in good agreement: 4,2±0,1 and 4,3±0,2 eV, respectively.

The chemical stability of the active layer materials, under air and UV irradiance was examined using Fourier-Transform Infrared Spectroscopy (FTIR) spectroscopy. No significant change in substance IR absorption spectrum, before and after air/UV treatment, was observed. The initial purity of the material 99%, rest unchanged.

An optical study of the solar cell was made, with a computer simulation. For this, layer thickness, refraction index (**n**) and extinction coefficient (**k**) for each cell material were supplied to a computer program. **n** and **k** were calculated from spectroscopic measurements of material reflection and transmission in the visible region. The optical cell simulation yielded the sun light intensity distribution in the solar cell, depending on the material properties. The simulation showed that the good absorption properties of ZnPc and C60 are not fully utilized. The intensity distribution of the wavelengths, beneficial for the two materials (570-720 nm for ZnPc, 420-520 nm for C_{60}), is very wide, thus no wavelength is absorbed completely by the narrow layers. This is an indication of the big potential of these solar cells, if geometry can be modified. In addition, the optical simulation demonstrates, that wavelengths around the sun energy

spectrum maximum ($\approx$540 nm) are very weakly absorbed, thus broadening the potential of these cells to better absorption through additional absorber dye mixing or extending the current absorption with chemical modifications.

The optical simulation of the solar cell emphasized on the importance of precise layer thickness. As a standard, calibration of the deposition controllers is done with profilometer, despite its 10% error. The calibration was revised with X-ray reflection and Ellipsometry. X-ray reflection showed for ZnPc 20% and for C_{60} 7% higher thicknesses, than measured with the deposition controllers. Ellipsometry confirmed for ZnPc and C_{60} a thickness with 14%, respectively 17% higher, than by the measurements of the deposition controllers. The structure of the ZnPc film was determined with a fit of the x-ray reflection data and two different molecule orientations were found. Ellipsometry proved BCP and C_{60} to have too high roughness for x-ray analysis.

As the main highlight of the present work, the chemical modification of the ITO surface with monomolecular layer, has the objectives to adjust its conduction band to the valence band (HOMO) of ZnPc and improve the electrical conductivity through this interface. Two general approaches were examined.

Introducing an aromatic passivation on the ITO surface, consisting of covalently bound 8-Hydroxyquinoline, yielded a solar cell with 1,3% efficiency (η), compared to 0,8% for untreated ITO. The cell parameter, contributing mostly for this improvement, is the increased short circuit current (J_{sc}) $5,5.10^{-3} A/cm^2$. The corresponding value for J_{sc} of untreated ITO cell is $4,56.10^{-3} A/cm^2$. Comparison showed also, that the fitted serial resistance (R_s) of the passivated cell $15,19\pm0,28\ \Omega.cm^2$ is roughly four times less than the one for non-passivated ITO cell $63,25\pm0,76\ \Omega.cm^2$. Most likely, the serial resistance is influenced by improved contact resistance, at this interface. Since conductivity between ITO and ZnPc is improved with an aromatic termination of the ITO surface, it is concluded that an aromatic ITO passivation is helpful for the cell performance.

Creation of a surface dipole, by dipping ITO in acidic solutions, increased its work function from $4,2\pm0,2$ eV for untreated ITO to $4,8\pm0,1$ eV for H_3PO_4 passivated and $4,8\pm0,1$ eV for HIO_4 passivated ITO. This had positive influence on the solar cell parameters. Improved were mainly the fill factor (FF) and J_{sc} which for H_3PO_4 passivated ITO were: FF 0,54%, I_{sc} $6.10^{-3} A/cm^2$ and for HIO_4 FF 0,54%, I_{sc} $5,28.10^{-3} A/cm^2$. The cell parameter improvement contributed to the efficiency (η) the following way: η_{H3PO4} 1,72%, η_{HIO4} 1,5%. Both acid passivations brought the Rs of the solar cells to very lower values, $3,06\pm0,0025\ \Omega.cm^2$ for H_3PO_4 and $2,82\pm0,039\ \Omega.cm^2$ for HIO_4, thus improving the contact resistance of the ITO-ZnPc interface and charge carrier transport from the organic layer to the TCO electrode. XPS proved that phosphoric acid creates very stable (up to $\approx$300°C) adsorption species on ITO surface.

A surface dipole in the opposite direction, created with an alkaline treatment of ITO (NH_3 solution), ruined the solar cell, which showed no photocurrent at all.

From all tested ITO surface chemical modifications, organic and acid passivations had the biggest contribution to solar cell performance.

To combine both requirements contributing to cell performance, aromatic passivation and anionic (acid) surface dipole, a new chemical passivation for ITO was designed, namely Zincphthalocyaninetetraphosphonic acid (ZnPc4P). This concept of combining organic and acid in one substance for TCO passivation was never reported before. ZnPc4P was never used for a TCO passivation in organic solar cells up to the present. It is a water soluble, aromatic acid molecule, even from the phthalocyanine class. It has four $-PO_3H_2$ groups, covalently bound to the benzene rings of the four benzopyrrole rests. The acid groups were chosen by the high stability of adsorbed phosphate species on ITO, proven by XPS studies. ZnPc4P retained this property, so that after passivating ITO with it, the blue coloration could not be removed by washing with water. This passivation created a surface dipole, which pushed the ITO work function to the highest value of 5,2 eV, comparable to that of PEDOT:PSS. Solar cells, made on ITO passivated with ZnPc4P, had the highest FF ever observed by us: 57%. The open circuit voltage (V_{oc}) is at the upper limit, which this cell concept ever showed 0,54V. J_{sc} with a value of $4,2.10^{-3}A/cm^2$ was not significantly improved. The fitted R_s of the cell $2,55\pm0,1\ \Omega.cm^2$ is the lowest ever measured by us and is attributed to an improved contact resistance on the ITO-ZnPc interface. R_p of $1351\pm62\ \Omega.cm^2$ is almost the double, compared to other passivations, and stands for extremely low recombination of charge carriers and lack of leakage currents. Although the power conversion efficiency is 1,3%, the influence of this new treatment on the cell parameters proves the potential of the cell concept.

In order to obtain a better understanding of V_{oc}, a counter-electrode study was made, where instead of the standard aluminum, Ca and Mg as materials with different work function were used. It showed that V_{oc} is in linear dependence of the back-electrode work function in these solar cells. This was attributed to the creation of an energetic barrier hindering electron transport from the bulk to the contact.

It can be summarized, that in the present dissertation the charge transport through the interface ITO-organics in $ZnPc/C_{60}$ organic solar cells was studied and optimized. Using a self designed chemical passivation, the work function of ITO electrode was adjusted for optimal charge transport. It is shown that driving the TCO work function to higher values exhausts its contribution to cell improvement, so different ways of optimization have to be sought. In this work it was shown that mono-molecular layers can be used as buffers in solar cells and thus they can be made thinner and economical in production through buffer layer substitution.

6 Zusammenfassung

Diese Arbeit befasst sich mit der Untersuchung einer organischen Solarzelle, deren aktive Schichten aus Zink-Phthalocyanin (ZnPc), Fullerenen (C_{60}) und Bathocuproin (BCP) mit einer Gesamtdicke von 70 nm bestehen,. Innerhalb dieses Systems dominieren Grenzschichtenprozesse gegenüber den Volumeneigenschaften. Diejenigen Grenzflächen, die die größte Herausforderung darstellen, liegen zwischen anorganischen Elektroden und organischen, photoaktiven Schichten, in deren Bereich ein ohmscher Kontakt nur schwer hergestellt werden kann. In der vorliegenden Dissertation wurde eine umfassende Studie über die Grenzfläche zwischen Indium-Zinnoxid (ITO) und organischer Schicht durchgeführt. Der Schwerpunkt dieser Arbeit liegt auf der Reduktion des Kontaktwiderstandes durch chemische Passivierung der ITO-Oberfläche, um eine Verbesserung des Ladungstransports durch diese Grenzfläche zu erreichen.

Die Oberfläche der ITO-Elektrode ist ein Fokus der vorliegenden Dissertation und wurde deshalb eingehend untersucht, bevor jegliche Modifizierungen vorgenommen wurden. Zum besseren Verständnis kommerzieller ITO-Substrate wurden unterschiedliche, von der Industrie zur Verfügung gestellte ITO-Typen verglichen. Durch Gegenüberstellung der optischen Transmissionen, elektrischen Widerstände und Oberflächenhomogenitäten wurde ein ITO mit 5 Ohm/square als besonders geeignet ausgewählt.

In-situ-Messungen des Widerstandes solcher Elektroden in Temperexperimenten zeigten, dass dieser sich bis 250°C mit der Temperatur reversibel ändert. Irreversible Veränderungen hinsichtlich des Widerstands scheinen erst oberhalb dieser Temperatur einzutreten. Die Austrittsarbeit von ITO als wichtiger Parameter und als Referenzwert wurde mittels Röntgenphotoelektronenspektroskopie (XPS) und Kelvinsondenkraft-mikroskopie (KPFM) gemessen. Die daraus resultierenden Messwerte, 4,2±0,1 und 4,3±0,2 eV, verzeichneten eine gute Übereinstimmung.

Die chemische Stabilität von ZnPc und C_{60} unter dem Einfluss von Luft und UV-Bestrahlung wurde mittels Fourier-Transform-Infrarot-(FTIR)-Spektroskopie untersucht. Nach der Luft/UV-Behandlung waren im IR-Absorptionsspektrum der Substanzen keine signifikanten Veränderungen zu beobachten. Die anfängliche Reinheit des 99%-igen Materials blieb unverändert.

Für eine optische Studie der Zelle wurden die einzelnen Schichten in Transmission und Reflexion spektroskopisch vermessen. Aus diesen Spektren wurden dann Brechungsindex n und Extinktionskoeffizient k für den ganzen sichtbaren Spektralbereich berechnet. Diese Werte dienten in einer optischen Computersimulation zur Bestimmung der Intensitätsverteilung innerhalb der Zellschichten. Die Simulation demonstrierte, dass die guten Absorptionseigenschaften von ZnPc und C_{60} nicht vollständig genutzt werden. Die (stationäre) räumliche Intensitätsverteilung bei den Wellenlängen, die in den beiden Materialien absorbiert werden können (570-720 nm für ZnPc, 420-520 nm für C_{60}), ist viel breiter als die entsprechende Schicht. Daher wird in beiden Fällen das Licht von den Schichten nicht vollständig absorbiert. Außerdem treffen die Intensitätsmaxima der genannten Spektralbereiche nicht in die Mitte der Schichten. Daraus ergibt sich das große Potential dieser Solarzellen, falls

die Geometrie modifiziert werden kann. Zudem zeigt die Studie, dass Wellenlängen nahe dem Maximum des Sonnenenergiespektrums ($\approx$540 nm) wenig absorbiert werden. D.h. diese Zelle hat weiteres Potential die Absorption dadurch zu verbessern, dass einerseits durch Beimischung von zusätzlichen Farbstoffen oder andererseits durch Verbreiterung der aktuellen Absorption mittels chemischer Modifikationen.

Die optische Simulation der Solarzelle unterstrich die Wichtigkeit der genauen Angabe der Schichtdicken. Standardmäßig wird die Kalibrierung der Schichtdickenmeßgeräte mit einem Profilometer durchgeführt. Diese Kalibrierung wurde durch Röntgenreflexion und Ellipsometrie überprüft. Die Röntgenreflexion zeigt für ZnPc und C_{60} um je 20% und 7% höhere Dicken als mit dem Schichtdickenmeßgerät gemessene. Die Ellipsometrie bestätigte diese Tendenz für ZnPc und C_{60} mit den Werten von 14% bzw. 17% höherer Dicke. Außerdem wurde die Struktur der ZnPc-Schicht anhand einer Modellierung der Röntgenreflexionsdaten untersucht und Hinweise für zwei unterschiedliche Molekülorientierungen gefunden.

Ein Hauptpunkt der vorliegenden Arbeit – die chemische Modifikation der ITO-Oberfläche mit einer monomonekularen Schicht – verfolgt das Ziel, dessen Leitungsband ans Valenzband (HOMO) von ZnPc anzupassen, um die elektrische Leitfähigkeit durch diese Grenzschicht zu verbessern. Zwei Methoden wurden untersucht.

Die erste Methode besteht darin, durch eine kovalent gebundene, aromatische Monolage, bestehend aus 8-Hydroxyquinolin, die ITO-Oberfläche chemisch zu passivieren. Bei der zweiten Methode wird durch nasschemische Behandlung mit verschiedenen anorganischen Säuren ein Oberflächendipol auf der ITO-Oberfläche erzeugt, der zu einer Erhöhung der Austrittsarbeit der Elektrode führt.

Solarzellen, die auf derart präparierten Substraten hergestellt wurden, zeigten im ersten Fall einem Wirkungsgrad von 1,3% (η) im Vergleich zu 0,8% bei unbehandeltem ITO. Die Verbesserung ist vor allem dem hohen Kurzschlussstrom von J_{sc}= 5,5.10^{-3}A/cm^2 zuzuschreiben. Der entsprechende Wert für eine Zelle mit unbehandeltem ITO ist J_{sc} = 4,56.10^{-3}A/cm^2. Ein Vergleich zeigte ebenfalls, dass der serielle Widerstand (R_s) der passivierten Zelle mit 15,19$\pm$0,28 Ω.cm^2 etwa viermal kleiner ist als derjenige für die nicht-passivierte ITO-Zelle mit 63,25$\pm$0,76 Ω. cm^2. Höchstwahrscheinlich wurde der serielle Widerstand durch einen verbesserten Kontaktwiderstand an dieser Grenzfläche beeinflusst. Daraus lässt sich schließen, dass eine aromatische Passivierung des ITO die Zelleigenschaften positiv beeinflusst.

Die Bildung eines Oberflächendipols durch das Eintauchen von ITO in Säurelösungen erhöhte dessen Austrittsarbeit von 4,2$\pm$0,2 eV bei unbehandeltem ITO auf 4,8$\pm$0,1 eV bei H_3PO_4– oder HIO_4–passiviertem ITO. Dies beeinflusste die Solarzellenparameter in positiver Weise. Hauptsächlich wurden Füllfaktor (FF) und J_{sc} verbessert. Für H_3PO_4-passiviertes ITO betrugen sie FF=54% und I_{sc}= 6. 10^{-3}A/cm^2 und für HIO_4-passiviertes ITO FF=54% und I_{sc}=5,28.10^{-3}A/cm^2. Die Verbesserung der Zellparameter trugen wie folgt zur Effizienz (η) bei: η_{H3PO4}= 1,72%, η_{HIO4}= 1,5%. Beide Säurepassivierungen drückten R_s der Solarzellen auf sehr niedrige Werte, indem sie den Kontaktwiderstand der ITO-ZnPc-Grenzfläche verringerten. XPS zeigte, dass auf der ITO-Oberfläche sehr stabile Verbindungen (bis zu $\approx$300°C) der Phosphorsäure existieren.

Ein Oberflächendipol in entgegen gesetzter Richtung, hergestellt durch eine alkalische Behandlung (in NH_3-Lösung) von ITO, zerstörte die Solarzelle, die keinerlei Photostrom mehr aufwies.

Von allen getesteten, chemisch modifizierten ITO-Oberflächen, brachten organische und Säurepassivierungen die größte Steigerung im Wirkungsgrad.

Um die beiden Vorteile, resultierend aus aromatischer Passivierung und anionischem Oberflächendipol, zu kombinieren, wurde eine neue chemische Passivierung für ITO mittels Zink-Phthalozyanintetraphosphonische Säure (ZnPc4P) designt. Dabei handelt es sich um ein wasserlösliches, aromatisches Säuremolekül, das vier $-PO_3H_2$ Gruppen aufweist, die kovalent an die Benzolringe der vier Benzopyrrolreste gebunden sind und das zudem aus der Klasse der Phthalozyanine stammt. Die Stabilität der Phosphat-ITO-Verbindung bleibt auch hier erhalten, so dass nach der Passivierung mit ZnPc4P die blaue Färbung auf ITO nicht mit Wasser entfernt werden konnte. Diese Passivierung schuf einen Dipol, der die ITO-Austrittsarbeit auf den höchsten Wert von 5,2 eV verschob und damit nur mit PEDOT:PSS vergleichbar war. Solarzellen auf Basis von ZnPc4P-passiviertem ITO hatten den höchsten von uns beobachtete FF von 57%. Die offene Klemmenspannung (V_{oc}) liegt am oberen Limit, das dieses Zellkonzept jemals aufwies: 0,54V, während J_{sc} mit einem Wert von 4,2. $10^{-3}A/cm^2$ nicht bedeutend verbessert wurde. Der ermittelte Wert für R_s der Zelle ist mit 2,55±0,1 $\Omega.cm^2$ der niedrigste in dieser Arbeit gemessene und wird einem verbesserten Kontaktwiderstand an der ITO-ZnPc-Grenzfläche zugeschrieben. R_p mit einem Wert von 1351±62 $\Omega. cm^2$ ist im Vergleich zu anderen Passivierungen beinahe doppelt so hoch und steht für eine äußerst niedrige Rekombination von Ladungsträgern und geringe Leckströme. Obgleich der Wirkungsgrad nur 1,3% beträgt, beweist der Einfluss dieser neuen Behandlung auf die Zellparameter das Potential sowohl des Zell- wie auch des Passivierungskonzepts.

Zum besseren Verständnis von V_{oc} wurde eine Studie an der Rückelektrode durchgeführt. Anstatt einer Standardelektrode aus Al wurde hier Ca und Mg mit ihren niedrigeren Austrittsarbeiten verwendet. Die Studie zeigte, dass V_{oc} sich proportional zur Austrittsarbeit der Rückelektroden verhält. Dieses Ergebnis wurde der Bildung einer Energiebarriere, die den Elektronentransport an der Grenzfläche zur Rückelektrode behindert, zugeschrieben.

Abschließend lässt sich sagen, dass in der vorliegenden Dissertation der Ladungstransport an der ITO-ZnPc-Grenzfläche in $ZnPc/C_{60}$ Solarzellen untersucht und optimiert wurde. Die Verbesserung der Zellparameter lediglich durch Erhöhung der ITO- Austrittsarbeit mittels Säurepassivierung war erschöpft. Es mussten neue Wege zur Optimierung erkundet werden. Dafür wurde hier eine neu designte chemische Passivierung vorgeschlagen, wodurch die Austrittsarbeit der ITO-Elektrode angepasst wie auch der Kontaktwiderstand für einen optimalen Ladungstransport verringert wurde. Gleichzeitig wurde gezeigt, dass mono-molekulare Schichten als Puffer in Solarzellen genutzt werden können.

7 Appendix

7.1 Appendix A: Theoretical basis of material constants "n" and "k" calculation [71]

In chapter 3.3 a theoretical computer simulation of our cell is done, in order to learn about the distribution of light within the cell layers and be able to optimize this. For the computer simulation one needs to input data for each separate layer. This data includes the refraction index "**n**" and extinction coefficient "**k**" of each substance. These parameters can not be measured directly, so they have to be calculated from other measured data. With the program "Optik", written by Kristian Peter, this is possible. From measured reflection "**R**" and transmission "**T**" of each separate layer, **n** and **k** can be calculated.

In the following section the principle of calculating **n** and **k** from **R** and **T** is described.
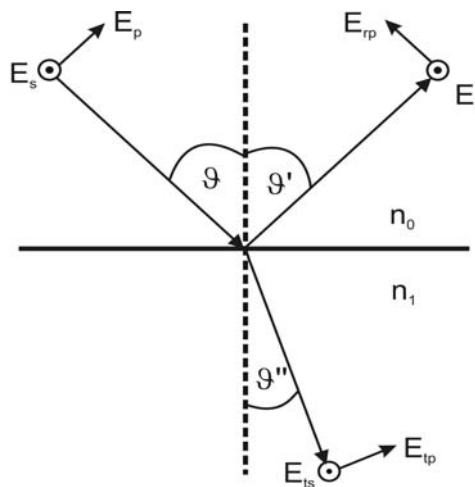
Figure 65. Reflection and transmittance of a plane wave at an interface; indices: s-perpendicular, p-parallel, r-reflected, t-transmitted

The reflection and transmittance of a plane wave $\vec{E}$ at an interface of two mediums (Figure 65) is characterized by Fresnel-law:

$$r_\perp = \frac{n_0 \cos\vartheta - n_1 \cos\vartheta''}{n_0 \cos\vartheta + n_1 \cos\vartheta''} \qquad r_\| = \frac{n_1 \cos\vartheta - n_0 \cos\vartheta''}{n_1 \cos\vartheta + n_0 \cos\vartheta''} \qquad (1)$$

$$t_\perp = \frac{2n_0 \cos\vartheta}{n_0 \cos\vartheta + n_1 \cos\vartheta''} \qquad t_\| = \frac{2n_0 \cos\vartheta}{n_1 \cos\vartheta + n_0 \cos\vartheta''} \qquad (2)$$

$r_\|, t_\|$: Reflection- and transmittance coefficient describing the component of the E-vector parallel to plane of incidence;

$r_\perp, t_\perp$: Reflection- and transmittance coefficient describing the component of the E-vector perpendicular to plane of incidence;

Regarding transmittance the refracted wave continues without phase skipping.

Concerning the reflected wave, two cases have to be considered:

1. $n_0 < n_1$:There is a phase shift of π in the perpendicular component. If $\vartheta + \vartheta'' > \dfrac{\pi}{2}$ then the parallel component has also a phase shift of π.

2. $n_0 > n_1$:The perpendicular component has no phase-shift, but the parallel component has a shift of π in case $\vartheta + \vartheta'' > \dfrac{\pi}{2}$.

Concerning absorbing materials, the refractive index $\bar{n}$ becomes complex:

$$\bar{n} = n + ik \qquad (3)$$

and the absorbing coefficient α is defined as $\alpha = \dfrac{4\pi k}{\lambda}$, where **k** is the so called extinction coefficient.

In the case of perpendicular incidence of light the Frensel formulas can be simplified to:

$$r = r_\perp = \frac{\bar{n}_0 - \bar{n}_1}{\bar{n}_0 + \bar{n}_1} \qquad (4)$$

112

$$t = t_\perp = \frac{2\overline{n_0}}{\overline{n_0} + \overline{n_1}} \tag{5}$$

For reflection: $R = |r|^2 = \dfrac{\left(n_0 - n_1\right)^2 + \left(k_0 - k_1\right)^2}{\left(n_0 + n_1\right)^2 + \left(k_0 + k_1\right)^2}$

$$\tag{6}$$

The transmittance can be calculated by using the equation: $T = 1 - R$

$$\tag{6a}$$

In order to analyze the transmittance and reflection of a thin film on a thick coplanar substrate we have to divide the problem into two sections. First reflection and transmittance of a thin coplanar film will be considered and finally reflection and transmittance of a thick coplanar layer will be examined.

Reflection and transmittance of a thin coplanar film

A thin coplanar film with thickness d and refractive index $\overline{n_1}$, which is located between two mediums with $\overline{n_0}$ and $\overline{n_2}$ is examined. A multiple reflection on the upper- and lower-side of the film occurs (Figure 66).
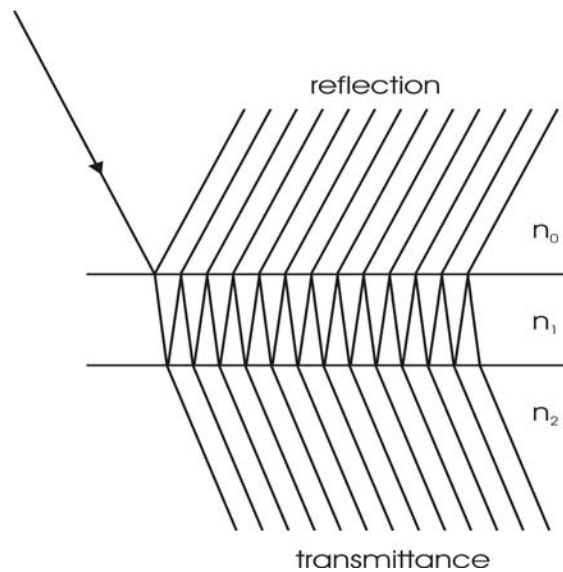

Figure 66. Thin coplanar film and its interaction with light

113

The amplitude decreases by the factor $\exp\left(-\dfrac{2\pi k d}{\lambda}\right)$ when the layer is penetrated once. Moreover a phase shift of $\Delta\varphi = \dfrac{2\pi n d}{\lambda}$ occurs. These effects will be taken into account by multiplying the plane wave with $e^{i\delta}$. For δ we have the formula:

$$\delta = \frac{2\pi d(n+ik)}{\lambda} \tag{7}$$

The following formulas will include the indices "i" and "j". The index "i" means that light comes from the medium i and the index "j" denotes the medium where the light is reflected respectively where it penetrates. The reflection- and transmittance-coefficients are r_{ij} and t_{ij} correspondingly.

For the calculation of the complete transmittance coefficient after infinite reflection in the layer one get the equation:

$$t = \left[t_{01} e^{i\delta} \sum_{j=0}^{\infty} \left(r_{12} r_{10} e^{2i\delta} \right)^{j} \right] \cdot t_{12} \tag{8}$$

Explanation of equation (8):

$t_{01} e^{i\delta}$ • The light penetrates in the medium 1 and is weakened because of covering a distance of one layer thickness. It reaches the interface 1-2.

$\displaystyle\sum_{j=0}^{\infty} \left(r_{12} r_{10} e^{2i\delta} \right)^{j}$ • The light will be reflected into the layer infinite number of times. Every time the amplitude decreases by the factor $e^{2i\delta}$ because the light has to go twice through the layer thickness d until it will be back at the interface 1-2. The components of the light which have already been reflected more often are weaker. For this reason there is the exponent "j" in the sum.

t_{12} • Every time the light goes with the „probability" t_{12} through the interface 1-2.

Appendix A. Theoretical basis of material constants "n" and "k" calculation

Accordingly there is an equation for the reflection coefficient:

$$r = r_{01} + \left[t_{01}r_{12}e^{2i\delta} \sum_{j=0}^{\infty} \left(r_{12}r_{10}e^{2i\delta} \right)^j \right] \cdot t_{10} \qquad (9)$$

Explanation of equation (9):

r_{01}
- The part of light which is reflected immediately at the interface 0-1.

$t_{01}r_{12}e^{2i\delta}$
- The part which is transmitted at the interface 0-1 and reflected at the interface 1-2. The light has covered a distance of 2d when it reaches the interface 0-1 again. The amplitude has decreased by $e^{2i\delta}$.

$\sum_{j=0}^{\infty} \left(r_{12}r_{10}e^{2i\delta} \right)^j$
- The light will be reflected into the layer infinite times. Every time the amplitude decreases by the factor $e^{2i\delta}$ because the light has to go twice through the layer thickness d. The components of the light which have already been reflected more often are weaker. For this reason there is the exponent j in the sum.

t_{10}
- Every time the light goes with the „probability" t_{12} through the interface 1-0

In order to simplify the equations (8) and (9) it is used $r_{01} = -r_{10}, t_{10} = 1 - r_{10}$ and the equations (4) and (5). Furthermore the equations (8) and (9) include geometric series which can be written as $\sum_{k=0}^{\infty} q^k = \dfrac{1}{1-q}$ if 0<q<1.

Consequently the following formulas arise from these transformations:

$$r = \frac{r_{01}e^{-i\delta} + r_{12}e^{i\delta}}{e^{-i\delta} + r_{01}r_{12}e^{i\delta}} \quad (10) \qquad t = \frac{t_{01}t_{12}}{e^{-i\delta} - r_{10}r_{12}e^{i\delta}} \quad (11)$$

Using the formulas (4) and (5) (that are valid for the reflection and transmittance on an interface) for $r_{01}, r_{12}, t_{01}, t_{12}$ we obtain the complete reflection and transmittance coefficient of a thin coplanar layer.

$$r = \frac{(\bar{n}_0 - \bar{n}_1)(\bar{n}_1 + \bar{n}_2)e^{-i\delta} + (\bar{n}_1 - \bar{n}_2)(\bar{n}_0 + \bar{n}_1)e^{i\delta}}{(\bar{n}_0 + \bar{n}_1)(\bar{n}_1 + \bar{n}_2)e^{-i\delta} + (\bar{n}_0 - \bar{n}_1)(\bar{n}_1 - \bar{n}_2)e^{i\delta}} \tag{12}$$

$$t = \frac{4\bar{n}_0\bar{n}_1}{(\bar{n}_0 + \bar{n}_1)(\bar{n}_1 + \bar{n}_2)e^{-i\delta} + (\bar{n}_0 - \bar{n}_1)(\bar{n}_1 - \bar{n}_2)e^{i\delta}} \tag{13}$$

The reflection and transmittance will be calculated with:

$$R = |r|^2 \ \textbf{(14)} \ \text{and} \ T = \left|\frac{\bar{n}_2}{\bar{n}_0}\right| \cdot |t|^2 \ \textbf{(15)}.$$

Reflection and transmittance of a thick coplanar layer

While treating this problem it is assumed that the thick layer has no interference effects and that phase shifting has not to be considered. For this reason the formulas include similar sums like the equations (8) and (9) but here calculations can be started immediately by using the intensities and not the coefficients:

$$R = R_{01} + \frac{T_{01}^2 R_{12}e^{-2\alpha d}}{1 - R_{12}R_{10}e^{-2\alpha d}} \ \textbf{(16)} \qquad T = \frac{T_{01}T_{12}e^{-\alpha d}}{1 - R_{12}R_{10}e^{-2\alpha d}} \ \text{(17)}$$

The parts R_{ij} and T_{ij} are the reflection and transmittance of an interface which can be calculated with the equations (6) and (6a).

Reflection and transmittance of a thin film which is located on a thick coplanar substrate
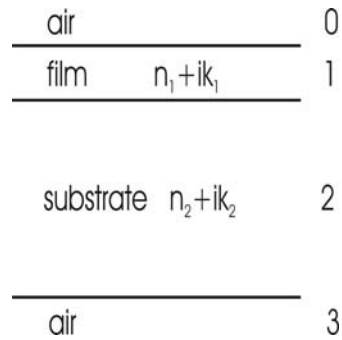
Figure 67. Thin film on a thick coplanar substrate.

Setup is similar to a real-life measurement configuration

It is assumed that a thin film shows interference but the thick substrate does not.

The task has to be solved in two steps:

1. The reflection and transmittance of the thin film between two mediums will be calculated like it was already described. The results will be denoted: R_{02}, R_{20}, T_{02} and T_{20}. Moreover it is valid: $T_{02} = T_{20}$.

2. Finally the whole system will be calculated like a thick coplanar layer. The thin film will be regarded as an interface 0-2.

For the reflectivity we obtain:

$$R = R_{02} + \frac{T_{02}^2 R_{23} e^{-2\alpha_2 d_2}}{1 - R_{23} R_{20} e^{-2\alpha_2 d_2}} \tag{18}$$

For the transmittance:

117

$$T = \frac{T_{02}T_{23}e^{-\alpha_2 d_2}}{1 - R_{23}R_{20}e^{-2\alpha_2 d_2}} \tag{19}$$

The values R_{23} and T_{23} can be calculated with: $R_{23} = \dfrac{(n_2 - 1)^2 + k_2^2}{(n_2 + 1)^2 + k_2^2}$ (compare equation 6 using $n_3 = 1$ and $k_3 = 0$ for air) and $T_{23} = 1 - R_{23}$.

For evaluating the values of R_{02}, T_{02} and R_{20} the formulas for the case of a thin absorbing coplanar layer between two mediums are used (equations 12 and 13 in connection with the equations 14 and 15).

Solving the equations

If the thickness of the layers is known the refractive index **n** and the extinction coefficient **k** can be determined from the measurement of reflectivity R and transmittance T. The equations (18) and (19) cannot be solved by analytical methods. For this reason the two-dimensional Newton-Raphson algorithm is used as an approximation.

In principle this method works in the same way like the Newton algorithm. How does the Newton-algorithm work? It is applied a tangent on the graph in the point $(x_0, f(x_0))$. You get a point of intersection with the x-axis, which is the value x_1. In the point $(x_1, f(x_1))$ is applied a tangent again. The procedure will be iterated until the null of the function f(x) has been found with the wanted accuracy (Figure 68).
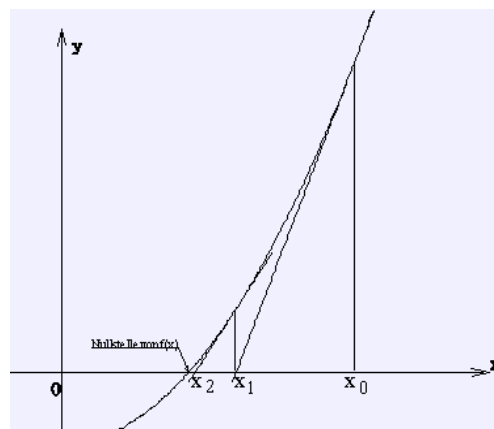

Figure 68. The Newton algorithm

In our case the reflection and transmittance depend from two parameters, n and k. That is why the algorithm has to be accomplished in a two dimensional way (Newton-Raphson algorithm).

The following system of equations has to be solved:

$$R_{ex} - R(n,k) = 0$$
$$T_{ex} - R(n,k) = 0$$

R_{ex} and T_{ex} are the experimental found values. Before beginning the approximation we have to set start values $R(n_0, k_0) = R_0$ and $T(n_0, k_0) = T_0$.

Then a Taylor expansion of R(n, k) at R_0 is done (linearization):

$$R = R_{ex} = R_0 + \left(\frac{\partial R}{\partial n}\right)_0 (n - n_0) + \left(\frac{\partial R}{\partial k}\right)_0 (k - k_0)$$

$$T = T_{ex} = T_0 + \left(\frac{\partial T}{\partial n}\right)_0 (n - n_0) + \left(\frac{\partial T}{\partial k}\right)_0 (k - k_0)$$

The following equation is obtained for the first approximation values n_1 and k_1:

$$\begin{pmatrix} n_1 \\ k_1 \end{pmatrix} = \begin{pmatrix} n_0 \\ k_0 \end{pmatrix} - M^{-1} \begin{pmatrix} R_{ex} - R_0 \\ T_{ex} - T_0 \end{pmatrix}$$

M is the Jakobi matrix:

$$M = \begin{pmatrix} \dfrac{\partial R}{\partial n_0} & \dfrac{\partial R}{\partial k_0} \\ \dfrac{\partial T}{\partial n_0} & \dfrac{\partial T}{\partial k_0} \end{pmatrix}$$

This procedure will be iterated until the values n_n and k_n deviate from n_{n-1} and k_{n-1} in the wanted limits.

The Newton-Raphson algorithm is not applicable when several solutions are possible. For that reason we used a program called "Optik", written by Kristian Peter. It

uses a special calculation routine. The **n** and **k** plane is scanned in a chosen interval. For every pair of **n** and **k** the Newton-Raphson-algorithm is made. If the wanted interval for **n** and **k** is exceeded or the iteration not finished after ten steps, the procedure is interrupted and the next values for **n** and **k** are taken.

7.2 Appendix B: Cell up-scaling – sample holder, mask, encapsulation

In order to be able to perform space resolved I/V measurements on organic solar cells, they needed to be up-scaled to a size of approximately 1 cm^2 and reshaped to a rectangular form. This was made possible by designing and using during UHV material evaporation a new sample holder with a modified mask.
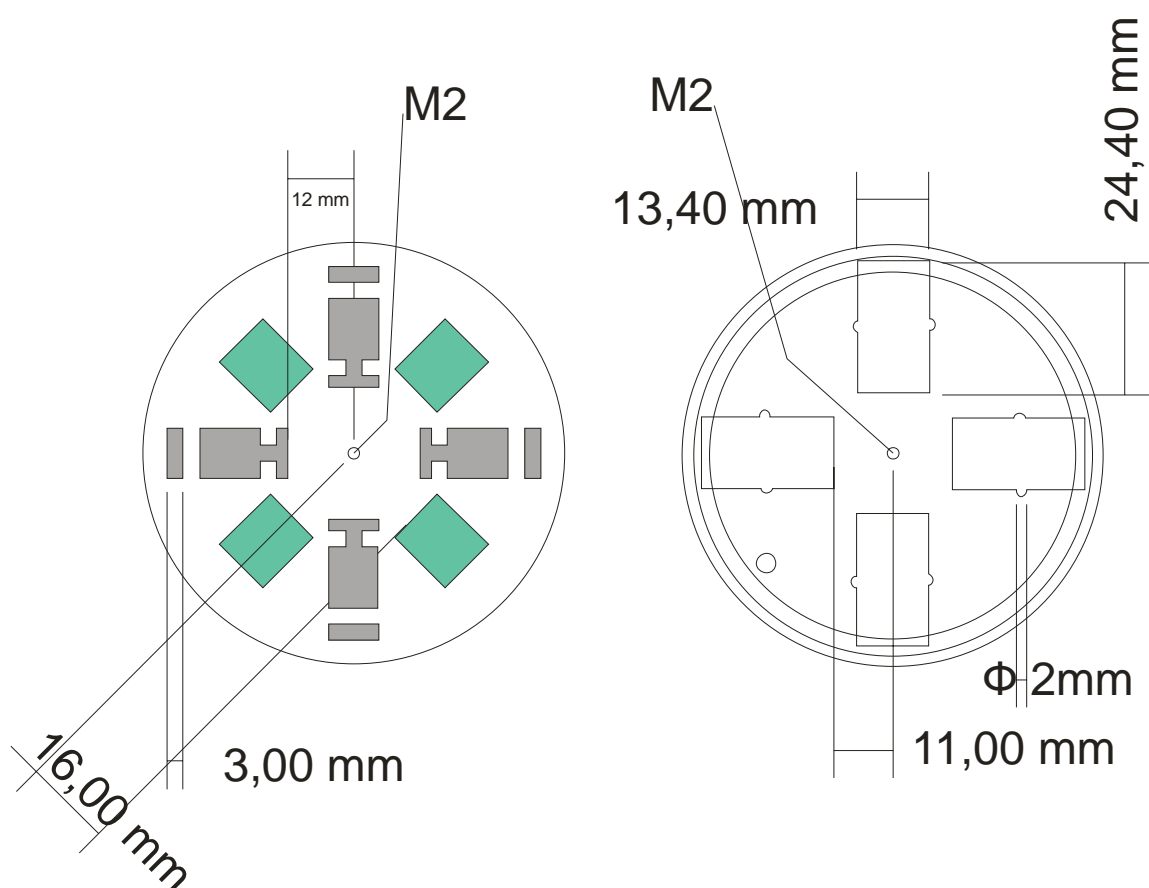
Figure 69. Mask for up-scaled solar cells (left) and sample holder (right). On the mask, the green areas are the openings through which the organics is shaped in the rectangular form of the cell. The grey areas are the openings giving shape to the aluminum contacts and defining the actual cell. The mask is being switched to 45° before contacts are being evaporated

The mask (Figure 69, left) was cut out of 1 mm thick stainless steel sheet with a laser. It was then fitted in the sample holder ring under the sample stabilizer (right on the same figure). Mask and holder were fixed together only by the holder ring, thus a

free rotation of the mask at 45° was possible, for switching between organic and metal contact openings.

The up-scaled solar cells were evaporated on ITO glass substrates with size 13x24 mm. The substrates were structured with a laser cut 5 mm from the short edge, to isolate the front from the back contact (Figure 70).
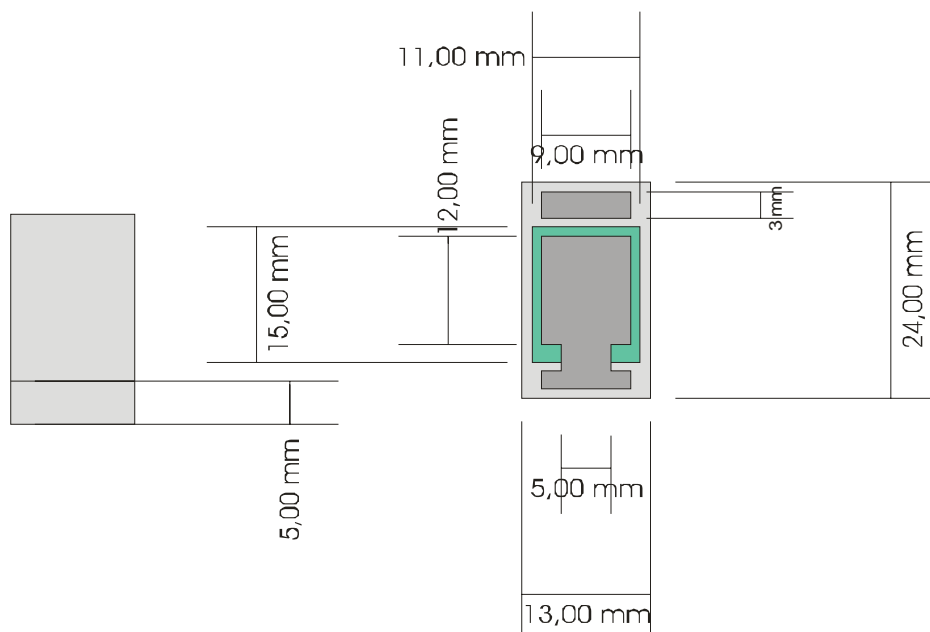
Figure 70. Scheme of a structured ITO glass for solar cell substrate (left). The ITO layer is interrupted 5 mm from the edge, done by a laser cut. Thus the front contact is separated from the back electrode, eliminating a shortcut. A scheme of the ready solar cell (right) shows how organics and contacts are situated.

The schematic view can be compared with solar cells photos on Figure 71.

Figure 71. Photographs of the up-scaled solar cells, seen from the metal contact side (left) and through the glass (right). The green-blue coloring is the organic layer part of the cell

The up-scaled solar cells, of course degrade as their smaller predecessors. That is why a corresponding encapsulation had to be designed (Figure 72).

Figure 72. Up-scaled solar cell encapsulation box (left) and lid (right). The lid is fitted with an o-ring, which upon closure presses on the substrate, keeping the cell isolated from atmosphere

The encapsulation serves as an environment insulator, which keeps the solar cell under inert atmosphere. This allows longer measurements or characterizations with slowed cell degradation.

8 Literature and references

1 K. Heinloth, "Die Energiefrage; Bedarf und Potentiale, Nutzung, Risiken und Kosten"., 2te erweiterte und aktualisierte Auflage, Friedr. Vieweg & Sohn Verlaggesellschaft mbH, Braunschweig/Wiesbaden, 2003

2 R. Hezel, R. Meyer, A. Metz, "A new generation of crystalline silicon solar cells: Simple processing and record efficiencies for industrial-size devices", Solar Energy Materials & Solar Cells, Vol. 65 (2001) 311-316

3 A. J. Boorshtein, "Kinetics of internal photoeffect in organic semiconductors of anthracene type", Journal of Catalysis, Vol. 4, Issue 2 (1965) 313-314

4 C. W. Tang, "Two-layer organic photovoltaic cell", Appl. Phys. Lett., Vol. 48 No.2 (1986) 183-185

5 P. Peumans, A. Yakimov, S. Forrest, "Small molecular weight organic thin-film photodetectors and solar cells", J. Appl. Phys., Vol. 93 No. 3 (2003) 3693-3723

6 D. Gebeyehu, B. Maennig, J. Drechsel, K. Leo, M. Pfeiffer, „Bulk-heterojunction photovoltaic devices based on donor-acceptor organic small molecule blends", Solar Energy Materials & Solar Cells, Vol. 79 (2003) 81-92

7 J. Bernède, H. Derouiche, V. Djara, „Organic photovoltaic devices: influence of cell configuration on its performances", Solar Energy Materials & Solar Cells, 87 (2005) 261-270

8 V. Singh, B. Parsarathy, R. Singh, A. Aguilera, J. Anthony, M. Payne, "Characterisation of high-photovoltage CuPc-based solar cell structures", Solar Energy Materials & Solar Cells, Article in press (2005)

9 M. Muccini, "Optical properties of solid C_{60}", Synthetic metals, Vol. 83 (1996) 213-219

10 R. Lof, M. van Veenendaal, B. Koopmans, H. Jonkman, G. Sawatzky, „Band gap, Excitons, and Coulomb Interaction in Solid C_{60}", Physical Review Letters, Vol. 68, No. 26, (1992) 3924-3927

11 O. Molodtsova, T. Schwieger, M. Knupfer, „Electronic properties of organic semiconductor hetero-interface CuPc/C_{60}", Applied Surface Science, Article in press (2005)

12 C. Weisbuch, H. Benisty, R. Houdbrè, „Overview of fundamentals and applications of electrons, excitons and photons in confined structures", Journal of Luminescence, Vol. 85 (2000) 271-293

13 S. Barth and H. Baessler, "Intrinsinc photoconduction in PPV-Type conjugated polymers.", Phys. Rev. Lett., Vol. 79 (1997) 4445-4448

14 H. Kerp, H. Donker, R. Koehorst, T. Schaafsma, E. Van Faassen, „Exciton transport in organic dye layers for photovoltaic applications", Chem. Phys. Lett., Vol. 298 (1998) 302-308

15 Peumans, S. Forrest, "Separation of geminate charge-pairs at donor–acceptor interfaces in disordered solids" Chem. Phys. Lett., Vol. 398 (2004) 27-31

16 K. Coakley, M. McGehee, "Conjugated Polymer Photovoltaic Cells" J. Chem. Mater., 2004

17 Y. Wang, F. Teng, Q. Zhou, Y. Wang, „Multiple roles of bathocuproine employed as a buffer-layer in organic light-emitting diodes", Applied Surface Science, Article in press (2005)

18 J. Kroon, M. Wienk, W. Verhees, J. Hummelen, „Accurate efficiency determination and stability of conjugated polymer / fullerene solar cells", Thin Solid Films, Vol. 403-404 (2002) 223-228

19 D. Gebeyehu, C. Brabec, N. Sariciftci, „Solid-state organic/inorganic hybrid solar cells based on conjugated polymers and dye-sensitized TiO_2 electrodes", Thin Solid Films, Vol. 403-404 (2002) 271-274

20 H. Neugebauer, C. Brabec, J. Hummelen, R. Janssen, N. Sariciftci, „Stability Studies and Degradation Analysis of Plastic Solar Cell Materials by FTIR Spectroscopy", Synthetic Metals, Vol. 102 (1999) 1002-1003

21 H. Neugebauer, C. Brabec, J. Hummelen, N. Sariciftci "Stability and photodegradation mechanisms of conjugated polymer/fullerene plastic solar cells", Solar Energy Materials & Solar Cells, Vol. 61 (2000) 35-42

22 T. Jeranko, H. Tributsch, N. Sariciftci, J. Hummelen "Patterns of efficiency and degradation of composite polymer solar cells", Solar Energy Materials & Solar Cells, Vol. 83 (2004) 247-262

23 K. Furukawa, Y, Terasaka, H. Ueda, M. Matsumura, "Effect of plasma treatment of ITO on the performance of organic electroluminescent devices", Synthetic Metals, Vol. 91 (1997) 99-101

24 K. Sugiyama, H. Ishii, Y. Ouchi "Dependence of indium-tin-oxide work function on surface cleaning, method as studied by ultraviolet and x-ray photoemission spectroscopies", J. Appl. Phys., Vol. 87 (2000) 295-298

25 S. Karuppuchamy, K. Nonomura, T. Yoshida, T. Sugiura, H. Minoura, "Cathodic electrodeposition of oxide semiconductor thin films and their application to dye sensitized solar cells", Solid State Ionics, Vol. 152 (2002) 19-27

26 M. Tetto "Tuning the ITO work function by surface modification with hydroxyquinoline derivatives" Princeton University Press, 2001

27 B. Johnev, "Research and modification of the contact interface of $InSnO_x$ in organic solar cells", Diploma work, Sofia University, October 2002

28 S. Takeda, M. Fukawa "Role of surface OH groups in surface chemical properties of metal oxide films", Mat. Sci. and Eng., Vol. 119 (2005) 265-267

29 G. Märkl, K. Gschwendner, I. Rötzer P. Kreitmeier "Tetrakis(diethyl-phosphonat)-, Tetrakis(ethyl-phenylphosphinat)- und Tetrakis(diphenylphosphin-oxid)-substituierte Phthalocyanine", Helv. Chim. Act., Vol. 87 (2004) 825

30 C. Waldauf, P. Schilinsky, J. Hauch, C. Brabec, „Material and device concepts for organic photovoltaics: towards competitive efficiencies", Thin Solid Films, Vol. 451-452 (2004) 503-507

31 M. Vogel, „Diplomarbeit: Herstellung und Charakterisierung organischer Solarzellen auf Basis von C60 und Zink-Phthalocyanine", FU-Berlin, October 2002

32 M. Tivanov et al., "Determination of solar cell parameters from its current-voltage and spectral characteristics", Solar Energy Materials & Solar Cells, Vol. 87 (2005) 457-465

33 T.P. Russel, "On the reflectivity of polymers: Neutrons and X-rays", Physica B, Vol. 221 (1996) 267-283

34 C. Himcinschi et al., "Contributions to the static dielectric constant of low-*k* xerogel films derived from ellipsometry and IR spectroscopy", Thin Solid Films, Vol. 455-456 (2004) 433-437

35 J. Hilfiker et al., "Optical characterization in the vacuum ultraviolet with Variable Angle Spectroscopic Ellipsometry: 157 nm and below", submitted at SPIE Microlithography 2000 Conference

36 C. Himcinschi et al. "Characterization of silica xerogel films by variable-angle spectroscopic ellipsometry and infrared spectroscopy", Semicond. Sci. Technol., 16 (2001) 806-811

37 U. Zerweck et al., "Accuracy and resolution limits of Kelvin probe force microscopy", Phys. Review B, Vol. 71 (2005) 125424

38 Ch. Sommerhalter et al., "High-sensitivity quantitative Kelvin probe microscopy by noncontact ultra-high-vacuum atomic force microscopy", Appl. Phys. Lett., Vol. 75, No. 2 (1999) 286-288

39 R.G. Gordon, "Criteria for Choosing Transparent Conductors", MRS Bulletin, August 2000

40 Neal R. Armstrong, C. Carter, C. Donley, A. Simmonds, P. Lee, M. Brumbach, B. Kippelen, B. Domercq, S. Yoo "Interface modification of ITO thin films: organic photovoltaic cells", Thin Solid Films, Vol. 445 (2003) 342–352

41 G. Greczynski, Th. Kugler, M. Keil, W. Osikowicz, M. Fahlman, W. Salaneck, "Photoelectron spectroscopy of thin films of PEDOT–PSS conjugated polymer blend: a mini-review and some new results", Journal of Electron Spectroscopy and Related Phenomena, Vol. 121 (2001) 1-17

42 PGO GmbH Website, "http://www.pgo-online.com/intl/", Oct. 2005

43 F. Yang, M. Shtein, S. Forrest, „Controlled growth of a molecular bulk heterojunction photovoltaic cell", Nature Materials, Vol. 4 (2005) 37-41

44 D. Zheng, Z. Gao, X. He, F. Zhang, L. Liu, "Surface and interface analysis for Copper phthalocyanine (CuPc) and indium-tin-oxide (ITO) using X-ray photoelectron spectroscopy (XPS)", Applied Surface Science 211 (2003) 24–30

45 http://telstar.ote.cmu.edu/environ/m3/s2/02sun.shtml, Oct. 2005

46 S. Siebentritt, „Untersuchung der Mechanismen von Ladungsträgererzeugung und Ladungsträgertransport in Zink-Phthalozyanin-Dünnfilmen", Dissertation, Universität Hannover, 1992

47 P. Milani, M. Manfredini, et al., *Solid State Communications*, volume 90, issue 10, June 1994, p. 639

48 A. Richter, et al., *Appl. Phys.* A 61, p. 163-170

49 T. Russel, "On the reflectivity of polymers: Neutrons and X-rays", Physica B, Vol. 221 (1996) 267-283

50 R. Könnenkamp et al. "Carrier mobilities and influence of oxygen in C_{60} films", Physical Review B, Vol. 60, No. 16 (1999) 11804-11808

51 N. Armstong et al., "Interface modification of ITO thin films: organic photovoltaic cells", Thin Solid Films, Vol. 445 (2003) 342-352

52 J. Kim et al., „Indium–tin oxide treatments for single- and double-layer polymeric light-emitting diodes: The relation between the anode physical, chemical, and morphological properties and the device performance", J. Appl. Phys., Vol. 84, No. 12 (1998) 6859-6870

53 G. Greczynski, Th. Kugler, M. Keil, W. Osikowich, M. Fahlman, W. Salaneck, "Photoelectron spectroscopy of thin films of PEDOT–PSS conjugated polymer blend: a mini-review and some new results", Journal of Electron Spectroscopy, Vol.121 (2001) 1-17

54 S. Karuppuchamy, K. Nonomura, T. Yoshida, T. Sugiura, H. Minoura, "Cathodic electrodeposition of oxide semiconductor thin films and their application to dye-sensitized solar cells", Solid State Ionics, Vol. 151 (2002) 19-27

55 J. Kim, N. Johansson, R. Daik, F. Cacialli "Indium–tin oxide treatments for single- and double-layer polymeric light-emitting diodes: The relation between the anode physical, chemical, and morphological properties and the device performance", J. Appl. Phys., Vol. 84, No. 12 (1998) 6859-6870

56 F. Nüesch, E. Forsythe, Q. Le, Y. Gao, L. Rothberg, "Importance of indium tin oxide surface acido basicity for charge injection into organic materials based light emitting diodes", J. App. Phys., Vol. 87, No. 11 (2000) 7973-7980

57 F. Nüesch, L. Rothberg, „A photoelectron spectroscopy study on the indium tin oxide treatment by acids and bases", J. Appl. Phys., Vol. 74, No, 6 (1999) 880-882

58 I. Fujiwara, M. Maeda, M. Takagi, "Preparation of Ferrocyanide-Imprinted Pyridine-Carrying Microspheres by Surface Imprinting Polymerization", Analytical Sciences, Vol. 19 (2003) 617-620

59 M. Vogel, Dissertation: "Grenzflächen in Phthaloczanin-C_{60}-Solarzellen", F.U.-Berlin, Oct. 2005

60 E. Coquet, J. Crettez, J. Pannetier, J. Bouillot, J. Damien, "Effect of Temperature on Interatomic Distances in Pyroelectric –LiIO3", Acta Cryst. Vol. 39 (1983) 408-413

61 M.Knupfer, H. Peisert, „Electronic properties of interfaces between model organic semiconductors and metals", Phys. Stat. Sol., Vol. 21, No. 6 (2004) 1055-1074

62 C. Hamann, "Organische festkörper und organische dünne schichten", Leipzig, Akademische Verlaggeselschaft Geest & Portig K.-G. 1978

63 K. Gschwendner, Dissertation: "Tetra-Phosphorsubstituierte Phthalocyanine", Uni-Regensburg, 1997

64 K. Gschwender, "Tetra-Phosporsubstituierte Phthalocyanine", Dissertation, Uni-Regensburg 1997

65 M. Al-Ibrahim et al., "The influence of the optoelectronic properties of poly(3-alkylthiophenes) on the device parameters in flexible polymer solar cells", Organic Electronics, Vol. 6 (2005) 65-77

66 N.P.G. Roeges, "A Guide to the Complete Interpretation of Infrared Spectra of Organic Structures", J. Wiley & Sons, Chichester, 1993.

67 Fourier Transform Infrared Spectroscopy, Griffiths & de Haseth, New York:Wiley, 1986

68 Brabec et al., Advanced Functional Materials, Vol. 11, No.5, (2001) 374-380.

69 N. Lang, W. Kohn, "Theory of Metal Surfaces: Work Function", Physical Review B, Vol. 3, No. 4 (1971) 1215-1223

70 J. Smith, "Self-Consistent Many-Electron Theory of Electron Work Functions and Surface Potential Characteristics for Selected Metals", Phys. Review, Vol. 181, No 2 (1969) 522-529

71 K. Peter, „Optische Charakterisierung von Halbleiterschichten", Diplomarbeit, Universität Konstanz, 1993